

# UC Berkeley

## UC Berkeley Electronic Theses and Dissertations

### Title

Investigating mechanisms of tissue growth control during development in *D. melanogaster*

### Permalink

<https://escholarship.org/uc/item/54x0h3kq>

### Author

Sumabat, Taryn

### Publication Date

2018

Peer reviewed|Thesis/dissertation

Investigating mechanisms of tissue growth control during development in *D.*  
*melanogaster*

by

Taryn Sumabat

A dissertation submitted in partial satisfaction of the

requirements for the degree of

Doctor of Philosophy

in

Molecular and Cell Biology

in the

Graduate Division

of the

University of California, Berkeley

Committee in charge:

Professor Iswar Hariharan, Chair

Professor Nicole King

Professor Lin He

Professor Elizabeth Purdom

Spring 2018

Investigating mechanisms of tissue growth control during development in *D.*  
*melanogaster*

Copyright 2018  
by  
Taryn Sumabat

## Abstract

Investigating mechanisms of tissue growth control during development in *D. melanogaster*

by

Taryn Sumabat

Doctor of Philosophy in Molecular and Cell Biology

University of California, Berkeley

Professor Iswar Hariharan, Chair

A remarkable feat of animal development is the precision with which organs grow to a consistent and characteristic size. The lengths of the right and left arm of a human, for instance, match with an accuracy of about 0.2%, and the size of adult mouse brains varies by only about 5%. How a developing organ—and the individual cells within—can know when it is time to stop growing has long-fascinated biologists.

Reciprocal organ transplantation experiments from the 1920s were among the first to demonstrate that, for an individual organ, growth is subject to both extrinsic and intrinsic programs. Working with two closely related but different-sized species of salamanders, the faster-growing yet smaller-sized *Ambystoma punctatum* and the slower-growing yet larger-sized *Ambystoma tigrinum*, Harrison found that the growth rate of a limb transplanted from one species to the other matched that of the host, but the overall size of the transplanted limb matched that of the donor. He concluded, therefore, that while some circulating factor, perhaps a hormone, dictated the rate of limb growth, the organ's size overall was determined by some intrinsic “growth potential.”

Now, close to a century later, we know the identities of many evolutionarily-conserved factors that are critical to achieving a properly-sized organ, but our understanding of what ultimately determines an organ's size remains far from complete. Much of what we do know about the mechanisms regulating tissue growth comes from studies using the model organism *Drosophila melanogaster*, whose genetic tractability and high reproducibility of organ size allow us to easily evaluate the effects of genetic perturbations on tissue growth.

In Chapter 1, I provide an overview of some of these growth-regulatory mechanisms and describe how genetic studies using a well-characterized tissue model of growth—the *Drosophila* wing imaginal disc—have helped to provide some clues into how these mechanisms might operate. I will highlight two signaling pathways—the Hippo pathway and the JNK pathway—that have very different functions but seem to both impact tissue growth in unique ways. Activities of both of these pathways have been areas of interest for my dissertation research.

The Hippo pathway regulates growth in most multicellular organisms and is altered (either directly or indirectly) in many human cancers. Since the elucidation of the core pathway approximately a decade ago, a key aim for researchers has been to identify the upstream signals that link this pathway to external cues and understand how these signals are sensed. An important upstream regulator of Hippo signaling is the transmembrane protein Fat (Ft), though the mechanistic link between the core pathway and this upstream factor is not fully clear. We identified the *Drosophila* F-box protein, Fbxl7, as a downstream effector of Ft activity that is important for regulating the cellular distribution of Dachs, a protein that mediates much of Ft's effect on tissue growth. This work, described in Chapter 2, provides a more complete understanding of the functional link between Ft signaling and the Hippo pathway.

The JNK pathway is a well-conserved pathway involved in several morphogenetic processes during development and commonly activated in response to stress. JNK signaling promotes apoptosis, yet—quite paradoxically—is also important in promoting tissue proliferation during regeneration and tumorigenesis. The role this pathway plays in regulating growth during organ development is less established. We found that JNK signaling is active at low levels in the developing wing imaginal disc and regulates an enhancer of the gene *bantam* (*ban*), which encodes a microRNA that promotes growth. This *ban* enhancer activity is opposed by the transcriptional co-repressor CtBP, which we characterize as a negative growth-regulator in *Drosophila*. These findings, described in Chapter 3, support a role for JNK signaling in promoting tissue growth and suggest that CtBP may help to direct this broadly-functioning signaling pathway towards specific effects on growth during normal development.

During the course of these studies, I made the surprising observation that a common genetic technique used in *Drosophila*, namely shRNA-mediated gene knockdown using the Gal4/UAS system, can lead to an unexpected result: clonal expression of shRNAs causes knockdown in cells that do not express Gal4. Chapter 4 describes this phenomenon, which we term “shadow RNAi,” and shows how this effect can lead to erroneous conclusions regarding cell-autonomous vs. non-autonomous genetic functions. We outline how shadow RNAi can be mitigated, as well as how it can be exploited as an effective lineage-tracing tool.

Taken together, my work offers important clues for solving the mysteries of organ size control and explores new applications of standard genetic techniques, while potentially providing useful insights for the development of novel tools in cancer therapy and regenerative medicine.

*Nomina si pereunt, perit et cognitio rerum.*  
If the names are lost the knowledge also disappears.  
—Johann Christian Fabricius  
*Philosophia Entomologica*

This dissertation is dedicated to the memories of my two grandmothers,  
Flossie Sumabat (1929-2014) and Lillian Fong (1931-2016).

# Contents

<b>Contents</b>	<b>ii</b>
<b>List of Figures</b>	<b>iii</b>
<b>List of Tables</b>	<b>iv</b>
<b>1 Introduction</b>	<b>1</b>
1.1 A conceptual understanding of tissue growth . . . . .	2
1.2 The <i>Drosophila</i> wing disc as a model for organ growth . . . . .	3
1.3 Identification of factors that regulate tissue growth using <i>Drosophila</i> . . . . .	7
1.4 Summary of dissertation work . . . . .	13
<b>2 The F-box protein Fbx17 is a Fat effector that regulates Hippo signaling in <i>Drosophila</i></b>	<b>15</b>
2.1 Abstract . . . . .	16
2.2 Introduction . . . . .	16
2.3 Materials and Methods . . . . .	18
2.4 Results . . . . .	22
2.5 Discussion . . . . .	29
2.6 Figures . . . . .	33
<b>3 A JNK-CtBP pathway regulates the growth effector <i>bantam</i> in <i>Drosophila</i></b>	<b>51</b>
3.1 Abstract . . . . .	52
3.2 Introduction . . . . .	52
3.3 Materials and Methods . . . . .	53
3.4 Results . . . . .	55
3.5 Discussion . . . . .	62
3.6 Figures . . . . .	64
<b>4 Discovery and applications of persistent RNAi-mediated knockdown in <i>Drosophila</i></b>	<b>77</b>
4.1 Abstract . . . . .	78
4.2 Introduction . . . . .	78

4.3	Materials and Methods . . . . .	79
4.4	Results . . . . .	81
4.5	Discussion . . . . .	86
4.6	Figures . . . . .	88
	<b>References</b>	<b>96</b>

# List of Figures

1.1	<i>Drosophila</i> development and wing anatomy . . . . .	4
1.2	FLP/FRT-mediated mitotic recombination . . . . .	8
2.1	Fbxl7 negatively regulates growth through the Hippo pathway . . . . .	33
2.2	Fbxl7 is localized to apical membrane, cytoplasmic puncta, and the proximal side of planar polarized cells . . . . .	35
2.3	Fbxl7 physically interacts with Fat and regulates its apical localization . . . . .	37
2.4	Additional analysis of the relationship between Fbxl7 and Fat . . . . .	39
2.5	Relationship between Fbxl7 and the Fat pathway proteins Ds and Dco . . . . .	40
2.6	Fbxl7 functions in one of two growth-suppressing pathways downstream of Ft . . . . .	41
2.7	Domain D of Ft is required for the effects of Fbxl7 on Ft localization . . . . .	43
2.8	Fbxl7 regulates the localization of Dachs . . . . .	44
2.9	Fbxl7 does not affect Dachs ubiquitylation, and Fbxl7 affects the localization of Cindr . . . . .	46
3.1	Mutations in <i>CtBP</i> result in increased tissue growth . . . . .	64
3.2	Overexpression of unique CtBP protein isoforms causes impaired wing growth . . . . .	65
3.3	Analysis of Yki activity in <i>CtBP</i> mutant clones . . . . .	66
3.4	Increased <i>ban</i> activity is required for overgrowth of <i>CtBP</i> clones . . . . .	67
3.5	CtBP regulates a minimal <i>ban</i> enhancer, <i>brC12</i> via Yki-dependent and Yki-independent mechanisms . . . . .	68
3.6	<i>brC12</i> activity is dependent on JNK signaling . . . . .	70
3.7	Blocking JNK signaling abrogates the increased <i>brC12</i> activity caused by loss of <i>CtBP</i> . . . . .	72
3.8	Loss of distinct Fos isoforms leads to <i>brC12-lacZ</i> upregulation . . . . .	73
3.9	CtBP inactivation does not autonomously upregulate <i>puc-lacZ</i> expression . . . . .	75
3.10	A model for how CtBP could switch AP-1 from a transcriptional activator to repressor . . . . .	76
4.1	Gene knockdown in shadow RNAi clones when using the FLP-out Gal4 system . . . . .	88
4.2	Gene knockdown in shadow RNAi cells caused by dynamic expression of <i>ptc-Gal4</i> . . . . .	90
4.3	RNAi persistence does not require past expression of target transcripts . . . . .	91

4.4	RNAi persistence requires Ago2 but not other RISC components . . . . .	92
4.5	The i-TRACE system . . . . .	93
4.6	Reversible cell-fate switching at compartment boundaries in the wing disc . . . .	94

# List of Tables

2.1	Oligonucleotide sequences . . . . .	48
2.2	Co-localization of FLAG-Fbx17 and vesicle markers . . . . .	50
4.1	Summary of genes targeted by RNAi and knockdown transgenes tested . . . . .	95

## Acknowledgments

I am deeply grateful to many individuals who helped see this dissertation come to a completion and who, like some of the molecules described in this work, have played important roles in my own growth—both professionally and personally. Since part of this maturation probably involves refraining from the use of groan-inducing metaphors, I will resist the temptation to liken aspects of my graduate career to the “wandering stage” of larval development or to refer to the culmination of this work as a “metamorphosis.” Instead, I will begin by thanking my advisor, Iswar Hariharan, for constantly supporting me, teaching me, challenging me, checking in with me, and believing in me these past six years. Iswar’s encouragement of thinking in terms of first principles, his ability to tie together threads from seemingly unrelated bodies of work into one cohesive scientific model, and the ease with which he is able to explain these models and their rationale have all helped to shape my understanding of what it means to be a good scientist. His kindness and sincere respect for others, along with his commitment to integrity, have helped me appreciate what it means to be a good person. Thanks to Iswar, I feel proud of the work I have done in his lab, and I am truly fortunate to have had him as a mentor.

In addition to Iswar, I want to recognize some incredible individuals whom I’ve had the privilege of calling my labmates over the years. Justin Bosch’s patience and mentorship during my rotation was a big reason why I chose to join the Hariharan lab. He was so generous with his time and advice, and I am lucky to have had the chance to collaborate on two chapters in this dissertation with such a talented scientist. Melanie Worley’s earnest scientific curiosity, brilliant ideas, and commitment to scientific rigor have all played a huge part in shaping my development as a scientist. Many of the conversations we have had at our bay, in the fly room, or on our walks to/from the gym/Starbucks have helped me interpret confusing results or think about my data in new ways and provided me with ideas for experiments. It was convenient that we both ended up working on the same gene (though in different contexts), and I am grateful for Melanie’s willingness to share her results, recombinants, and other reagents with me. Linda Setiawan was incredibly helpful with scientific discussions and saved me many headaches by instilling in me early on the importance of double-balancing my stocks and setting up proper controls. Jo Downes Bairzin was my first friend in grad school and she has helped me through many hurdles both inside and outside of academia. In addition to being great colleagues, I also want to acknowledge Melanie, Linda, and Jo for being wonderful workout buddies, lunch companions, and, overall, amazing friends. I don’t think I could’ve imagined a better graduate experience without the three of them. I also want to acknowledge my former undergraduate mentee, Susan Wang, for her contributions to the CtBP project, her willingness to try out some of my experimental ideas, and for giving me the chance to grow as a mentor. Finally, thank you to the rest of the Hariharan lab, both past and present, for providing invaluable feedback on my work and for contributing to a fun and supportive environment that I have looked forward to coming to every day: Robin, Sa Kan, Maya, Jamie, Nick, Sophia, Danielle, and Riku.

Outside of the Hariharan lab, I wish to acknowledge the members of my thesis committee for taking the time to think about my work and provide guidance over the years: Nicole King, Lin He, and Elizabeth Purdom. I also want to thank David Bilder and the rest of the Bilder lab for sharing reagents and contributing helpful feedback. Thank you also to Nipam Patel for helping me become skillful at confocal microscopy and for giving me the opportunity to TA at Woods Hole for two rewarding summers.

And finally, I am indebted to my wonderful friends and family members who have been my cheerleaders since before I decided to even embark on this journey. Particularly, I wish to acknowledge both of my parents, Dianna and Ed, for their unconditional love and support. Thanks for flying down to visit me throughout the years, for planning fun trips together, and for sending me your Bitmoji messages (Mom) and pictures of Teddy and LJ (Dad)—I don't think I fully appreciated how important these things were at the time in keeping my spirits high. Last but not least, I want to acknowledge my partner and best friend, Jayaji More, who has celebrated my triumphs, empowered me when I felt defeated, and provided relentless love and encouragement throughout my entire time in grad school. For all those times you asked me, "Why were you in lab so late?" this dissertation is your answer.

# Chapter 1

## Introduction

Everywhere Nature works true to scale, and everything has its proper size accordingly.

---

—D’Arcy Wentworth Thompson  
*On Growth and Form*

## 1.1 A conceptual understanding of tissue growth

Organ growth is defined as an increase in the mass or overall size of a tissue. In general, the final size of an organ is determined by the number of cells it contains, the sizes of each of these cells, and the extracellular space between cells. I will focus on how two of these parameters—cell number and cell size—are determined, as the space between somatic cells is fairly similar (Yang and Xu, 2011). Overall cell number is balanced by the number of cell divisions and cell deaths within a tissue, while cell size depends on cell growth.

Though they are often (but not always) coupled during development, cell growth and cell division are fundamentally distinct processes. Cell growth occurs by increasing a cell’s overall mass. While water accounts for over 70% of total cell mass, macromolecules including proteins, nucleic acids, and carbohydrates make up the bulk of dry weight within a cell (Cooper, 2000). Cell growth thus relies heavily on growth factors and systemic nutrient levels as well as the internal machinery involved in synthesizing these macromolecules. Cell division is the final step of a fixed sequence of events—the cell cycle—in which a cell divides into two. Thus, while cell growth alone can yield an increase in overall organ size, cell division without cell growth cannot do so. During development, mitogens stimulate the activity of cyclin-dependent kinases (Cdks), which pair with cyclins to coordinate cell cycle progression. Typically, this involves a concordant degree of cell growth. (Some exceptions to this include the cleavage stage of embryogenesis, during which cells of the fertilized egg rapidly divide with little growth, and the cells of the *Drosophila* salivary glands, which repeatedly replicate their DNA without dividing, resulting in large cells with giant polytene chromosomes.)

Cell death can be a critical aspect of an organ’s development, allowing for the elimination of unnecessary tissue. Digit formation during vertebrate limb morphogenesis, for instance, involves the death of interdigital tissue (Garcia-Martinez et al., 1993; Mori et al., 1995). This is achieved by apoptosis, which is an intrinsically-regulated process in which the activation of caspase proteins results in cell morphological changes that culminate in the cell’s destruction. Apoptosis may be triggered by developmental cues or cells may be programmed to die unless they receive a specific survival factor.

It is clear that for each of these processes—cell growth, cell division, and cell death—extrinsic factors are linked to an intrinsic cellular program. Because organ growth is ultimately a collection of these individual cell behaviors, understanding how these processes are coordinated during development is key to understanding size control.

## 1.2 The *Drosophila* wing disc as a model for organ growth

The larval structures of *Drosophila* that give rise to adult organs and appendages have provided an excellent system for studying many fundamental aspects of biology. These epithelial structures, called imaginal discs, are internal tissues that, in the span of just a few days prior to metamorphosis, undergo a fixed program of growth and patterning, ultimately forming external adult structures of characteristic size and shape (Figure 1.1B). Significantly, the organization of cells within imaginal discs is highly similar to that of most epithelial tissues found throughout the animal kingdom, including those that make up most human organs (Tyler, 2003).

### Growth and development of the wing imaginal disc

The wing imaginal disc (Figure 1.1C), in particular, is perhaps one of the best-studied models of organ growth (Shingleton, 2010; Hariharan, 2015; Irvine and Harvey, 2015). This tissue arises from a cluster of approximately 30 undifferentiated cells of the embryonic ectoderm, which together invaginate to form a flattened sac (García-Bellido and Merriam, 1971; Madhavan and Schneiderman, 1977; Worley et al., 2013). As larval development proceeds, these cells undergo roughly 10 rounds of cell divisions so that by the onset of pupariation, the wing disc consists of approximately 30,000-50,000 cells (Milán et al., 1996b; Martín et al., 2009; Worley et al., 2013). By this stage, much of the tissue's patterning has been established. Most cells complete two additional divisions during the pupal stage before arresting in the cell cycle (Milán et al., 1996a). During metamorphosis, the wing disc will evert to form the adult wing. Cells of the adult wing do not grow or divide; thus, the final size of the adult wing can serve as a direct readout for the degree of tissue growth that occurred during development.

The wing imaginal disc is not a homogeneous tissue. Patterning events during embryogenesis and larval development set up distinct subpopulations of cells within the tissue, that can be distinguished by selector genes and cell-fate markers and which will contribute to specific parts of the adult. The wing disc will give rise to three structures in the adult: the wing pouch will evert during morphogenesis and become the wing blade, the hinge attaches the wing to the body wall, and the notum contributes to the dorsal thorax (Figure 1.1C-D). In addition to these distinct fates, anterior-posterior (A/P) and dorsal-ventral (D/V) compartment boundaries subdivide the disc into lineage-restricted cell populations which do not intermix (Figure 1.1C). Despite these differences, cell division is fairly uniform throughout the wing disc, though there is some evidence that it is not random (García-Bellido and Merriam, 1971). For instance, we have long-appreciated the existence of a stripe of cells along the D/V boundary, termed the “zone of non-proliferating cells,” that arrest in the cell cycle near the end of larval development (O’Brochta and Bryant, 1985). In addition, non-clonal clusters of cells with similar cell cycling rates have been observed (Gonzalez-Gaitan et al.,

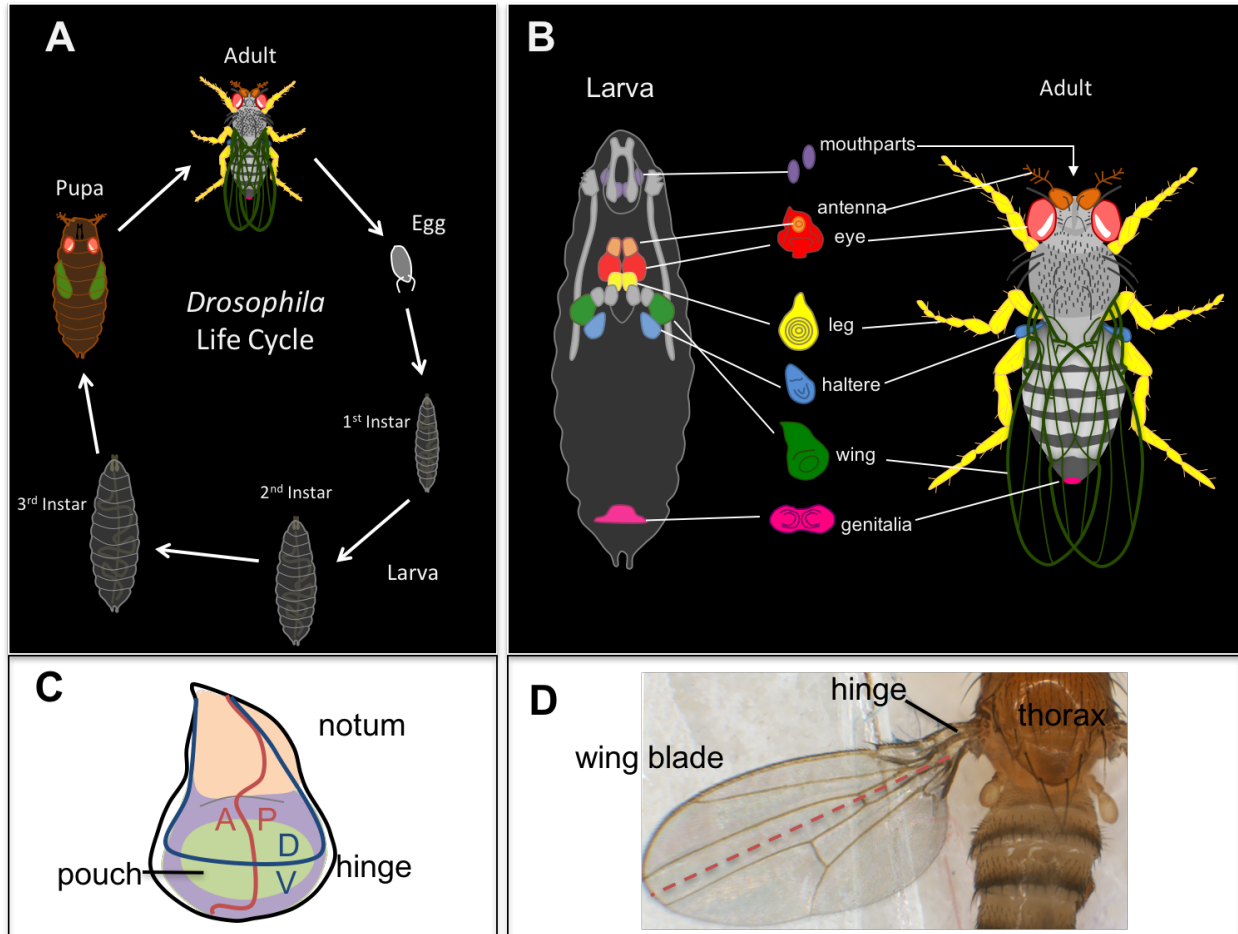


Figure 1.1: *Drosophila* development and wing anatomy.

(A) The *Drosophila* life cycle (B) The larval imago discs that give rise to adult structures. (C) *Drosophila* wing imago disc showing compartment boundaries and identities of different parts of the tissue. The red line is the anterior-posterior (A/P) compartment boundary, and the blue line is the dorsal-ventral (D/V) compartment boundary. The pouch gives rise to the wing blade, and the notum gives rise to parts of the thorax. (D) Adult fly labeled with the structures derived from the parts of the wing imago disc shown in (C). The dashed red line approximately marks the A/P compartment boundary.

1994; Milán et al., 1996b; Dubatolova and Omelyanchuk, 2004), suggestive of localized proliferative zones. While the zone of non-proliferating cells is clearly established by signals that emanate from the D/V boundary, how these proliferative zones are set up is poorly understood. Beyond the confines of normal development, it has become increasingly clear that some areas of the disc have a greater capacity to form tumorous overgrowths than others when tumor-initiating genetic manipulations are performed (Froldi et al., 2010; Khan et al., 2013; Tamori et al., 2016), yet any model consolidating proliferative zones during developmental growth with so-called “tumor hotspots” will require future work.

## Disc-autonomous regulation of wing growth

We know from classical disc transplantation experiments that the wing disc has the capacity to sense its overall size and stop growing disc-autonomously. For example, if a wing disc from a young larva or a fragment of a wing disc is transplanted into the abdomen of an adult female, it will grow until it reaches its approximately normal size and shape, (Hadorn, 1963; Bryant, 1971; Schubiger, 1971; Bryant and Levinson, 1985).

A size-sensing mechanism also appears to be a property of individual compartments within the disc. At least for the A/P compartments, it has been demonstrated that slowing the growth rate of one compartment will force the other compartment to slow down and eventually stop its own growth to allow the slower-growing compartment to “catch up,” so that both compartments achieve their correct final size (Martín and Morata, 2006; Mesquita et al., 2010). However, it has also been observed that increasing the growth of one compartment results in reduced growth of the other compartment (Ferreira and Milán, 2015). It is worth noting that the genetic pathways that are perturbed in these studies in order to affect growth rates are not identical.

As discussed in Section 1.1, tissue growth ultimately results from the individual actions of constituent cells. Thus, any disc- or compartment-autonomous size control mechanism must ensure that localized growth is coordinated. There are several models for how this coordination could be achieved. One that has been subject to intensive testing and refinement is the morphogen-gradient model. In this model, signaling molecules—called morphogens, which emanate from small groups of cells along compartment boundaries, set up concentration gradients that provide receiving cells with instructive cues about their individual fates and growth activities. Supporting this are many classic studies finding that morphogens such as Decapentaplegic (Dpp; the *Drosophila* TGF- $\beta$ /BMP family protein) and Wingless (Wg; the *Drosophila* Wnt family protein) are critical for normal wing size (reviewed in [Restrepo et al., 2014; Swarup and Verheyen, 2012]). Accounting for the fact that growth within the disc does not occur in a concentration-dependent manner, a number of possibilities have been put forth, and I will not detail all of them here (for more in-depth reading, see [Schwank and Basler, 2010; Wartlick et al., 2011; Restrepo et al., 2014; Irvine and Harvey, 2015; Hariharan, 2015]). One idea is that detection of the slope drives proliferation. In other words, signal-receiving cells compare their concentrations with neighboring cells and the detection of differences above a threshold results in a proliferative response. This proliferation would

result in the addition of new cells to intercalate between once-neighboring cells, resulting in a leveling out of the slope. Eventually these differences would fall below the critical threshold, and disc growth would cease. An alternative possibility is that the gradient itself does not matter; rather, concentrations above a single threshold trigger proliferation. Significantly, improvements in gene editing tools are now providing opportunities to test these models in new ways; that a flurry of work over the past several years has stimulated intense debate over if and how these classical morphogen gradients regulate organ growth suggests we will soon see careful refinement of these growth-regulatory models.

Another idea that is receiving increasing attention is that mechanical feedback offers a way to control tissue size. In epithelia, high levels of mechanical stress, such as compression of cells dividing within a defined two-dimensional space, can impede growth (Shraiman, 2005). In the context of wing disc development, this model suggests that the increasing compression of cells at the center of the disc—i.e. where concentration of a morphogen is highest—is what slows and eventually terminates disc growth. Consolidating aspects of the morphogen-gradient model, it has been proposed that, for cells at the center, once the growth-stimulatory effect of any morphogen is overcome by the growth-inhibitory effect of mechanical compression, growth ceases (Aegerter-Wilmsen et al., 2007; Hufnagel et al., 2007). Cell proliferation at the periphery of the disc could result from stretching induced by growth in the disc center (Aegerter-Wilmsen et al., 2007) or graded signals (Shraiman, 2005), or both, but would ultimately cease according to any of the growth-inhibitory mechanisms described. These mechanical feedback models have not been as rigorously tested as morphogen-gradient models, and the results of recent studies have been difficult to reconcile. Quantifications of mechanical compression show that it is indeed highest at the center of the disc and increases with disc size (Nienhaus et al., 2009; LeGoff et al., 2013), but altering tissue constriction by manipulating the basement membrane has not been found to influence tissue size (Ma et al., 2017). Still, there is mounting evidence that activity of the Hippo Pathway (one of the key pathways known to regulate developmental growth, which I will describe later on in this chapter) is modulated by tensile forces that arise during disc development (Rauskolb et al., 2014). The concept of mechanosensation as a size-sensing mechanism is an attractive model but further investigation of its significance during development is clearly needed.

## Systemic regulation of wing size

In addition to these mechanisms regulating autonomous disc growth, the wing imaginal disc also integrates extrinsic cues that can affect its growth. These cues can include information about the animal's environment: nutrient-starvation, high temperatures, and crowding during larval development can cause adults to be smaller in size overall, with proportionally reduced wings (Shingleton et al., 2009).

Additionally, circulating growth factors such as hormones coordinate organ growth with organismal development, ensuring that not only are organs sized properly, but they are correctly proportioned as well. If growth of the wing disc is slowed or perturbed by damage, for instance, developmental progression will delay—that is, the larva will pupate later than

normal—and the other organs in the body will slow their growth so that the ratios of organ size to one another are maintained (Parker and Shingleton, 2011; Halme et al., 2010; Jaszczak et al., 2015). Thus, the individual organ has a way of communicating its growth status to the rest of the body.

During larval development, an endocrine organ called the prothoracic gland synthesizes the molting hormone ecdysone in a series of ever-increasing pulses. The larval-to-pupal developmental transition is triggered by a steep increase in ecdysone levels. Studies of damaged or abnormally-growing discs have found that these discs can secrete factors that inhibit ecdysone production (Halme et al., 2010; Colombani et al., 2012; Garelli et al., 2012), and there is some evidence that discs during normal development produce factors that impede ecdysone synthesis (Boone et al., 2016; Setiawan et al., 2017 *preprint*).

### 1.3 Identification of factors that regulate tissue growth using *Drosophila*

Now that I have described the wing disc as a model for studying tissue growth, I will provide an overview of how powerful genetic approaches in *Drosophila* provide us with an ideal system to identify factors that regulate growth. I will then highlight some of the key growth-regulatory pathways that have been identified and studied in *Drosophila*.

#### Mosaic analysis and targeted gene expression

A powerful tool for studying the function of essential genes is the use of mosaic analysis, in which clones of cells that are homozygous for an otherwise lethal mutation are generated within a heterozygous animal. This is routinely achieved by *Drosophila* researchers using FLP/FRT-mediated mitotic recombination (see Figure 1.2). The FLP/FRT system has been used by several labs (including ours) to screen for genes with tumor-suppressive functions. Many of these screens were conducted using a version of FLP that is only expressed in the developing eye imaginal disc, and involved screening in the adult eye, where mutant clones can be visually marked by the absence of red pigment. Because mitotic recombination will produce an adult eye with a roughly 1:1 ratio of mutant to wild-type tissue, mutations that affect negative regulators of growth can be identified in eyes with more mutant to wild-type tissue—or a “white-over-red” phenotype. Versions of these white-over-red screens led to the recovery of a wide range of mutations that eventually led to the identification and characterization of many genes required for normal tissue growth.

In addition to these classical screening approaches, targeted mis-expression or RNAi-based knockdown of genes of interest is performed with ease using the Gal4/UAS system (reviewed in Adams and Sekelsky, 2002). Excitingly, the advent of CRISPR/Cas9-mediated gene editing techniques has introduced UAS-Cas9 lines to the *Drosophila* researcher’s toolkit (Xue et al., 2014), making it possible to perform conditional mutagenesis. Applications that combine the Gal4/UAS and FLP/FRT systems, including the MARCM and FLP-out Gal4

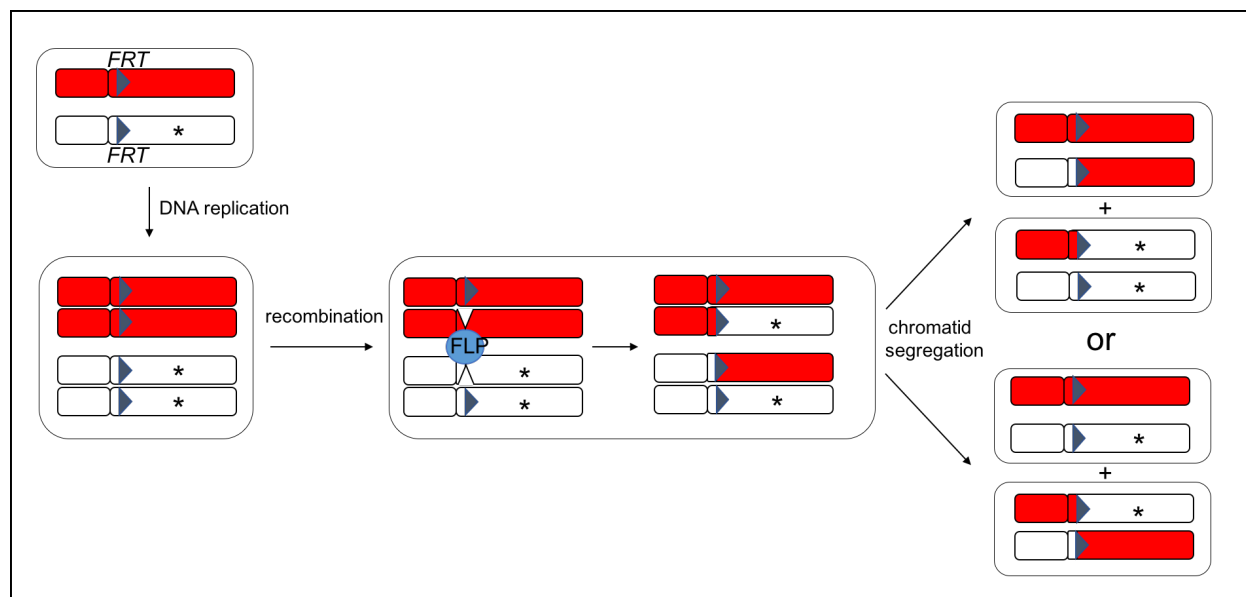


Figure 1.2: **FLP/FRT-mediated mitotic recombination.**

In cells heterozygous for a hypothetical mutation (\*), activation of the FLP recombinase will result in recombination between homologous chromosomes at the *FRT* site. Cytokinesis will result in two possible pairs of daughter cells: a homozygous WT cell and a homozygous mutant cell (top) or two cells that are both heterozygous for the mutation of interest (bottom). In the latter case, if activity of the FLP recombinase persists, future rounds of mitoses could result in the generation of homozygous daughter cells. Proliferation of homozygous cells will result in clones. Typically, genes encoding visual markers are carried on the WT chromosome, distal to the *FRT* site, enabling detection of unmarked mutant clones

clonal systems, expand our ability to perform mosaic analysis. The existence of literally thousands of transgenic RNAi lines, mis-expression libraries, and Gal4 lines—many of which have unique expression patterns—that are available to the *Drosophila* community, along with many tools that provide for precise temporal control of the expression of transgenes, has significantly transformed our ability to assess how specific genetic perturbations affect growth. While none of these genetic tools are without technical limitations—such as off-target effects, unintended gene misexpression (Vissers et al., 2016), or perdurance of both proteins and even shRNAs—many of which a researcher can overlook, they provide an extremely powerful system for determining the functional significance of many genes.

## Identification of key growth-regulatory pathways

Many of the factors that were identified using the genetic approaches just described fall into one of six “main” pathways that regulate imaginal disc growth: the Insulin/PI3 kinase pathway, the receptor tyrosine kinase (RTK)/Ras/MAPK pathway, the Rheb/Tor pathway,

the Hippo pathway, the Myc pathway, and the JAK/STAT pathway (Hariharan, 2015). Importantly, each of these pathways is evolutionarily-conserved, underscoring their functional significance—as well as the utility of using *Drosophila* to study tissue growth. As well, components of many of these pathways are mis-regulated during tumorigenesis, indicating the importance of understanding their functions in order to devise better cancer therapeutic strategies.

These pathways do not function in isolation, nor is it the case that any of these pathways function solely to regulate growth. Thus, it is important to bear in mind that when attempting to understand growth that a perturbation to one pathway could impact the activities of another pathway, while also affecting the behavior of another developmental process altogether. Thus, an important goal for future studies will be to determine how these different pathways crosstalk with one another. Incorporating approaches from systems biology may help to improve our understanding of these complexities.

## The Hippo pathway

The Hippo pathway has emerged as a key regulator of organ size, and many components of this pathway are evolutionarily conserved even in the unicellular amoeboid *Capsaspora owczarzaki*, suggesting this pathway may have premetazoan origins (Sebé-Pedrós et al., 2012). Work in vertebrates has shown that the Hippo pathway is strongly involved in several processes of cancer progression and, in general, has important regulatory functions in organ development, regeneration and stem cell biology. The pathway is typically classified into three main parts: a central core kinase cassette, downstream transcriptional regulatory proteins, and multiple upstream regulatory inputs (reviewed in [Irvine and Harvey, 2015]).

At the core of the Hippo tumor-suppressor pathway in *Drosophila* is a four-member complex consisting of the kinases Hippo (Hpo; Mst1/2 in mammals) and Warts (Wts; Lats1/2 in mammals) and their adaptor proteins Salvador (Sav; Sav1 in mammals) and Mats (Mob1A/B in mammals). These proteins act to repress tissue growth by phosphorylating and thereby preventing the nuclear localization of the key transcriptional coactivator, Yorkie (Yki; YAP/TAZ in mammals). Under growth-stimulatory conditions, nuclear-localized Yki activates the transcription of a suite of genes, whose functions include promoting cell proliferation and inhibiting apoptosis.

Two primary goals for researchers studying the Hippo pathway are to understand both how the Hippo pathway is regulated and the critical downstream events it controls. I will describe some of the progress that has been made towards both of these goals.

### Regulation of Hippo signaling by cell-cell interactions and the cytoskeleton

A striking aspect of the Hippo pathway is that its activity has been found to be modulated by many of the mechanisms that could coordinate tissue growth at a local level. Many of the upstream proteins that are known to regulate Hippo signaling are concentrated at cell junctions, and provide a way for the core pathway to integrate information from neighboring

cells. For example, the proteins Kibra, Merlin, and Expanded (Ex) regulate Hippo signaling and co-localize junctionally (McCartney et al. 2000; Yu et al., 2010; Genevet et al., 2010; Baumgartner et al., 2010). These proteins have been found to interact biochemically and losing each results in similar overgrowth phenotypes, but there is growing evidence that they have non-overlapping functions in affecting Hippo signaling. It is still unclear how these proteins influence Hippo activity, as well as how they are individually regulated. One factor that has been shown to affect the activities of at least Kibra and Ex is the transmembrane protein Crumbs (Chen et al., 2010; Ling et al. 2010; Su et al., 2017). Homophilic interactions of Crb at the apical domain of neighboring cells could provide a way for cell-cell adhesion to regulate Hippo signaling (Hafezi et al. 2012). Similarly, the protein Echinoid binds to itself on adjacent cells at the adherens junction to regulate pathway activity.

Another important cell-cell interaction is the binding of the protocadherins Fat (Ft) and Dachshous (Ds) at the sub-apical domain of adjacent cells. Ft-Ds signaling regulates the Hippo pathway by influencing the protein levels of Wts, and Ft-Ds interactions are modulated by the kinase Four-Jointed (Fj). Significantly, both Ds and Fj are expressed in gradients that are established by Dpp, Wg, and Notch signaling (Rogulja et al., 2008), thus linking Hippo signaling to the influence of morphogen patterning.

Studies in both *Drosophila* and cultured human cells have shown that Hippo pathway activity is modulated by the actin cytoskeleton. For instance, when cells are stretched or cultured at low cell density, they form extensive actin stress fibers and proliferate due to high activity of YAP/TAZ (Dupont et al., 2011; Wada et al., 2011). In imaginal discs, certain manipulations that increase the polymerization of actin filaments result in tissue overgrowth via the activity of Yki (Fernández et al., 2011; Sansores-Garcia et al., 2011). How cytoskeletal changes influence Hippo signaling is still an open area of investigation. One mechanism by which this could occur involves the protein Ajuba (Jub). Both Jub and its mammalian homolog have been shown to interact with  $\alpha$ -catenin (Rauskolb et al., 2014; Marie et al., 2003), a protein that links cadherins at the adherens junction to the actin cytoskeleton (Desai et al., 2013). Increased tension within the actin cytoskeleton causes Jub to localize with Wts at adherens junctions, and this could promote tissue growth by impeding activity of the core Hippo pathway (Rauskolb et al., 2014). In addition, loss of spectrin—a cytoskeletal protein that crosslinks with short F-actin to form a lattice-like structural lining along the intracellular side of the plasma membrane—has been observed to lead to Yki-mediated disc overgrowth (Fletcher et al., 2015; Deng et al., 2015).

In addition to these upstream signals, there is a growing body of work on the role of cellular metabolism and G-protein coupled receptor signaling in regulating the Hippo pathway in mammals (reviewed in [Watt et al., 2017]). Whether these regulatory mechanisms are conserved in *Drosophila* is unclear. Ultimately, determining how these upstream signals feed into the Hippo pathway to drive a physiological program of growth requires an understanding of the transcriptional program underlying tissue growth.

## Yorkie as an effector of tissue growth

Though mammals possess two functional homologs of Yki, in *Drosophila* virtually all transcriptional events downstream of the Hippo pathway seem to occur through Yki (Huang et al., 2005). Yki itself lacks DNA-binding activity, relying instead on interactions with DNA-binding transcription factors to regulate target gene expression. Yki’s primary binding partner seems to be Scalloped (Sd; TEAD1-4 in mammals), but growth-promoting physical interactions between Yki and additional transcription factors have been demonstrated. The extent to which Yki switches between binding partners to regulate organ growth during development is still an unsettled issue. Another open question is how, specifically, Yki activates transcription. At least for Sd, it is thought that Yki may activate growth by relieving Sd-mediated repression. This model suggests that Yki competes with a transcriptional co-repressor that is, by default, engaged with Sd (Koontz et al., 2013; Guo et al., 2013). Biochemically, Yki has been found to associate with GAGA Factor, the Brahma complex (the *Drosophila* SWI/SNF chromatin remodeling complex), components of the Mediator complex, and a subunit of the Trithorax-related histone H3K4 methyltransferase complex, thus linking Yki to chromatin modifiers and the transcriptional machinery (Oh et al., 2013; Qing et al., 2014).

An important goal towards understanding Yki-regulated growth is to determine what its transcriptional targets are during development. We already know of some that could help explain Yki’s growth-promoting effects. These include *cyclin E*, *thread/diap1*—which encodes the anti-apoptotic factor Diap1, and *bantam (ban)*—a microRNA that promotes growth. Additionally, Yki can activate the expression of genes encoding many of the factors that regulate growth upstream of the core Hippo pathway, indicating a mechanism of negative feedback. Recently, *dilp8*, which encodes a hormone that suppresses ecdysone biosynthesis, was identified as a transcriptional target of Yki, thus suggesting a way for the organ to communicate its growth status systemically. (Boone et al., 2016) From a combination of work using ChIP-seq, DamID-seq, and RNA-seq, it has recently been estimated that a little over 100 genes seem to be direct targets of Yki (Oh et al., 2013; Zhang et al., 2017). Validating and further characterizing these prospective targets to understand when they are expressed and how they function will be an important next step in determining at least one of the transcriptional programs that underlies growth.

One observation that has puzzled our group and likely many others is that, at least in the developing wing disc, both fluorescently-tagged and endogenous Yki—as visualized by a Yki antibody (Oh and Irvine, 2008), appears almost exclusively cytoplasmic. Yet, based on virtually all published studies of Yki to date, the majority of Yki activity occurs in the nucleus. In fact, the analyses using ChIP-seq and DamID-seq suggest that Yki associates with approximately 5000-6000 sites in the genome! It is likely that a predominantly cytosolic Yki reflects its “true” state during developmental growth, and this detection of high chromatin-association could arise from experimental bias. When and how often during the growth of the wing disc does Yki enter the nucleus to effect its transcriptional program are questions that few studies to date have addressed. Despite our extensive repertoire of genetic tools,

super-resolution microscopy and live imaging of developing discs are technical milestones the *Drosophila* community have yet to achieve, but could one day help shed light on some of the mysteries surrounding Yki.

## The JNK pathway

The Jun-N-terminal Kinase (JNK) pathway is an evolutionarily-conserved kinase cascade that is involved in several morphogenetic processes in *Drosophila*, such as dorsal closure of the embryo and imaginal disc eversion. It is also the key stress-response pathway and is triggered by various stress stimuli, including inflammatory cytokines, reactive oxygen species, heat shock, and physical wounding. Though it is not typically thought of as a key growth-regulatory pathway, it does play a critical role in regulating compensatory proliferation and tumorigenesis—two processes that invoke many of the components underlying developmental growth. Additionally, there is evidence suggesting a role for JNK activity in promoting normal wing growth (Willsey et al., 2016), though how this occurs is poorly understood.

In vertebrates, individual components of the JNK pathway are represented by large gene families, which has complicated genetic analysis, but in flies the pathway is far less complex (Biteau et al., 2011). The *Drosophila* JNK signaling pathways consists of a single JNK (Basket), two JNKKs (Hemipterous and the relatively understudied dMKK4) and a number of JNKKKs. Although JNK phosphorylates several substrates, its effects are primarily mediated through the transcription factor AP-1. AP-1 is a heterodimer consisting of the bZIP proteins Jun (Jra) and Fos (Kayak/Fra), that typically functions as a transcriptional activator to modify the expression of specific target genes.

It is well-documented that over-active JNK signaling, in an otherwise “normal” context, triggers apoptosis (Igaki, 2009). However, in damaged tissues, the activation of JNK activity promotes wound healing and compensatory proliferation to replace the lost tissue (Bosch et al., 2005; Ryoo et al., 2004). Activating apoptosis in a subset of cells in the wing imaginal disc has been shown to increase the activities of Wg, Dpp, and Yki in neighboring cells via JNK signaling, to induce a proliferative response (Ryoo et al., 2004; Pérez-Garijo, et al., 2009; Sun and Irvine, 2011). In addition to its role in compensatory proliferation, JNK signaling is also important for the neoplastic overgrowth of epithelial tumors arising from disruptions in apico-basal polarity (Uhlirva et al., 2005; Igaki et al., 2006). Several studies examining the role for JNK in promoting neoplastic overgrowth have shown that JNK signaling can activate Yki (Sun and Irvine, 2011; Enomoto and Igaki, 2013; Enomoto et al., 2015). Thus, there is a clear link between the JNK and Hippo pathways, and there is evidence demonstrating that JNK can phosphorylate Jub, which could promote the association of Jub and Wts (thereby promoting the nuclear localization of Yki) (Sun and Irvine, 2013; Enomoto et al., 2015). The extent to which these interactions mediate disc growth during normal development remains an open question.

## 1.4 Summary of dissertation work

In order to better understand the mechanisms underlying tissue size control, our lab conducted a series of unbiased mosaic screens for mutations that affect tissue growth. Using versions of this screen, our lab uncovered alleles of many tumor suppressor genes, that all generally fell into one of the well-conserved growth regulatory pathways mentioned previously in this chapter. Our lab still has about two dozen unmapped mutants (“hits”) recovered in these screens, none of which obviously appears to affect known growth-regulatory factors and most of which form single-member complementation groups. As part of my dissertation work, I chose to pursue further characterization of some of these hits.

A former graduate student in our lab, Justin Bosch, had identified a few hits recovered from these screens as mutations of the *Drosophila Fbxl7* gene, which encodes an F-box protein. These mutations resulted in tissue overgrowth and the upregulation of many transcriptional targets of Yki, suggesting that Fbxl7 may affect Hippo signaling. Additional *Fbxl7* mutant phenotypes were suggestive of impaired Ft-Ds signaling—one of the upstream regulatory branches of the Hippo pathway described earlier in this chapter that helps to propagate local coordination of tissue growth via cell-cell interactions. A clear link between Ft-Ds signaling and the core Hippo pathway is the protein Dachs (D), an atypical myosin that represses Wts activity. Ft-Ds signaling modulates the distribution of D within a cell, but the mechanism by which this occurs is poorly understood. Using a combination of genetic and biochemical experiments, Justin and I found that Fbxl7 binds to Ft and co-localizes with it to a particular edge of cells, which is important for regulating the localization of Dachs. This work, described in Chapter 2, thus helps to fill in a gap in our understanding of how Ft-Ds signaling regulates tissue growth via the Hippo pathway.

Our screening also turned up a hit that formed a single-member complementation group (recovered by a former postdoc in our lab, Brett Pellock), which I ultimately identified as a mutation in the *Drosophila CtBP* gene. *CtBP* encodes a well-conserved transcriptional co-repressor that, at least in *Drosophila*, has mainly been regarded as a general transcriptional regulator. Little is known about its function in regulating growth in *Drosophila*. Coincidentally, right around the time that I began pursuing such a function, a current postdoc in our lab, Melanie Worley, had independently identified mutations of CtBP in a screen for factors involved in maintaining cell fate following tissue damage. Consistently, these mutations in *CtBP* also caused tissue overgrowth. I found that these overgrowth phenotypes are largely due to elevated *ban* microRNA levels in *CtBP* mutant tissue. In investigating how CtBP regulates *ban* expression, I found that a minimal *ban* enhancer is regulated by the JNK pathway, indicating that JNK signaling is active at basal levels in the developing wing imaginal disc and may be significant for organ growth. Chapter 3 describes these results and discusses how an antagonistic interaction between CtBP and JNK signaling may help to control overall organ size during development.

During the course of my experiments on CtBP, I made the surprising discovery that transiently knocking down *CtBP*, using a publicly-available shRNA, resulted in persistent knockdown, often complicating genetic analysis. As coincidence would have it, this hap-

pened to be around the same time that my former colleague, Justin, was observing a similar phenomenon using shRNAs targeting transgenic fluorescent proteins. Together, we explored how this phenomenon could be arising and how it could be exploited by researchers as an effective lineage-tracing technique. Chapter 4 highlights this work, along with some of my preliminary findings that this phenomenon may be used as a research tool for studying cytokinetic abscission, the process by which daughter cells are finally separated from each other following cell division.

## Chapter 2

# The F-box protein Fbx17 is a Fat effector that regulates Hippo signaling in *Drosophila*

This chapter is a partial reproduction of the following paper:

Bosch, J. A., Sumabat, T. M., Hafezi, Y., Pellock, B. J., Gandhi, K. D., and Hariharan, I. K. (2014). The *Drosophila* F-box protein Fbx17 binds to the protocadherin Fat and regulates Dachs localization and Hippo signaling. *eLife* 2014(3), e03383.

My contributions were to Figures 2.2B; 2.3A,D-E,H; 2.4D; 2.5A-B,F,H-I; 2.6D-F; and 2.8A-B,D-F and to Table 2.2. I helped with study design, performed immunohistochemistry and imaging, and edited the manuscript with JAB and IKH.

## 2.1 Abstract

The *Drosophila* protocadherin Fat (Ft) regulates growth, planar cell polarity (PCP) and proximodistal patterning. A key downstream component of Ft signaling is the atypical myosin Dachs (D). Multiple regions of the intracellular domain of Ft have been implicated in regulating growth and PCP but how Ft regulates D is not known. Mutations in *Fbxl7*, which encodes an F-box protein, result in tissue overgrowth and abnormalities in proximodistal patterning that phenocopy deleting a specific portion of the intracellular domain (ICD) of Ft that regulates both growth and PCP. Fbxl7 binds to this same portion of the Ft ICD, co-localizes with Ft to the proximal edge of cells and regulates the levels and asymmetry of D at the apical membrane. Fbxl7 can also regulate the trafficking of proteins between the apical membrane and intracellular vesicles. Thus Fbxl7 functions in a subset of pathways downstream of Ft and links Ft to D localization.

## 2.2 Introduction

An important goal for developmental biologists is to understand how organs achieve a predictable size and shape at the end of their development. The Hippo signaling pathway has emerged as a key regulator of organ size (reviewed by Pan, 2010; Halder and Johnson, 2011; Tapon and Harvey, 2012). While most components of this pathway were originally discovered using genetic screens in *Drosophila*, mammalian orthologs of those genes perform similar functions. Additionally, mutations in several components of the pathway have been described in human cancers. An exciting aspect of the Hippo pathway is that its growth-regulating activity can be modulated by cell-surface proteins that are capable of binding to ligands expressed on adjacent cells. Such interactions may be especially important for achieving precise control of growth at a local level that is necessary for generating the detailed features of an organ.

Of the proteins that regulate the Hippo pathway, much research has focused on the protocadherin Fat (Ft). In addition to regulating growth, Ft also regulates planar cell polarity (PCP), oriented cell division and proximodistal patterning of appendages (reviewed in Thomas and Strutt, 2012; Sharma and McNeill, 2013) and its regulated activity therefore impacts the size and shape of organs. The Ft protein localizes to the cell membrane just apical to the adherens junctions (Ma et al., 2003). It has a large extracellular domain composed of 34 cadherin domains as well as 4 EGF-like domains and 2 laminin G domains (Mahoney et al., 1991) that binds to another large cadherin, Dachsous (Ds) (Clark et al., 1995), on adjacent cells (Matakatsu and Blair, 2004). Ft-Ds interactions are modulated by the kinase Four-Jointed (Fj), which resides in the Golgi and phosphorylates the extracellular domains of both Ft and Ds (Ishikawa et al., 2008; Brittle et al., 2010; Simon et al., 2010). Both Ds and Fj are expressed in gradients in *Drosophila* imaginal discs where they function in patterning the disc along a major axis (e.g., equatorial to polar or proximodistal) (Yang et al., 2002; Ma et al., 2003).

While cadherins are known to have important functions in cell-cell adhesion, a key aspect of Ft function is its role as a signaling molecule (Matakatsu and Blair, 2006). Ft regulates the Hippo pathway in two ways. First, Ft influences the protein levels of Warts (Wts), a kinase that regulates the activity and subcellular location of the pro-growth transcriptional co-activator Yorkie (Yki) (Cho et al., 2006; Rauskolb et al., 2011). Additionally, mutations in *ft* disrupt the localization of Expanded (Ex), a FERM-domain protein that functions upstream of Hippo (Hpo) (Bennett and Harvey, 2006; Silva et al., 2006; Willecke et al., 2006), though other studies suggest Ft and Ex act in parallel (Feng and Irvine, 2007).

A key downstream target of Ft is the atypical myosin Dachs (D). The strong overgrowth elicited by *ft* mutations can be completely suppressed by loss of D function (Cho et al., 2006). Additionally, PCP defects in *ft* mutants are partially rescued by loss of D (Mao et al., 2006). D localizes to the apical membrane where, in cells of the wing disc, it localizes preferentially to the distal edge of the cell (Mao et al., 2006; Mao et al., 2011; Ambegaonkar et al., 2012; Bosveld et al., 2012; Brittle et al., 2012). In *ft* mutants, increased levels of D are observed apically and D is redistributed around the entire perimeter of the cell (Mao et al., 2006; Brittle et al., 2012). However, the overall levels of D protein are not obviously changed (Mao et al., 2006). It has been proposed that Ft restricts growth by negatively regulating the levels of D at the apical membrane and that it regulates the D-dependent PCP functions by maintaining D asymmetry (Rogulja et al., 2008).

An important gap in our current understanding of Ft function is how Ft regulates the levels and localization of D at the apical membrane. Ft does not bind to D itself, indicating that there must be one or more proteins that bind to Ft and mediate its regulation of D localization at the membrane. In an attempt to identify signaling pathways downstream of Ft, several recent studies have made systematic deletions in the intracellular domain (ICD) of Ft (Matakatsu and Blair, 2012; Bossuyt et al., 2013; Pan et al., 2013; Zhao et al., 2013). These deletion studies implicate multiple non-overlapping regions in the ICD that differentially affect growth, PCP and organ shape, suggesting that Ft signals via multiple effector pathways. Additionally, several proteins have been shown to bind to the Ft ICD including the transcriptional repressor Atrophin/Grunge which regulates PCP (Fanto et al., 2003), the novel protein Lowfat that regulates Ft protein levels (Mao et al., 2009), and the casein kinase I protein Discs overgrown (Dco) that phosphorylates the Ft ICD (Feng and Irvine, 2009; Sopko et al., 2009). Also, the palmitoyltransferase approximated (App) is needed for D localization to the membrane (Matakatsu and Blair, 2008). However, for each of these proteins, their role in mediating the regulation of D levels or asymmetry by Ft is not well understood.

Here we describe the *Drosophila* ortholog of the *Fbxl7* gene, which encodes an F-box protein and is a novel component of the Ft signaling pathway. Inactivation of *Fbxl7* results in increased tissue growth via the Hippo pathway and abnormalities in wing shape and proximodistal patterning of appendages. *Fbxl7* localizes preferentially to the proximal edge of cells in the wing pouch where it binds to and co-localizes with Ft. We find a role for *Fbxl7* in one of the growth-suppressing signaling pathways downstream of Ft and also demonstrate a role for *Fbxl7* in regulating the amount of D at the apical membrane as well as its distribution

around the edge of the cell.

## 2.3 Materials and Methods

### *Drosophila* stocks and husbandry

Crosses were maintained on standard fly food at 25°C unless otherwise noted.

*Fbxl7*<sup>C616Y</sup> and *Fbxl7*<sup>Q201X</sup> alleles were isolated in two EMS screens, while *Fbxl7*<sup>W389X</sup> was found fortuitously in a separate fly stock. All *Fbxl7* alleles are on chromosomes bearing a *FRT82B* insertion. *Fbxl7* overexpression stocks used were *UAS-FLAG-Fbxl7* (this study, attP40 and attP2), *UAS-FLAG-Fbxl7*<sup>C616Y</sup> (this study, attP40), and *P{XP}CG4221*<sup>d08178</sup> (BL19289). *Fbxl7* RNAi stocks used were *UAS-Fbxl7*<sup>RNAi</sup> (JF01515 [BL31065], VDRC108628). All RNAi experiments performed in flies used *UAS-Dcr2*, which increases knockdown. The *fat*<sup>61</sup> allele was isolated in an EMS screen for supercompetitor mutations (T4854I amino acid change).

Additional stocks used were: *FRT82B dco*<sup>le88</sup> (Jursnich et al., 1990), *P[acman]-Fat+*; *P[acman]-FatΔD*, *P[acman]-FatΔF* (Pan et al., 2013), *Diap1 3.5-GFP* (Zhang et al., 2008), *FRT40A ft*<sup>Grv</sup>, *textitFRT40A ds*<sup>38k</sup>, *UAS-Fat* (Simon, 2004), *FRT40A*, *FRT82B* (Xu and Rubin, 1993), *UAS-GFP-cindr-PC* (Johnson et al., 2008), *Dachs-GFP* (Bosveld et al., 2012).

Remaining stocks used were from, or derived from, the Bloomington Stock Center (Bloomington, IN): *UAS-dcr2*; *nub-Gal4* (BL25754), *eyFLP*; *FRT82B ubi-GFP* (BL5580, BL5188), *FRT82B ubi-RFPnls* (BL30555), *hsFLP*; *Act>CD2>Gal4 UAS-GFP* (BL26902, BL4780), *FRT82B MARCM* (BL30036), *FRT40A MARCM* (BL5192), *FRT82B dco*<sup>3</sup> (BL44250), *FRT40A d*<sup>GC13</sup> (BL28289), *UAS-d.v5* (BL28291), *Df(3R)BSC515* (BL25019), *Df(3R)BSC728* (BL26580), *GFP-Cindr*<sup>CA06686</sup> (BL50802), *tub-Gal4* (BL5138), and *FRT40A ft*<sup>8</sup> (BL44257).

### Tissue immunohistochemistry

*hsFLP*-induced clones were generated by incubating larvae at 37°C at 48 hr after egg deposition (AED). A 30-min incubation was used for experiments using *Act>CD2>Gal4* and 2-hr incubation for experiments using *MARCM*. Immunostainings were performed by dissecting imaginal discs from wandering third instar larvae, fixing discs in 4% paraformaldehyde + PBS, followed by blocking in PBS + 0.1% Triton-X + 5% normal goat serum (NGS), incubation with primary antibodies overnight at 4°C and incubation with secondary antibodies overnight at 4°C. Immunostainings with anti-Fbxl7 antibodies required a separate optimized protocol: Larvae were dissected in 0.1 M NaPO<sub>4</sub>, fixed in PLP-fixative (2% paraformaldehyde, 0.01 M NaIO<sub>4</sub>, 0.075 M lysine, 0.037 M NaPO<sub>4</sub>), washed with 0.1 M NaPO<sub>4</sub> containing 0.1% saponin, blocked with 0.1 M NaPO<sub>4</sub> containing 0.1% saponin and 5% NGS, primary and secondary antibodies were diluted in 0.1 M NaPO<sub>4</sub> containing 0.1% saponin and 5% NGS. Samples were imaged on a Zeiss 700 confocal microscope (Germany).

The anti-Fbx17 antibody was generated by immunizing guinea pigs (Pocono Farms, Canadensis, PA) with purified Fbx17 (amino acids 22-324) produced at the UC-Berkeley MacroLab (His-Fbx17 purified on a Nickel column), and used at 1:1000 for tissue staining.

Other antibodies used: rat anti-Dachs (1:500, Brittle et al., 2012), rat anti-Fat (1:1600, Feng and Irvine, 2009), rat anti-Dachsous (1:5000, Yang et al., 2002) rat anti-Ecad (1:100, DCAD2, DHSB, Iowa City, IA), mouse anti-FLAG (1:1000, F3165; Sigma, St. Louis, MO), rabbit anti-FLAG (1:1000, F7425; Sigma) mouse anti-V5 (1:500, R960-25; Invitrogen, Carlsbad, CA), mouse anti-Arm (1:100, N2 7A1; DHSB), rabbit anti-LacZ (1:500, #559762; MP Biomedicals, Santa Ana, CA), anti-Cleaved Caspase-3 (1:200, 9661; Cell Signaling, Beverly, MA). Actin was visualized with Phalloidin-TRITC (1:500, Sigma) or Alexa Fluor 633 Phalloidin (1:500, Invitrogen). Nuclei were visualized with DAPI (1:1000).

## Plasmids and molecular biology

Plasmids were constructed using conventional ligation-based molecular cloning techniques. Oligonucleotide sequences are listed in Table 2.1. Fbx17 was amplified from clone LD38495 (DGRC, Bloomington, IN) by designing oligonucleotides to amplify the single predicted coding sequence CG4221-RA and add Not1 and Xba1 restriction sites. The Not1-Fbx17-Xba1 PCR fragment was digested and ligated into pUAS-FLAG attB (adds an N-terminal FLAG tag) to generate pUAS-FLAG-Fbx17 attB. The C616Y amino acid change was introduced by site directed mutagenesis, generating pUAS-FLAG-Fbx17<sup>C616Y</sup> attB. Transgenic flies were made from pUAS-FLAG-Fbx17 attB and pUAS-FLAG-Fbx17<sup>C616Y</sup> attB using PhiC31 integration (BestGene, Chino Hills, CA), inserting into attP40 and attP2 landing sites.

Fbx17 truncation plasmids were generated by amplifying Fbx17 $\Delta$ 1 (389-772aa), Fbx17 $\Delta$ 2 (445-772aa), and Fbx17 $\Delta$ 3 (1-388aa) and ligating into pUAS-FLAG attB using Not1/Xba1. pUAS-FLAG-EGFP attB was generated by amplifying EGFP from pEGFPattB (K Basler) and cloning into pUAS-FLAG attB using In-Fusion (Clonetech, Mountain View, CA).

SkpA and Cull1 coding sequence were amplified from genomic DNA and clone LD20253 (DGRC), respectively. Not1/Xba1 sites were added to oligos that amplified SkpA, and Kpn1/Not1 was added for Cull1. PCR fragments were digested and ligated into pMT-HA (adds a C-terminal HA tag), generating pMT-SkpA-HA and pMT-Cul1-HA. dCul1<sup>DN</sup> is a C-terminal truncation (1-451aa) which corresponds to 1-452aa of dominant negative human hCul1DN (Wu et al., 2000) and was cloned into pMT-HA as for full length dCul1.

pMT-FatICD-V5 was generated by amplifying FatICD coding sequence from pUAS-FatICD-V5 (K. Irvine), adding Not1/Xba1 sites with oligos. PCR fragments were digested and ligated into pMT-V5/6xHis (Invitrogen). pMT-FatICD $\Delta$ D-V5, pMT-FatICD $\Delta$ F-V5, and pMT-FatICDmutV-V5 were generated by using the same oligos to amplify from pUAS-FatICD $\Delta$ D-V5, pUAS-FatICD $\Delta$ F-V5, and pUAS-FatICDmutV-V5 (Irvine), respectively. pMT-FatICD61-V5 was generated by site directed mutagenesis of pMT-FatICD-V5 to make the change T4854I.

pUAS-HA-Ub attB was generated by amplifying Ubi-p5E coding sequence from genomic DNA, adding an N-terminal HA tag with primers, and inserting into pUAS attB (K Basler).

pMT-cindr-V5 was generated by amplifying the longest predicted isoform cindr-RC from S2R+ cell cDNA, adding Not1/Xba1 sites, and ligating into pMT-V5/6xHis (Invitrogen).

Other plasmids used are pMT-Dco-V5 (Ko et al., 2002), pUAS-Dachs-V5 (Mao et al., 2006).

## **Western analysis of wing discs and S2R+ cells, co-immunoprecipitation, and *in vivo* ubiquitylation assays**

S2R+ cells were cultured and transfected using conventional techniques. S2R+ cells were cultured in Schneiders medium containing 10% FBS at 27°C, transfected with Effectene (Qiagen, Germany) in six-well dishes, and harvested 72 hr later. 500  $\mu$ M CuSO<sub>4</sub> was added 24 hr before harvesting to induce expression from plasmids with metallothionein promoters. For Co-IP and *in vivo* ubiquitylation assays, 50  $\mu$ M MG132 (C2211; Sigma) was added to transfected cells four hours before harvesting to inhibit proteasome activity. For experiments using dsRNA, S2R+ cells were transfected with dsRNA  $\pm$  plasmids and were harvested as needed for protocols described above.

Unless otherwise stated, wing discs or S2R+ cells were boiled in 1x or 2x SDS Sample buffer, run on 7.5% Mini-Protean TGX gels (Bio-Rad, Hercules, CA), and transferred to nitrocellulose membrane. Protein bands were detected with primary antibodies and secondary antibodies conjugated to HRP, and imaged using ECL detection reagent (RPN2232; Amersham, UK).

For co-IP assays, 50  $\mu$ M MG132 (C2211; Sigma) was added to transfected cells 4 hr before harvesting to inhibit proteasome activity. Cells were washed once with ice cold PBS, and lysed in lysis buffer (20 mM HEPES 7.5 pH, 5 mM KCl, 1 mM MgCl<sub>2</sub>, 0.1% NP-40, 'Complete' EDTA free protease inhibitor tablet [Roche, Switzerland]). Insoluble material and nuclei were removed by centrifugation at 13,000g for 30 min at 4°C, and soluble cell lysate was incubated with anti-FLAG M2 affinity gel (A2220; Sigma) overnight at 4°C. Beads were washed twice in lysis buffer and denatured by boiling in SDS sample buffer for 10 min. For SkpA, Cul1, and Cindr co-IP assays, to avoid detection of non-specific binding of transfected proteins to beads, FLAG-protein complexes were eluted off beads by incubating with 400 ng/ $\mu$ l 3x FLAG peptide (F4799; Sigma) for 30 min at 4°C.

For *in vivo* ubiquitylation assays, 50  $\mu$ M MG132 was added to transfected cells 4 hr before harvesting. Cells were washed once with ice cold PBS, and proteins denatured by boiling in 100  $\mu$ l 1% SDS in PBS for 10 min 400  $\mu$ l of 0.5% BSA, 1% Triton-X, in PBS was added, and samples were sonicated, then centrifuged at 13,000g for 10 min. Supernatant was diluted to 1 ml with 5% BSA, 1% Triton-X and incubated with anti-HA agarose beads (A2095; Sigma) overnight at 4°C. Beads were washed twice with 1% Triton-X in PBS and boiled in SDS sample buffer for 10 min. For *in vivo* ubiquitylation of Dachs-V5 from larval tissue, 12 hr before dissection larvae were heat-shocked at 37°C for 1 hr to induce UAS transgenes by hs-Gal4. 30 brain-eye-antennal complexes per genotype were dissected in Schneiders medium and incubated with 50  $\mu$ M MG132 for 4 hr. Complexes were boiled, diluted, sonicated,

and centrifuged as above. Supernatant was diluted to 1 ml with 5% BSA, 1% Triton-X and incubated with Protein G Sepharose (P3296; Sigma) for 1 hr at 4°C, replaced with Protein G Sepharose plus 1  $\mu$ l mouse anti-V5 antibody (R960-25; Invitrogen) and incubated overnight at 4°C. Beads were washed twice with 1% Triton-X in PBS and boiled in SDS sample buffer for 10 min.

For experiments using dsRNA, S2R+ cells were transfected with dsRNA  $\pm$  plasmids and were harvested as needed for protocols described above. dsRNA was generated by PCR amplifying DRSC15513 and DRSC38270 from genomic DNA, and GFP coding sequence from pattB-EGFP (K Basler), adding T7 sequence to forward and reverse primers, and in vitro transcribing dsRNA (AM1333; Megascript T7 Transcription Kit, Invitrogen).

For anti-Fat western blots from wing discs, 20 wing discs were dissected from third instar larvae in PBS and immediately boiled in 2x SDS Sample buffer. The amount loaded on gels was adjusted to load equivalent amounts of protein.

For anti-Dachs westerns from wing discs, 20 wing discs were dissected from third instar larvae in PBS and lysed in 1x RIPA buffer. Total protein was quantified (Micro BCA kit, 23235; Fisher, Hampton, NH) and adjusted equally among samples. Secondary antibodies conjugated to LiCor fluorescent dyes were used to detect protein bands using a LiCor Odessey imager (Lincoln, NE).

Western blots were probed with the following antibodies: Guinea pig anti-Fbx17 (1:1000), rat anti-Fat (1:25,000, K Irvine), rat anti-Dachs (1:5,000, D Strutt), mouse anti-Tubulin (1:100, E7; DHSB), mouse anti-FLAG (1:10,000, F3165; Sigma), mouse anti-V5 (1:5,000; R960-25, Invitrogen), rabbit anti-V5 (1:5000, V8137; Sigma) rabbit anti-HA (1:1,000, 3724; Cell Signaling), rabbit anti-Ub (1:1,000, Z0458; DakoCytomation, Carpinteria, CA), mouse anti-Lamin (1:100, ADL67.10; DHSB), goat anti-rat-HRP (112-035-003; Jackson, West Grove, PA), goat anti-rabbit-HRP (111-035-003; Jackson), goat anti-mouse-HRP (172-1011; Bio-Rad), goat anti-guinea pig-HRP (106-035-003; Jackson), goat anti-rat-IR680 (926-68,076; Licor), goat anti-mouse-IR800 (827-08,364; Licor).

## Quantification of dimensions of adult structures

Wings or legs were mounted onto slides using Canadian Balsam medium (Gary's Magic Mount) and imaged on a Leica transmitted light microscope (TL RCI, Germany). Wing area and cross vein distance was quantified in ImageJ. For cross veins, we measured the distance of a straight line drawn from intersection of the anterior cross vein and L4 to the intersection of the posterior cross vein and L4. Statistical significance between groups was determined by one-way ANOVA using (Tukey's or Dunnett's test).

## Quantification of Dachs asymmetry in wing discs

Quantifications were performed as in Brittle et al. (2012) using ImageJ. Wing discs were immunostained for Dachs and F-actin and imaged under identical settings at 20 $\times$  to determine P-D orientation, and at 63 $\times$  to image the dorsal portion of the wing pouch where Dachs

asymmetry is highest. Images were rotated so that the P-D axis of the wing pouch oriented vertically (90° and 270°). A cropped  $24.8 \times 24.8 \mu\text{m}$  ( $500 \times 500\text{px}$ ) square was used to quantify the mean fluorescence intensity of Dachs or actin along each cell edge while recording the angle of the cell edge relative to the P-D orientation. Cell edge data were measured using a 1 pixel width line. Mean fluorescence of cell edges oriented in the P-D orientation (45°–135°) or the A-P orientation (0°–45°; 135°–180°) was isolated into two different lists, which were each averaged. The ratio of mean fluorescence of the A-P orientation to P-D orientation gives the P-D/A-P localization. For example, asymmetric localization to the P-D sides of cells will give higher mean intensities on cell edges in the A-P orientation. Quantifications were performed on eight cropped boxes from different discs for each group. Statistical significance between groups was determined by one-way ANOVA using (Tukey’s test).

## 2.4 Results

### **Fbxl7 functions as a negative regulator of tissue growth and modulates signaling via the Hippo pathway**

In two different genetic screens, one for mutations that caused cells to outgrow their neighbors (described in Tapon et al., 2001) and another for mutations that enabled cells to promote the elimination of their slower-growing neighbors by cell competition (Hafezi et al., 2012), we identified mutant alleles of the *Drosophila Fbxl7* gene (*CG4221*), which encodes a protein with an F-box and 11 leucine-rich repeats (LRRs) (Figure 2.1A). Fbxl7 has a conserved human ortholog (FBXL7) that shares 49% amino acid identity over the region spanning the F-box and the LRRs. Most proteins with these motifs function as part of an SCF-type ubiquitin ligase, a protein complex which polyubiquitylates substrate proteins and targets them for degradation by the proteasome (Skaar et al., 2013). A third allele was identified fortuitously in an unrelated stock. Mutant clones of all three alleles were overrepresented in the adult eye when compared to clones of the parental *FRT82B* chromosome (Figure 2.1B), suggesting that these *Fbxl7* mutations cause increased tissue growth (Figure 2.1C-E). Two of the mutations generate premature stop codons upstream of all conserved domains, while the third causes a cysteine-to-tyrosine change in a conserved residue in one of the LRRs (Figure 2.1A) that likely interferes with the normal function of the protein, indicating that all three alleles reduce or eliminate *Fbxl7* function.

Although clones of mutant cells display a clear growth advantage, flies homozygous for each of these *Fbxl7* mutations are viable and fertile. However, the wings of *Fbxl7* homozygotes or hemizygotes (*Fbxl7*/Deficiency) are larger and more rounded than wild-type wings (Figure 2.1F-H,L) and the distance between the cross veins is reduced (Figure 2.1F-G). The same alterations in wing area and spacing between the cross veins were also observed when *Fbxl7* function was reduced by RNAi (Figure 2.1L) (Dui et al., 2012). The combination of overgrowth and reduced spacing of the cross veins is especially reminiscent of mutations in the Ft branch of the Hippo signaling pathway (Bryant et al., 1988; Mahoney et al., 1991;

Clark et al., 1995; Villano and Katz, 1995; Mao et al., 2006; Matakatsu and Blair, 2008; Mao et al., 2009).

Since we identified one of the *Fbxl7* alleles in a screen for mutations that made cells capable of eliminating their neighbors (Hafezi et al., 2012), we examined imaginal discs for evidence of cell death. We observed elevated levels of activated caspase-3, a marker of apoptosis, especially in wild-type cells adjacent to *Fbxl7* mutant clones (Figure 2.1M-M’). Thus *Fbxl7* mutant cells do indeed behave as supercompetitors similar to loss-of-function mutations in *ft* or in core components of the Hippo pathway such as *hpo* or *wts* (Tyler et al., 2007).

When we overexpressed *Fbxl7* in the wing imaginal disc, the adult wings were smaller and had a reduced distance between the cross veins (Figure 2.1I-L). This reduction in wing size was suppressed by heterozygosity of the *wts*<sup>X1</sup> allele (Figure 2.1P-R).

The Hippo pathway regulates the activity of the transcriptional co-activator Yki. In *Fbxl7* mutant clones in the eye imaginal disc, expression of a *diap1-GFP* reporter gene (Zhang et al., 2008) was increased, especially posterior to the morphogenetic furrow (Figure 2.1N-N’) consistent with increased Yki activity. Conversely, overexpression of *Fbxl7* reduced expression of an *ex-lacZ* reporter (Boedigheimer and Laughon, 1993; Hamaratoglu et al., 2006) (Figure 2.1O-O’). Taken together, these results indicate that *Fbxl7* functions as a negative regulator of growth via the Hippo pathway. Moreover, the multiple phenotypic similarities between alterations in *Ft* levels and *Fbxl7* levels suggest that *Fbxl7* functions in proximity to *Ft*.

## **Fbxl7 localizes to the apical membrane and is distributed asymmetrically**

A polyclonal antibody to an N-terminal portion of *Fbxl7* detects uniform *Fbxl7* expression throughout the wing imaginal disc (Figure 2.2A), with a slight enrichment at the dorsal-ventral boundary in the pouch as is also observed for *Ft* protein (Mao et al., 2009). At the cellular level, punctate staining is observed outlining the apical profiles of cells, which is absent in homozygous mutant clones of the *Fbxl7*<sup>Q201X</sup> allele (Figure 2.2B-B’) indicating that the truncated protein generated by this allele is likely unstable. In *Fbxl7*<sup>C616Y</sup> clones, apical puncta are absent but cytoplasmic staining is observed above background levels, indicating that the mutant protein is present but does not localize apically (not shown). An *Fbxl7* protein with an N-terminal FLAG epitope tag (FLAG-*Fbxl7*) exhibits an apical localization that is very similar to that of the endogenous protein (Figure 2.2C-F). Using either the anti-*Fbxl7* antibody (Figure 2.2C,E) or FLAG-*Fbxl7* (Figure 2.2D,F), we found that *Fbxl7* localizes to the subapical region of cells, apical to the adherens junctions marked by E-cadherin. FLAG-*Fbxl7* is also found in intracellular puncta (Figure 2.2G). In contrast, FLAG-*Fbxl7* protein bearing the C616Y missense mutation displays only diffuse cytoplasmic localization (Figure 2.2H) suggesting that the normal function of *Fbxl7* may be contingent upon its localization to the apical region or cytoplasmic puncta. In the flattened cells of the

peripodial epithelium (Figure 2.2I), confocal sections show puncta with diameters typically in the range of 400-500 nm (some as large as 1000 nm) with a hollow interior, consistent with the possibility that these might be vesicles.

In cells of the wing imaginal disc, Ft is preferentially expressed on the proximal side of cells and Ds and D on the distal surface (Ambegaonkar et al., 2012; Brittle et al., 2012). We generated small clones that expressed FLAG-Fbx17, which enabled us to examine the borders between FLAG-Fbx17-expressing cells and wild-type cells. In the dorsal part of the wing pouch, where polarization of D is most evident (Brittle et al., 2012), FLAG-Fbx17 localizes preferentially to the proximal side of cells (Figure 2.2J,K-K’’).

### **Fbx17 associates with Ft and regulates its localization**

Since the localization of Fbx17 is similar to that described for Ft, we examined whether the two proteins co-localize. Both anti-Fbx17 and anti-Ft revealed apical staining in a punctate manner with a considerable degree of overlap (Figure 2.3A-A’’). Additionally, we observed co-localization of FLAG-Fbx17 and Ft at the apical membrane (Figure 2.3B-B’’) as well as in cytoplasmic puncta (Figure 2.3B’’-B’’’, Figure 2.4A), many of which were basally located. Higher gain settings were required to visualize the comparatively faint Ft staining in puncta (Figure 2.3B’’’’). Because of a higher background level of cytoplasmic staining with anti-Fbx17, the FLAG-tagged Fbx17 protein was necessary to observe co-localization in puncta.

To determine whether Ft and Fbx17 can interact physically, we co-transfected S2 cells with tagged versions of Fbx17 and a portion of Ft that includes the transmembrane domain and the entire intracellular domain (FatICD). FatICD co-immunoprecipitates with FLAG-Fbx17, whereas association of FatICD with FLAG-Fbx17<sup>C616Y</sup> is greatly reduced (Figure 2.3C). We also examined the ability of truncated Fbx17 proteins to interact with Ft and find that Fbx17 interacts with Ft mostly via its LRRs (Figure 2.4B-C). A weaker interaction is also observed between Ft and the N-terminal portion of Fbx17. Thus wild-type Fbx17 can associate, either directly or indirectly, with the intracellular domain of Ft and this interaction mostly occurs via the LRRs of Fbx17.

The apical localization of Fbx17 was absent in *ft* clones (Figure 2.3D-D’’). However, an increase in diffuse cytoplasmic staining was observed (Figure 2.3E-E’’). Thus the localization of Fbx17 to the apical region is dependent upon Ft and in the absence of Ft, Fbx17 re-localizes to the cytoplasm. Since Ft and Fbx17 also co-localize to cytoplasmic puncta or vesicles, we examined whether this localization of Fbx17 also depends on Ft. Surprisingly, unlike the apical localization, punctate localization of FLAG-Fbx17 was still observed in *ft* clones indicating that the localization of Fbx17 in these cytoplasmic puncta is independent of Ft (Figure 2.3F-F’’).

Since proteins similar to Fbx17 often bind to their substrates via their LRRs and promote their polyubiquitylation and degradation (Skaar et al., 2013), we tested the effect of changes in Fbx17 on the levels and localization of Ft. Increasing Fbx17 levels resulted in clearly increased levels of apical Ft (Figure 2.3G-G’) and slightly increased cytoplasmic staining of Ft (Figure 2.4A). Surprisingly, a slight elevation of apical Ft levels was also observed in

*Fbxl7* mutant clones (Figure 2.3H-H’). The overall levels of Ft protein in imaginal discs, as assessed by Western blotting, were not obviously changed in either case (Figure 2.4D). These results are inconsistent with *Fbxl7* promoting Ft degradation and instead suggest that *Fbxl7* regulates Ft localization. In support of this, we do not observe an obvious increase in Ft ubiquitylation from expressing *Fbxl7* in S2 cells (not shown).

## The apical localization of *Fbxl7* does not require *Ds* or *Dco*

Since the phenotypic abnormalities of *Fbxl7* mutants resemble those of hypomorphic alleles of *ft*, and the recruitment of *Fbxl7* to the apical region of the cell is dependent upon Ft, we explored the relationship between *Fbxl7* and proteins known to regulate Ft in more detail. In *ds* mutant clones, the apical localization of *Fbxl7* is no longer observed as discrete puncta at cell edges but is rather more diffuse (Fig. 2.5A-A’). Moreover, in contrast to *ft* clones, we do not see an increase in cytoplasmic *Fbxl7* in *ds* clones at more basal focal planes, indicating that *Fbxl7* is still predominantly at an apical location (Figure 2.5B-B’). These changes in *Fbxl7* localization could simply be a consequence of the more diffuse localization of Ft that is observed in *ds* clones (Strutt and Strutt, 2002; Ma et al., 2003; Mao et al., 2009).

When *Fbxl7* is overexpressed in clones, cells have more prominent apical expression of *Ds* in puncta (Figure 2.5C-C’). Additionally, in wild-type cells bordering the *Fbxl7*-overexpressing clone, *Ds* staining is reduced and accumulates in prominent puncta at the surface that abuts the *Fbxl7*-overexpressing cells (Figure 2.5D-E’). Given that *Ds* can be drawn toward cells with greater levels of Ft (Ma et al., 2003), *Ds* may be drawn toward *Fbxl7*-overexpressing cells due to the increased Ft levels. Furthermore, the puncta of *Ds* in adjacent wild-type cells are in register with *Fbxl7* puncta, consistent with the coupling of *Ds* in wild-type cells to *Fbxl7*-bound Ft within the clone. In *Fbxl7* mutant clones, there is, at best, a very slight elevation of *Ds* levels (Figure 2.5F-F’). Thus, the effects of *Fbxl7* on *Ds* levels are minor compared to the effects on Ft levels. Additionally, we could not detect *Ds* in immunoprecipitates of *Fbxl7* when the two proteins were co-expressed in S2 cells (not shown). Together, these findings suggest that *Fbxl7* binds to and functions with Ft rather than *Ds*. Despite this, we did observe co-localization of *Fbxl7* and *Ds* at apical membranes and in more basally located cytoplasmic puncta (Figure 2.5G-G’). In the absence of evidence for direct interactions between *Fbxl7* and *Ds*, their co-localization, at least at the cell surface, may result from *Fbxl7* bound to Ft that is in turn bound to *Ds*.

*Ds* binding to Ft induces the phosphorylation of the ICD of Ft, which requires the protein kinase, *Dco* (Feng and Irvine, 2009; Sopko et al., 2009). Since some F-box proteins bind to phosphorylated proteins (Skaar et al., 2013), we tested whether the apical localization of *Fbxl7* was dependent upon *Dco* function. The apical localization of *Fbxl7* was not obviously changed in clones of the *dco*<sup>3</sup> allele that is unable to phosphorylate Ft (Figure 2.5H-H’) (Sopko et al., 2009). While *Dco* is capable of binding to *Fbxl7* as assessed by co-immunoprecipitation from S2 cells (Figure 2.5J), the apical localization of *Fbxl7* was still observed in clones of the null *dco* allele, *dco*<sup>le88</sup> (Figure 2.5I-I’), thus indicating that *Dco* function is altogether unnecessary for the apical localization of *Fbxl7*.

## Fbxl7 functions in one of two growth-suppressing pathways downstream of Ft

The primary amino acid sequence of the ICD of Ft does not predict any domains with enzymatic activity or known protein-protein interaction motifs. Hence, it has not been easy to understand how it functions in signal transmission. However, six blocks of sequence (labeled A-F in Figure 2.6A based on the nomenclature of Pan et al. (2013)) are conserved with the ICD of mammalian Fat4. A region between the conserved blocks B and C seems necessary for the major growth-suppressive function of Ft (Matakatsu and Blair, 2012; Bossuyt et al., 2013; Zhao et al., 2013). In our screen, we identified an allele of *ft*, *ft*<sup>61</sup> (Figure 2.6A), which displays strong overgrowth (Figure 2.6C,K) and is caused by a single amino acid change (T to I) within this region. *ft*<sup>61</sup> displays phenotypic abnormalities that are very similar to those described for *ft*<sup>sum</sup>, which also changes a single amino acid two residues N-terminal to *ft*<sup>61</sup> (Bossuyt et al., 2013). Additionally, in a *ft* null background, deletion of one of the conserved blocks (block D in Figure 2.6A) in a *ft* genomic rescue transgene was shown to cause overgrowth (Pan et al., 2013) albeit to a much lesser extent than for *ft*<sup>61</sup> and *ft*<sup>sum</sup>; flies had slightly overgrown, rounder wings with decreased spacing between the crossveins (Figure 2.6E).

In contrast to null alleles of *ft*, which display strong overgrowth and cause lethality well before the adult stage, flies lacking *Fbxl7* function are viable and fertile but have slightly overgrown wings that are rounded and have decreased spacing between the cross veins. Thus, their phenotypic abnormalities are very similar to those observed when the *ft* D region is deleted (*ft*Δ*D*). We therefore examined the localization of Fbxl7 in a *ft*Δ*D* background. When a heteroallelic combination of null *ft* alleles, *ft*<sup>Grv</sup>/*ft*<sup>8</sup>, is rescued by a wild-type version of *ft* (*ft*<sup>+</sup>), wings are normal (Figure 2.6D) and Fbxl7 displays normal apical localization (Figure 2.6D'-D''). However, apical localization of Fbxl7 is markedly reduced in *ft*<sup>Grv</sup>/*ft*<sup>8</sup>; *ft*Δ*D* (Figure 2.6E'-E''). We also examined a different deletion, *ft*Δ*F*, in which wings from these flies are not enlarged but have greatly reduced spacing between the cross veins (Figure 2.6F). In *ft*<sup>Grv</sup>/*ft*<sup>8</sup>; *ft*Δ*F* imaginal discs, the apical localization of Fbxl7 is not disrupted (Figure 2.6F'-F''). Similarly in *ft*<sup>61</sup> clones, which display strong overgrowth, Fbxl7 localization was normal (Figure 2.6G-G''). Thus, the apical localization of Fbxl7 requires the Ft D domain but neither the F domain nor the motif that is disrupted by the *ft*<sup>61</sup> allele.

To examine whether the effects on Fbxl7 localization in vivo correlated with the ability of Fbxl7 to physically interact with Ft, we tested the ability of these mutant Ft proteins to co-immunoprecipitate with FLAG-Fbxl7 (Figure 2.6H). Indeed, Ft<sup>61</sup> and FtΔ*F* proteins co-immunoprecipitated at levels comparable to wild-type Ft. However, the level of FtΔ*D* in FLAG-Fbxl7 immunoprecipitates was greatly reduced, as was that of Ft<sup>mutV</sup>, a mutant Ft protein in which a cluster of 10 serine/threonine residues overlapping the D domain was mutated to alanines. These sites were identified as candidates for phosphorylation by Dco (Pan et al., 2013). However, since Fbxl7 localizes normally in *dco* mutant clones, the inability of Fbxl7 to bind to Ft<sup>mutV</sup> might be caused by a change in its conformation that does not depend on phosphorylation by Dco. Indeed *ft*<sup>Grv</sup>/*ft*<sup>8</sup>; *ft*<sup>mutV</sup> flies also have phenotypic

abnormalities that are very similar to those of Fbxl7 mutants (Pan et al., 2013).

To test for a functional relationship between the D domain of Ft and Fbxl7, we monitored apical levels of Ft, Ft $\Delta$ D, and Ft $\Delta$ F under conditions of Fbxl7 overexpression. Ft and Ft $\Delta$ F levels are increased in cells overexpressing Fbxl7, while Ft $\Delta$ D levels do not increase (Figure 2.7). This demonstrates that the D domain is required for Fbxl7 to physically interact with and exert its effects on Ft localization.

If Ft<sup>61</sup> protein is still capable of recruiting Fbxl7 to its apical location, then overexpression of Fbxl7 might suppress the overgrowth observed in mutant discs. While ubiquitous Fbxl7 expression was unable to suppress *ft<sup>Grv</sup>/ft<sup>8</sup>* phenotypes (Figure 2.6L), the overgrowth and lethality of *ft<sup>61</sup>/ft<sup>8</sup>* discs was indeed suppressed, resulting in viable adult flies (Figure 2.6M,O). *dco<sup>3</sup>* mutant cells in the eye imaginal disc are overgrown and express higher Diap1 levels, an indicator of Yki activity (Figure 2.6P-P'). Fbxl7 overexpression can rescue both clone size and Diap1 levels in *dco<sup>3</sup>* mutant cells (Figure 2.6Q-Q'). Thus, mutant Ft<sup>61</sup> protein, or Ft protein that cannot be phosphorylated by Dco, can still bind to Fbxl7 and facilitate the growth-suppressive functions of Fbxl7. Taken together, these findings implicate Fbxl7 in one of two growth-suppressive pathways downstream of Ft and suggest that these two pathways might converge further downstream.

## Fbxl7 regulates the localization of the atypical myosin Dachs

Since Ft and Fbxl7 localized preferentially to the proximal side of cells, we compared the localization of Fbxl7 with that of D. In confocal z-sections, D and Fbxl7 co-localize at the subapical membrane in puncta, apical to the adherens junction marker Armadillo (Arm) (Figure 2.8A-A''). However, careful examination of these puncta in x-y sections shows that the Fbxl7 and D puncta are slightly offset in the proximodistal direction (Figure 2.8B-B'). D is localized at higher levels at the distal edge of the cell (Mao et al., 2006; Brittle et al., 2012) where it is likely stabilized by physical interaction with the cadherin Ds (Bosveld et al., 2012). Therefore, a likely explanation is that the formation of multimeric Ft-Ds complexes between cells results in the concomitant accumulation of Fbxl7 at the FatICD and D at the DsICD (Figure 2.8C).

To investigate whether Fbxl7 can regulate the levels or localization of D, we first examined *Fbxl7* mutant clones. The levels of apical D are increased throughout the clone (Figure 2.8D-D'') although not to the extent that occurs in *ft* clones. Thus Fbxl7 negatively regulates the level of D at the apical membrane. To determine whether Fbxl7 has a role in generating or maintaining the asymmetrical distribution of D, we examined the distribution of D in *Fbxl7* mutant wing discs. In these experiments, the distal edge of one cell cannot be distinguished from the proximal edge of its neighbor. However, in wild-type cells, endogenous D is preferentially observed on the proximal/distal edges and is found at lower levels at the other edges (Brittle et al., 2012; Figure 2.8E,G). In *Fbxl7<sup>Q201X</sup>* and *Fbxl7<sup>C616Y</sup>* homozygotes, this bias in the distribution of D within the cells is reduced (Figure 2.8F-G), indicating that Fbxl7 also has a role in regulating the asymmetric localization of D.

We examined the localization of Dachs-GFP in clones that overexpressed *Fbxl7*. In these clones there was reduction in the overall levels of apical D (Figure 2.8H-H’). In addition, Dachs-GFP puncta in neighboring wild-type cells are enriched against the border with *Fbxl7* overexpressing cells, reminiscent of Ds staining in Figure 2.5E-E’’. This likely resulted from the elevated levels of Ft in *Fbxl7*-overexpressing clones, which would cause an enrichment of Ds (and hence D) on the surface of wild-type cells contacting the clone. In z-sections, we observed subtle changes in the localization of D within the clone itself (Figure 2.8I-I’’). There was a slight increase in D throughout the cell, possibly at the expense of some of the bright puncta that are normally observed at the apical region. Thus, overexpression of *Fbxl7* may cause a shift in the overall distribution of D from the apical region to the interior of the cell.

## Changing *Fbxl7* levels does not alter the levels of Dachs ubiquitylation

To determine whether *Fbxl7* functions as part of an SCF-type ubiquitin ligase, we first tested whether *Fbxl7* was capable of interacting with either SkpA or Cull1. In co-transfection experiments in S2 cells, robust interactions were observed in both cases indicating that *Fbxl7* likely functions as part of an SCF complex (Figure 2.9A). Furthermore, when *Fbxl7* was cotransfected with HA-tagged ubiquitin, and ubiquitylated proteins immunoprecipitated with anti-HA, a high molecular weight smear above the size of wild-type *Fbxl7* was observed indicating that *Fbxl7* is ubiquitylated under these conditions (Figure 2.9B). This is expected, as F-box proteins that function in SCF complexes are often themselves ubiquitylated (Galan and Peter, 1999; Yen and Elledge, 2008). Interestingly, *Fbxl7*<sup>C616Y</sup>, which is incapable of binding to Ft, is also ubiquitylated suggesting that the incorporation of *Fbxl7* into an active SCF complex does not require Ft.

Since *Fbxl7* may function as a component of an E3 ubiquitin ligase, the most parsimonious explanation of its function would be that *Fbxl7* ubiquitylates Dachs directly and promotes its degradation by the proteasome. However, the overall levels of D are unchanged in *Fbxl7* mutant discs (Figure 2.8J). Since *Fbxl7* is localized apically and preferentially localizes to the proximal edge of the cell, *Fbxl7* could promote D degradation locally and this may not be reflected in the overall levels of D. We therefore tested whether *Fbxl7* was capable of promoting D ubiquitylation. These experiments were conducted in both S2 cells and imaginal discs. Ubiquitylated D was readily detected. However, the level of ubiquitylation was unchanged when *Fbxl7* was increased (Figure 2.9C). Additionally, we reduced *Fbxl7* in S2 cells by RNAi-mediated knockdown using two different dsRNAs and still observed no change in D ubiquitylation (Figure 2.9D). Thus we have no evidence that *Fbxl7* influences D ubiquitylation.

## Fbxl7 co-localizes with Cindr and displaces it from the apical membrane

If Fbxl7 negatively regulates the accumulation of D at the apical membrane, it may do so by promoting the trafficking of D into intracellular vesicles. Indeed, we observed a population of intracellular puncta, likely vesicles, that contain both Fbxl7 and D (Figure 2.8I-I’). Moreover Fbxl7 overexpression can cause an overall shift in D from the apical membrane to the interior of the cell (Figure 2.8I’). To further characterize the population of vesicles that contain Fbxl7, we examined the localization of FLAG-Fbxl7 with 59 different markers that each labeled a subpopulation of vesicles and with several proteins that have been identified as interactors of Ft in proteomic studies (Kwon et al., 2013). While most of these markers did not appear to co-localize with FLAG-Fbxl7, strong co-localization was observed with a protein-trap insertion of GFP in the *cindr* locus (results summarized in Table 2.2). Cindr is thought to be an adapter protein that links membrane proteins to the actin cytoskeleton. In basal sections, there is almost complete overlap between GFP-Cindr and FLAG-Fbxl7 in puncta (Figure 2.9E-E’). GFP-Cindr is normally localized to the subapical membrane, apical to E-cadherin, but its localization there is less punctate and more diffuse than that of FLAG-Fbxl7 (Figure 2.9F). When tagged versions of both proteins were expressed in S2 cells, Cindr co-immunoprecipitated with full length Fbxl7 or with a version containing only the LRRs (Fbxl7 $\Delta$ 2) (Figure 2.9G).

To determine whether Fbxl7 could influence the cellular localization of GFP-Cindr, we overexpressed FLAG-Fbxl7 in clones in *GFP-Cindr* animals. In these clones, we observed a dramatic re-localization of GFP-Cindr. GFP-Cindr is almost entirely eliminated from the apical membrane (Figure 2.9H-H’) and increased numbers of basally located vesicles are observed (Figure 2.9I-I’). Thus, Fbxl7 is capable of displacing a protein associated with the apical membrane into intracellular vesicles. We next tested whether changes in Cindr levels are capable of modifying Fbxl7 phenotypes. Indeed we find that the reduction in wing size from overexpression of Fbxl7 was suppressed by co-expression of GFP-Cindr (Figure 2.9J-L).

Under conditions of Fbxl7 overexpression, we did not observe any increase in Cindr ubiquitylation indicating that Cindr is unlikely to be a direct target of Fbxl7 (not shown). Moreover, reducing Cindr levels by RNAi did not elicit phenotypic abnormalities in wings suggestive of defects in Ft or D (not shown). However, the ability of Fbxl7 to cause changes in the localization of Cindr and Ft indicates that it can regulate trafficking of proteins between the apical membrane and the interior of the cell in either direction, and the pathways that regulate the trafficking of these proteins and D might share common components. Some of these shared components could potentially be direct targets of Fbxl7 ubiquitylation.

## 2.5 Discussion

The protocadherin Ft lies at the apex of multiple pathways that together regulate growth, several aspects of PCP, and proximodistal patterning. The mechanism by which Ft functions

as a signaling molecule remains poorly understood. We have now identified the F-box protein Fbx17 as an immediate effector of Ft, that functions to restrict the levels of the atypical myosin D at the apical membrane as well as its distribution around the perimeter of the cell. In addition, Fbx17 can regulate levels of Ft at the apical membrane.

## Multiple effector pathways downstream of Fat

Recent studies have revealed that Ft's effects on distinct pathways may be genetically separated, and that multiple effector domains can contribute to the same function. Indeed, the growth-suppressing function of Ft may occur via at least two regions of the Ft ICD. One or more regions between amino acids 4834 and 4899 in full-length Ft appear responsible for Ft's ability to regulate Hippo signaling (labeled HM in Figure 2.9M) (Matakatsu and Blair, 2012; Bossuyt et al., 2013; Zhao et al., 2013). Several mutations within this region compromise this function of Ft and cause massive tissue overgrowth (Bossuyt et al., 2013). Intriguingly, an allele of *ft*, *ft*<sup>61</sup>, which harbors such a mutation, showed neither an effect on the recruitment of Fbx17 to the apical membrane nor on the binding of Ft to Fbx17. Thus, signaling via this region of the ICD appears to be independent of Fbx17. A second, more C-terminal region of the Ft ICD (Region D in Figure 2.9M) that extends between amino acids 4975 and 4993 of full-length Ft, is removed by the *ft* $\Delta$ D deletion and also has a growth-suppressive function albeit weaker than that of HM (Pan et al., 2013). This second growth-suppressive pathway requires the function of Fbx17, as the protein generated by the *ft* $\Delta$ D allele cannot bind to Fbx17 nor can it localize Fbx17 to the apical membrane. Additionally, the phenotypic abnormalities of null alleles of *ft* rescued by *ft* $\Delta$ D are very similar, if not identical to those of *Fbx17* mutants.

We have shown that hyperactivation of the “weaker” Fbx17-dependent pathway can overcome the absence of the “stronger” Fbx17-independent pathway; overexpression of Fbx17 can suppress the overgrowth of *ft*<sup>61</sup>. Thus, while these two pathways can be dissociated at the level of the Ft ICD, they nevertheless seem to converge further downstream. This point of convergence likely involves D since the overgrowth of *ft* mutant tissue can be suppressed completely by eliminating D function (Cho et al., 2006). Indeed, it has previously been suggested that Ft regulates growth by restricting the levels of apical D, and regulates PCP by influencing the planar asymmetry of apical D (Rogulja et al., 2008; Pan et al., 2013).

Another key finding in our experiments is that *Fbx17* mutations perturb the distribution of D around the perimeter of the apical region of the cell. D is normally biased towards the distal edge of the cell; in *Fbx17* mutants, D is more evenly distributed around the cell perimeter. The asymmetric localization of D depends on at least two different regions of Ft (Pan et al., 2013). One is the region that binds to Fbx17 (Region D) and the other is composed of the last three amino acids at the C-terminus of the protein (Region F in Figure 2.9M), which is not necessary for Fbx17 localization to the apical membrane. Thus, for the regulation of D asymmetry as well, there appears to be an Fbx17-independent pathway. The existence of multiple downstream effector pathways that converge on common biological outcomes suggests that these pathways might function redundantly to some extent and thus

provide robustness. This might also explain why the phenotypes elicited by overexpression of Fbxl7 are, in general, more severe than those observed in loss-of-function mutations.

## Fbxl7 as a regulator of protein localization

Previous observations of the localization of Ft, Ds, and D to vesicles are suggestive of trafficking events being involved in Ft signaling (Ma et al., 2003; Matakatsu and Blair, 2004; Mao et al., 2006). We have demonstrated that, in addition to the apical membrane, Fbxl7 localizes to vesicles. Moreover, FLAG-Fbxl7 vesicles can contain Ft, Ds and D, and these may be related to the apical puncta observed on cell edges. This localization is likely specific, since we do not see Fbxl7 co-localization with other cell surface proteins such as Crumbs, Notch, and E-cadherin (not shown). Currently very little is known about the role of each of these proteins in vesicles. However, there is an increasing appreciation that most transmembrane proteins, and even proteins that are associated with the inner leaflet of the cell membrane are maintained at the plasma membrane by a dynamic process involving endocytosis and vesicle recycling (e.g., Schmick et al., 2014).

We provide evidence that Fbxl7 regulates Ft apical localization, but how this regulation relates to the Fbxl7 phenotypes is not clear. Since Fbxl7 overexpression increases Fat signaling, and rescues the overgrowth-inducing *ft<sup>61</sup>* allele, perhaps this is due to the increased levels of Ft protein at the apical membrane. However, Ft levels are slightly elevated in *Fbxl7* mutants, which display mild overgrowth. Therefore the mutant phenotype cannot be explained by the effect on Ft. Another known regulator of apical Ft levels is *lowfat (lft)* (Mao et al., 2009). Fbxl7 and Lft appear to regulate Ft in different ways. Lft overexpression, like Fbxl7, increases Ft levels. However, while Ft levels are decreased in *lft* mutant cells, Ft levels are increased in *Fbxl7* mutant cells, though less so compared to *Fbxl7* overexpression. Interestingly, for many proteins that regulate cellular trafficking, similar phenotypic abnormalities are observed with gain-of-function and loss-of-function mutations, since the normal execution of the process requires the protein to shuttle efficiently between two states (Park et al., 1993). Thus dynamic aspects of the localization of Ft, Ds and D clearly merit more attention.

The interactions we have observed between Fbxl7 and the adapter protein Cindr may provide clues for how Fbxl7 regulates D localization. Fbxl7-associated vesicles show almost complete overlap with GFP-Cindr and Fbxl7 can re-localize Cindr from the apical membrane to the interior of the cell. This finding, together with the observed increase in basal levels of D upon Fbxl7 overexpression (Figure 2.8I-I’’), suggests that Fbxl7 may function to regulate D trafficking in a similar manner. Cindr and its mammalian orthologues Cin85 and CD2AP are thought to regulate interactions between membrane proteins and actin cytoskeleton (Haglund et al., 2002; Petrelli et al., 2002; Soubeyran et al., 2002; Johnson et al., 2011, 2012). D is an atypical myosin with a predicted actin binding domain in its conserved head domain. Therefore, the vesicles which Fbxl7 associates with D and Cindr may be linked to the actin cytoskeleton. In addition, our finding of partial colocalization of Fbxl7

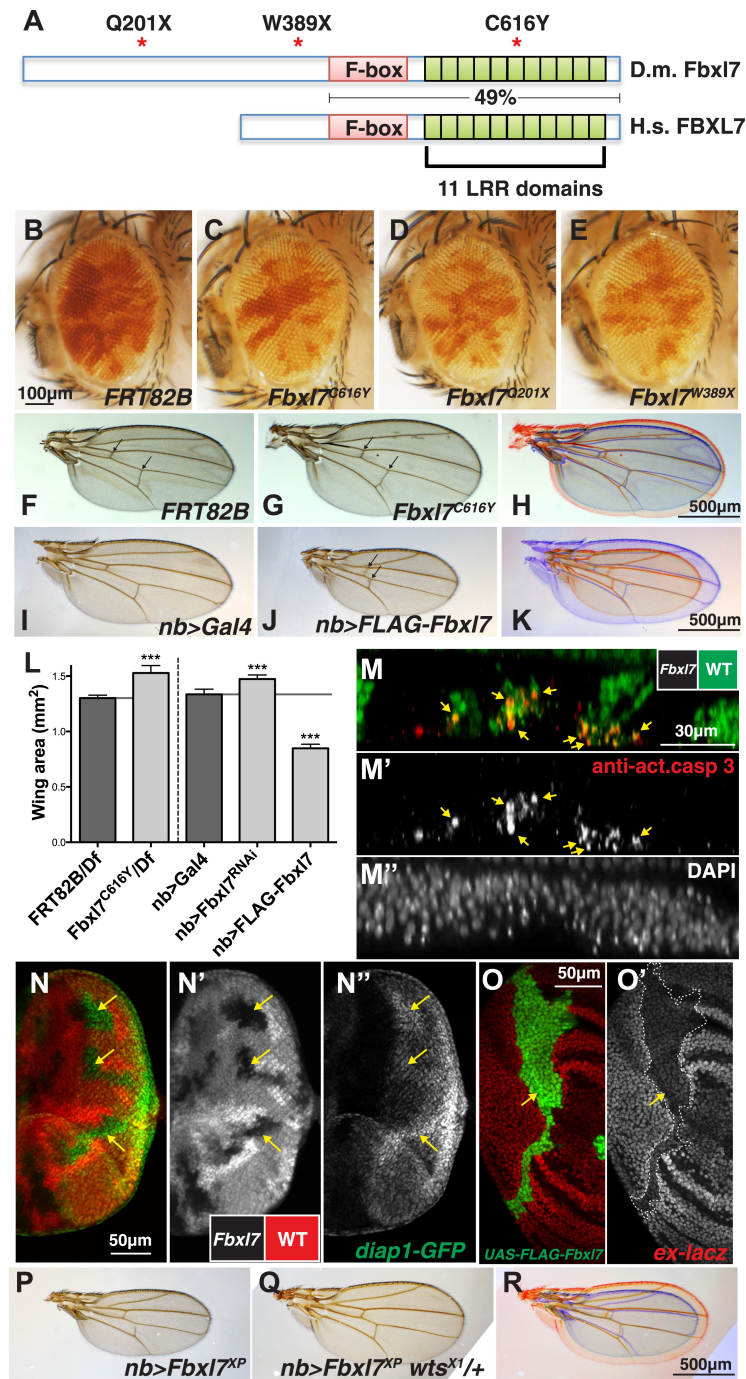
with retromer components further supports the possibility that Fbxl7 may have a role in protein trafficking.

## **Fbxl7 as a ubiquitin-ligase component**

Many F-box proteins associate with Skp1 and Cull1 to form an SCF E3 ubiquitin ligase complex (reviewed in Skaar et al., 2013). Recruitment of specific substrates results in their poly-ubiquitylation and degradation, or mono-ubiquitylation, which can have non-degradative signaling roles. In addition, some F-box proteins have SCF-independent roles (Nelson et al., 2013). Fbxl proteins are thought to recruit substrates to the SCF complex through the interaction with their LRR domains, and substrates have been identified for several Fbxls such as Skp2 (Fbxl1), which degrades p27 (Carrano et al., 1999; Sutterluty et al., 1999). However many, like Fbxl7, are still uncharacterized as “orphan” F-box proteins with no known substrates.

Since we find that Fbxl7 associates with Skp1 and Cull1, its potential substrates may be involved in Ft signaling. Fbxl7 has one described substrate in mice, Aurora A (Coon et al., 2012). However we do not believe Aurora A is a relevant substrate in *Drosophila*, as we do not observe Ft signaling defects when Aurora A is knocked down or overexpressed (not shown). The identification of F-box protein substrates has mainly been accomplished by unbiased approaches (Skaar et al., 2013). Similarly, a combination of unbiased approaches, involving proteomics, genetic interaction screens, and identifying proteins that co-localize with Fbxl7 in vesicles could be used to identify Fbxl7 substrates.

## 2.6 Figures

Figure 2.1: *Fbx17* negatively regulates growth through the Hippo pathway.

(A) Protein model of Drosophila Fbxl7 and Human FBXL7 showing the three alleles identified (red asterisks), F-box, and 11 Leucine Rich Repeat (LRR) domains. The two proteins have 49% amino acid identity throughout the F-box and LRR domains. (B-E) Mosaic adult eye assay. Heterozygous and wild-type cells have red pigment and homozygous mutant cells lack pigment. (B) Control mosaic eye. (C) *Fbxl7*<sup>C616Y</sup>, (D) *Fbxl7*<sup>Q201X</sup> and (E) *Fbxl7*<sup>W389X</sup> mosaic eyes are composed of more mutant cells. (F-K) Adult wings with overlays. Arrows indicate anterior and posterior crossveins. Compared to (F) *FRT82B* control wings, (G) *Fbxl7*<sup>C616Y</sup> homozygous wings are larger and crossveins are closer. (H) Merge shows F in blue and G in red. Compared to (I) *nubbin-Gal4* (*nb-Gal4*) control wings, (J) *nb>FLAG-Fbxl7* overexpressing wings are smaller and crossveins are closer. (K) Merge shows I in blue and J in red. (L) Quantification of wing area from *Fbxl7* loss-of-function, RNAi (*JF01515*), and overexpression.  $n \geq 20$  wings, \*\*\*  $p \leq 0.001$ , error bars show SD. (M-M'') Cell competition assay in the mosaic eye imaginal disc. (M) Wild-type cells are marked by GFP (green), while *Fbxl7* mutant cells are GFP-negative. (M') Activated caspase-3 (red) is detected in dying cells that are GFP positive (arrows). (M'') DAPI shows all nuclei. (N-N'') Mosaic eye imaginal disc with *diap1-GFP* (green) reporter. (N-N') Wild-type cells are marked with RFP (red) and *Fbxl7* mutant cells are RFP-negative. (N'') Mutant clones show higher levels of *diap1-GFP* (arrows). (O-O') Mosaic wing imaginal disc with *ex-lacZ* reporter (red). A clone overexpressing FLAG-Fbxl7 (green, cells marked by EGFP) has lower levels of *ex-lacZ* (arrow). (P-R) Wing size genetic interaction assay. Compared to (P) *nb>Fbxl7*<sup>XP</sup> alone, (Q) reducing the dosage of *wts* partially rescues the small wing phenotype. (R) Merge shows P blue and Q in red.

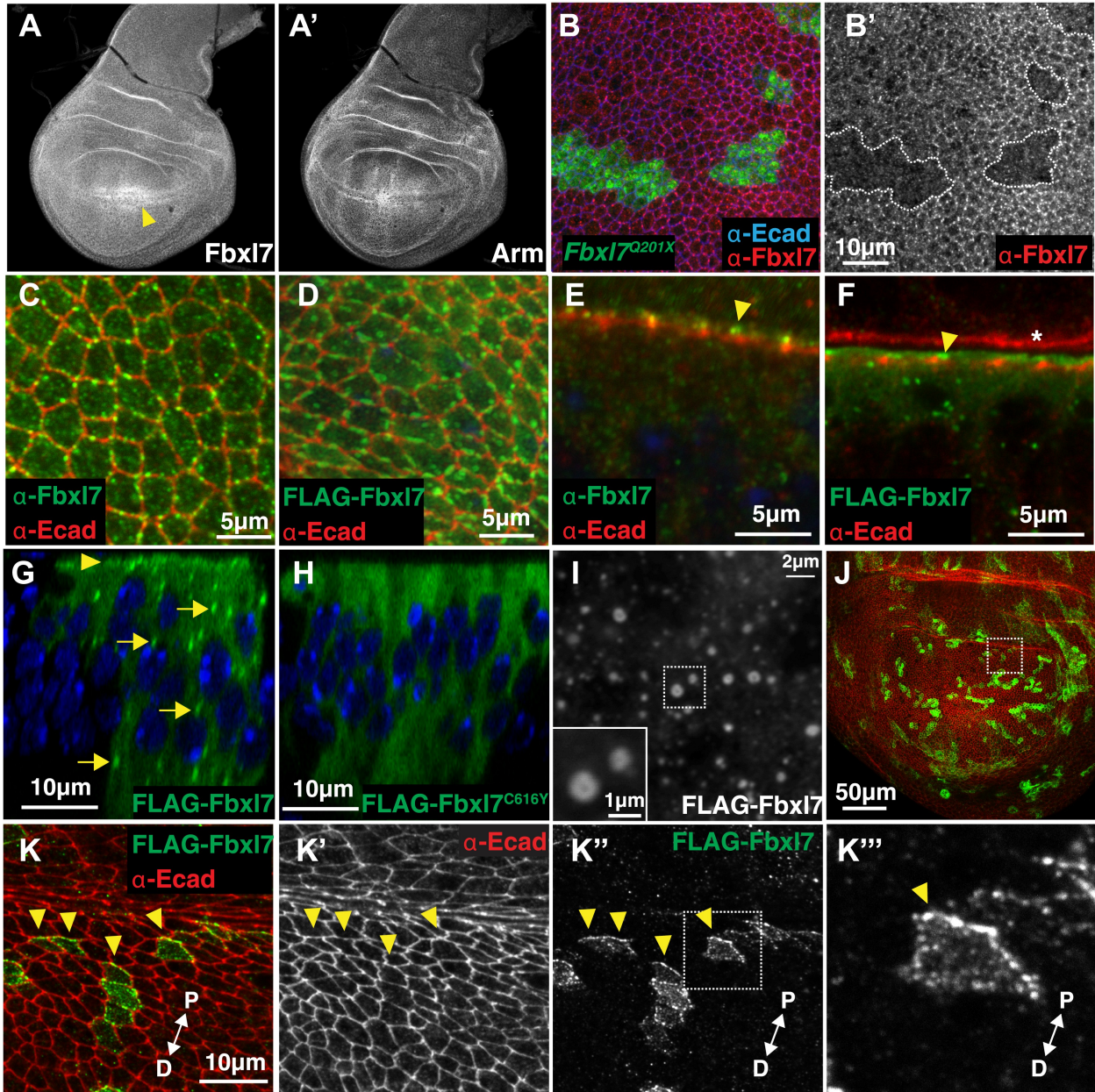


Figure 2.2: Fbx17 is localized to apical membrane, cytoplasmic puncta, and the proximal side of planar polarized cells.

Confocal slice of (A) endogenous Fbx17 and (A') Armadillo (Arm) in the wing imaginal disc. Arrow indicates enrichment of Fbx17 at the dorso-ventral boundary. (B-B') A confocal slice through the apical surface of wing disc cells. Fbx17 (red) accumulates at the apical membrane and is lost from MARCM *Fbx17<sup>Q201X</sup>* clones (green). (C-F) Endogenous Fbx17 and expressed FLAG-Fbx17 (green) are localized to apical puncta aligned with cell edges marked by E-cadherin (E-cad) (red). (C-D) Confocal slices through the apical surface of wing disc cells. (E-F) Confocal slice through folds in the wing disc. Fbx17 is apical to E-cad (arrowheads). (F) Asterisk indicates adjacent fold that does not express FLAG-Fbx17. (G-H) Confocal Z-slice through the wing disc with clones of cells expressing FLAG-Fbx17 or FLAG-Fbx17<sup>C616Y</sup> (green). Nuclei are shown with DAPI (blue). (G) FLAG-Fbx17 localizes to apical membrane (arrowhead) and cytoplasmic puncta (arrows), whereas (H) FLAG-Fbx17<sup>C616Y</sup> shows diffuse cytoplasmic localization. (I) Confocal section through peripodial membrane showing FLAG-Fbx17 localization to hollow puncta. Inset shows higher magnification of outlined box. (J-K'') Confocal slice of the wing disc pouch stained for E-cad (red) with clones expressing FLAG-Fbx17 (green). (K-K'') Magnified region from box in J, showing FLAG-Fbx17 enriched on proximal membrane (arrowheads). (K''') Magnified region from box in K''. D = distal, P = proximal.

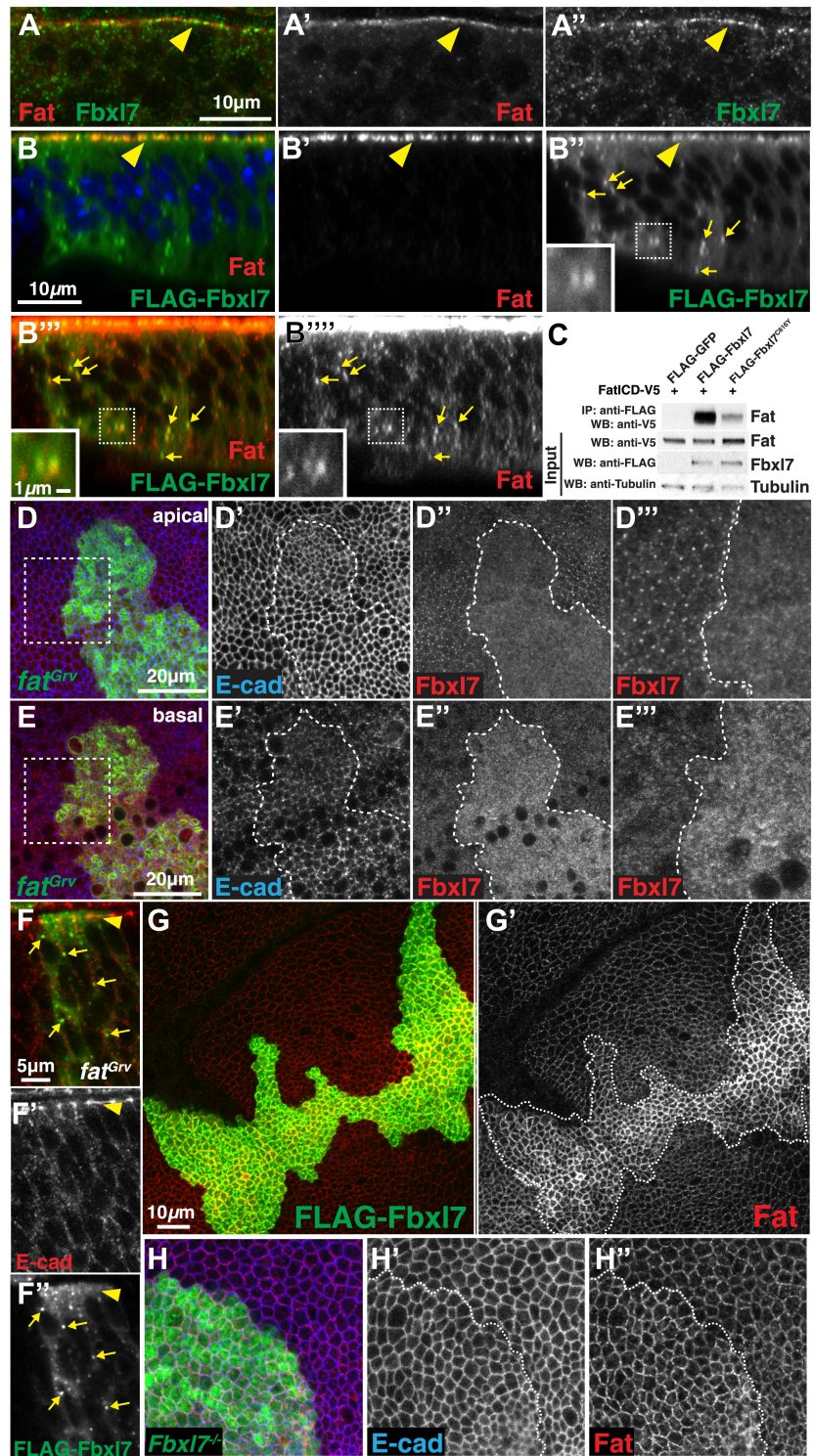


Figure 2.3: Fbx17 physically interacts with Fat and regulates its apical localization.

(A-A'') Confocal slice through a wing disc fold showing endogenous Fbx17 (green) and Fat (red) co-localize at apical membrane (arrowhead). (B-B'') Confocal Z-section showing FLAG-Fbx17 (green) and Fat (red) co-localize at (B-B'') apical membrane (arrowhead) and (B''-B''') cytoplasmic puncta (arrows). (B''-B''') Inset shows magnification of puncta. B''' uses higher gain settings than B' to visualize Fat in puncta. (C) Co-immunoprecipitation experiment in S2 cells. FatICD-V5 pulls down with FLAG-Fbx17, whereas pulldown is reduced with FLAG-Fbx17<sup>C616Y</sup>. (D-D'') Confocal slice of the wing disc at the apical surface. Apical Fbx17 (red) localization is lost from MARCM *fat<sup>Grv</sup>* clones (green), whereas (D') E-cad (blue) localization is unchanged. (D'') shows magnification of the box in D. (E-E'') A basal confocal slice through the same clone in D, showing increased cytoplasmic levels of Fbx17. (F-F'') Confocal slice through a fold showing a MARCM *fat<sup>Grv</sup>* clone (GFP marker not shown) which expresses FLAG-Fbx17 (anti-Flag, green). (F') E-cad (red) marks apical membrane. FLAG-Fbx17 is not apically localized in *fat<sup>Grv</sup>* clones (arrowhead), but does localize to cytoplasmic puncta (arrows). (G-G') Confocal slice through the apical surface of a disc overexpressing FLAG-Fbx17 (green) in clones. (G') Apical Fat (red) levels are elevated within the clone. (H-H'') Confocal slice through the apical surface with a MARCM *Fbx17<sup>Q201X</sup>* clone (green) showing (H') no change in levels of apical E-cad (blue) and (H'') slightly elevated levels of apical Fat (red).

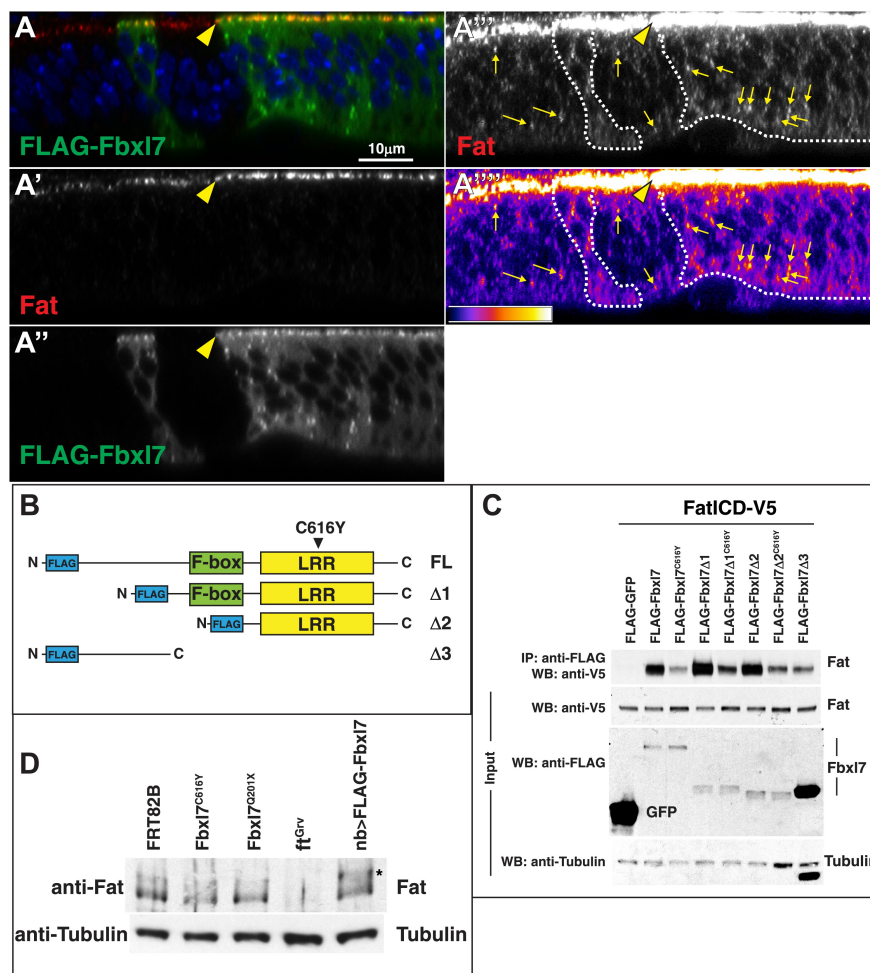


Figure 2.4: **Additional analysis of the relationship between Fbx17 and Fat.** (A) A confocal z-section through a wing disc with clones overexpressing FLAG-Fbx17 and stained for FLAG (green) and Fat (red). Apical membrane is towards the top of the image. Fat and FLAG-Fbx17 colocalize at apical membrane (yellow arrowhead). (A''-A''') Higher gain settings to observe Fat cytoplasmic punctae and heat map of fluorescence intensity. Fat localizes to punctae in both wild-type cells and FLAG-Fbx17 expressing cells (yellow arrows). Cytoplasmic Fat is slightly elevated in FLAG-Fbx17 expressing cells. (B) Schematics of FLAG-Fbx17 truncation constructs. (C) Western blots showing results of co-immunoprecipitation experiments from S2 cells expressing indicated transfected plasmids. FatICD co-immunoprecipitates with full length FLAG-Fbx17 as well as the LRR domain. The Fbx17<sup>C616Y</sup> protein reduces association with FatICD. The N-terminal domain of Fbx17 can weakly associate with FatICD. FLAG-Fbx17 $\Delta 3$  protein is found at higher levels than other Fbx17 proteins despite transfecting the same amount of plasmid and loading the same amount of total protein. (D) Western blots showing endogenous Fat protein from wing disc lysates of indicated genotypes. The asterisk indicates higher molecular weight Fat in discs overexpressing FLAG-Fbx17.

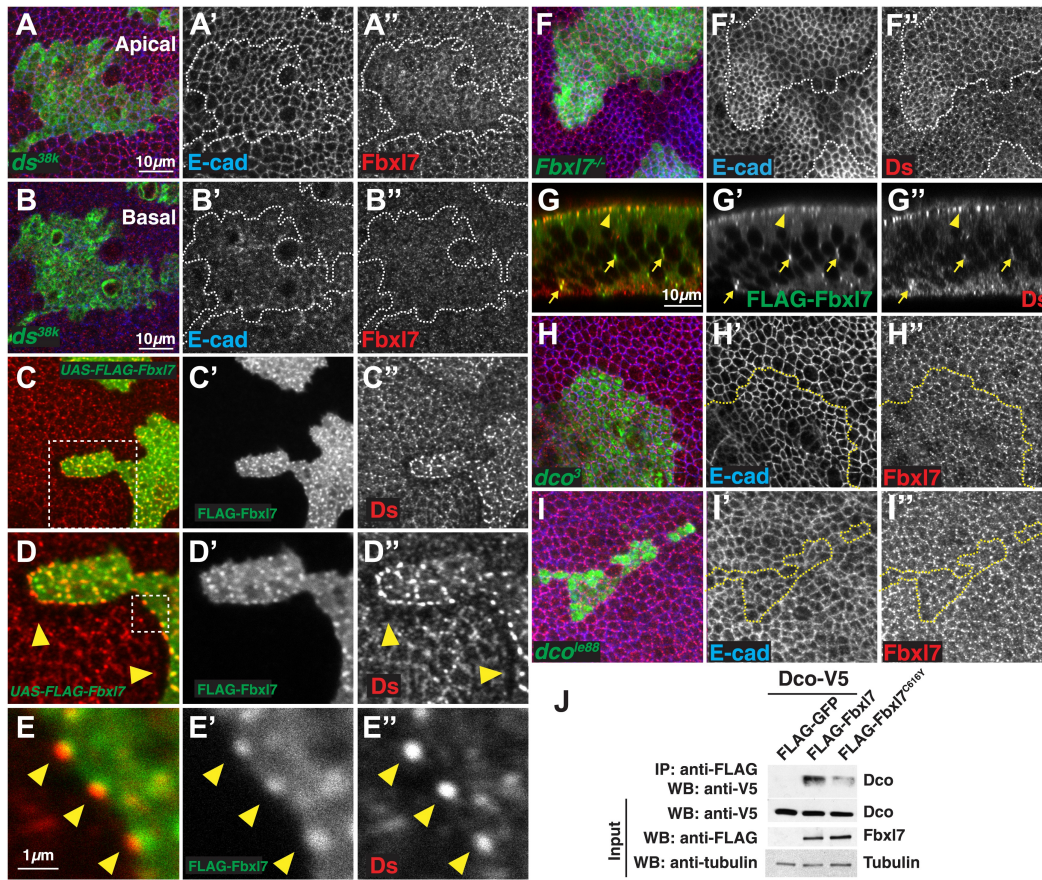


Figure 2.5: **Relationship between Fbx17 and the Fat pathway proteins Ds and Dco.** (A-A'') Confocal slice through the apical surface of a disc with MARCM *ds<sup>38k</sup>* clones (green) showing disturbed localization of Fbx17 (red). E-cad staining is not altered (blue) (B-B'') A basal confocal slice through the same clone in A, showing no change in Fbx17 cytoplasmic levels. (C-E'') Confocal slice through the apical surface of a disc with FLAG-Fbx17 overexpressing clones (green) and stained for Ds (red). (C-D'') Apical Ds levels appear higher and more punctate in FLAG-Fbx17 expressing clones. Wild-type cells immediately adjacent to the clone have reduced apical Ds (arrowheads). (E-E'') Ds and FLAG-Fbx17 puncta are aligned on either side of the clone boundary (arrowheads). (F-F'') Apical confocal slice of a disc containing MARCM *Fbx17<sup>Q201X</sup>* clones (green) and stained for Ds (red) and E-cad (blue). Ds levels are normal or slightly elevated, in clones. (G-G'') Confocal Z-section of a clone expressing FLAG-Fbx17 (green) and stained for Ds (red). Both are localized to apical membrane (arrowhead) and frequently co-localize in cytoplasmic puncta (arrows). (H-I'') Apical confocal slice of MARCM *dco<sup>3</sup>* or *dco<sup>le88</sup>* clones (green) and staining for Fbx17 (red) and E-cad (blue). Apical Fbx17 levels are unchanged in (H-H'') *dco<sup>3</sup>* and (I-I'') *dco<sup>le88</sup>* clones. (J) Co-immunoprecipitation experiment in S2 cells. Dco-V5 pulls down with FLAG-Fbx17, whereas pulldown is reduced with FLAG-Fbx17<sup>C616Y</sup>

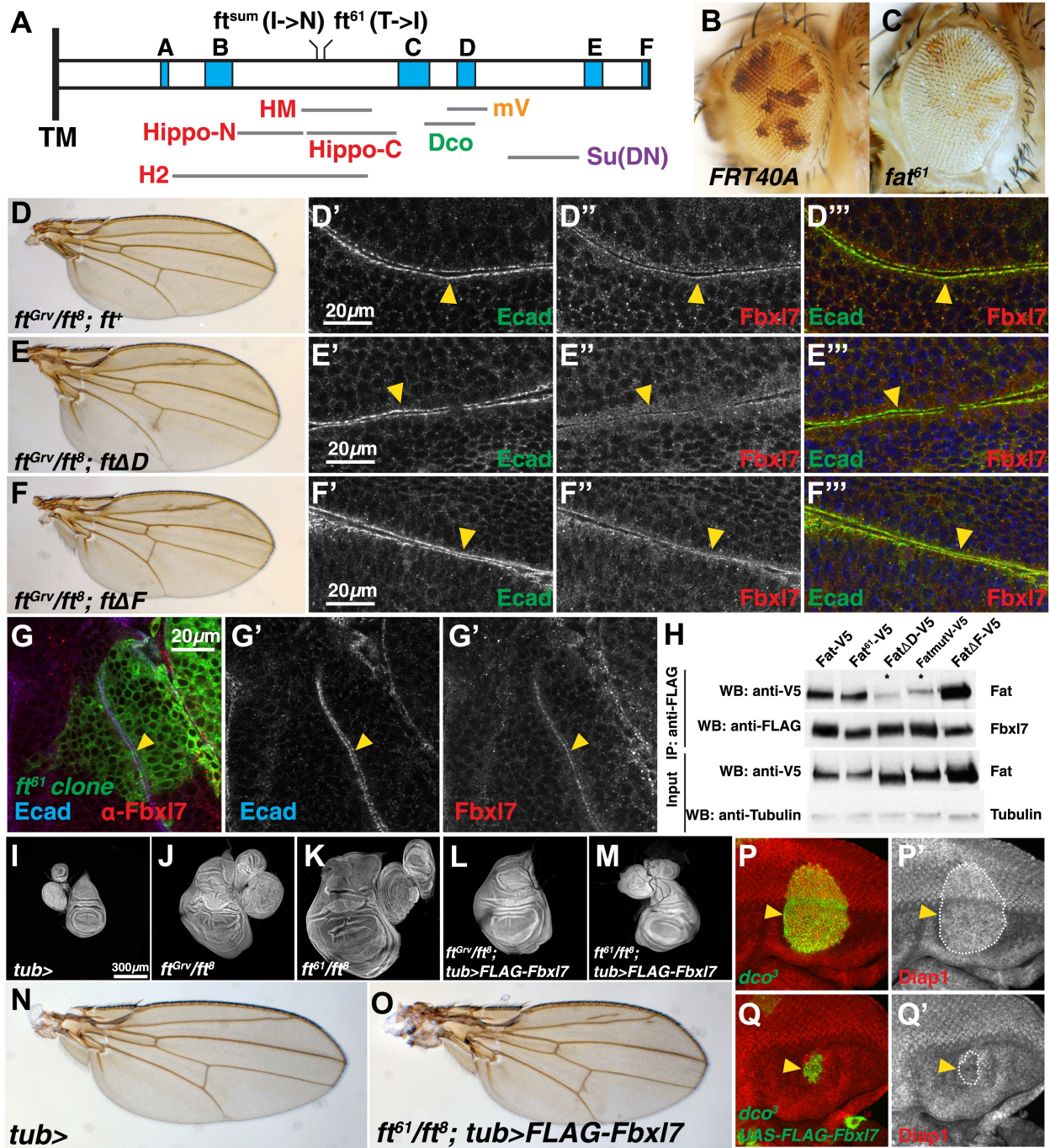
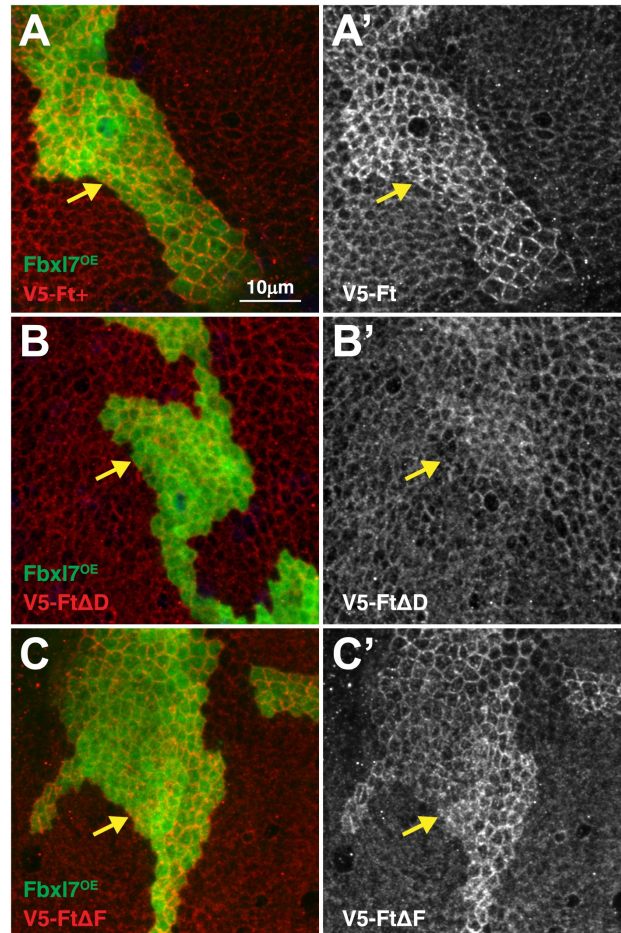


Figure 2.6: Fbx17 functions in one of two growth-suppressing pathways downstream of Ft.

(A) Protein model of the intracellular domain of Fat showing the transmembrane domain (TM), regions conserved with mammalian Fat4 (blue, A-F) (defined by Pan et al., 2013), regions associated with the major growth suppressive function of Fat (red) (HM, Bossuyt et al., 2013; Hippo-N, Hippo-C, Matakatsu and Blair, 2012; H2, Zhao et al., 2013), region required for Dco binding (green) (Sopko et al., 2009), mutV region (orange) (Pan et al., 2013), Su(DN) region (purple) (Matakatsu and Blair, 2012), and two point mutations,  $ft^{sum}$  (Bossuyt et al., 2013) and  $ft^{61}$  (this study). Size and position of regions are drawn to scale relative to the ICD. (B-C) Mosaic adult eye assay. Heterozygous wild-type cells have red pigment and homozygous mutant cells lack pigment. Compared to (B) control *FRT40A* mosaic eyes, (C)  $ft^{61}$  mosaic eyes are larger and have more mutant tissue. (D)  $ft^{Grv}/ft^8$ ;  $ft^+$  adult wing and (D'-D'') confocal slice of a wing disc showing that Fbx17 (red) is localized to the apical membrane similar to E-cad (green). (E)  $ft^{Grv}/ft^8$ ;  $ft^{\Delta D}$  adult wing and (E'-E'') confocal slice showing that Fbx17 (red) apical localization is disrupted. (F)  $ft^{Grv}/ft^8$ ;  $ft^{\Delta F}$  adult wing and (F'-F'') confocal slice showing that Fbx17 (red) apical localization is normal and similar to that in D'-D''. (G) Confocal slice of a disc containing a MARCM  $ft^{61}$  clone (green) and stained for Fbx17 (red) and E-cad (blue). Fbx17 apical localization is normal in  $ft^{61}$  cells (H) Co-immunoprecipitation experiment in S2 cells. Fat-V5, Fat<sup>61</sup>-V5, and Fat $\Delta F$ -V5 pull down with FLAG-Fbx17, whereas pull down of Fat $\Delta D$ -V5 and FatmutV-V5 is reduced. Expressed Fat proteins contain only transmembrane and cytoplasmic regions (ICD). (I-M) Wing imaginal discs (and associated leg and haltere discs) at low magnification. Compared to (I) control *tub-Gal4* discs, (J)  $ft^{Grv}/ft^8$  and (K)  $ft^{61}/ft^8$  discs are larger and have more folds. (L) Ubiquitous expression of Fbx17 does not rescue  $ft^{Grv}/ft^8$  disc overgrowth. (M) Ubiquitous expression of Fbx17 rescues disc overgrowth of  $ft^{61}/ft^8$ . (N-O) Adult wing from (N) control *tub-Gal4* and (O) ubiquitous expression of FLAG-Fbx17 in an  $ft^{61}/ft^8$  background. Animal lethality is rescued. (P-Q') Confocal slice through the eye imaginal disc showing MARCM clones (green) and anti-Diap1 staining (red). (P-P') *dco*<sup>3</sup> clones have elevated Diap1 levels and are overgrown, whereas (Q-Q') *dco*<sup>3</sup> clones expressing FLAG-Fbx17 have wild-type Diap1 levels and are reduced in size.



**Figure 2.7: Domain D of Ft is required for the effects of Fbx17 on Ft localization.** Confocal projection of apical membrane in wing disc cells stained for anti-V5 (red) with clones overexpressing FLAG-Fbx17 (green, marked by GFP) in different genetic backgrounds. Ft proteins are N-terminally tagged with V5. (A-A') V5-Ft+, (B-B') V5-Ft $\Delta$ D, (C-C') V5-Ft $\Delta$ F. Arrows indicate edge of clones. Apical levels of V5-Ft $\Delta$ D protein are not increased upon Fbx17 overexpression.

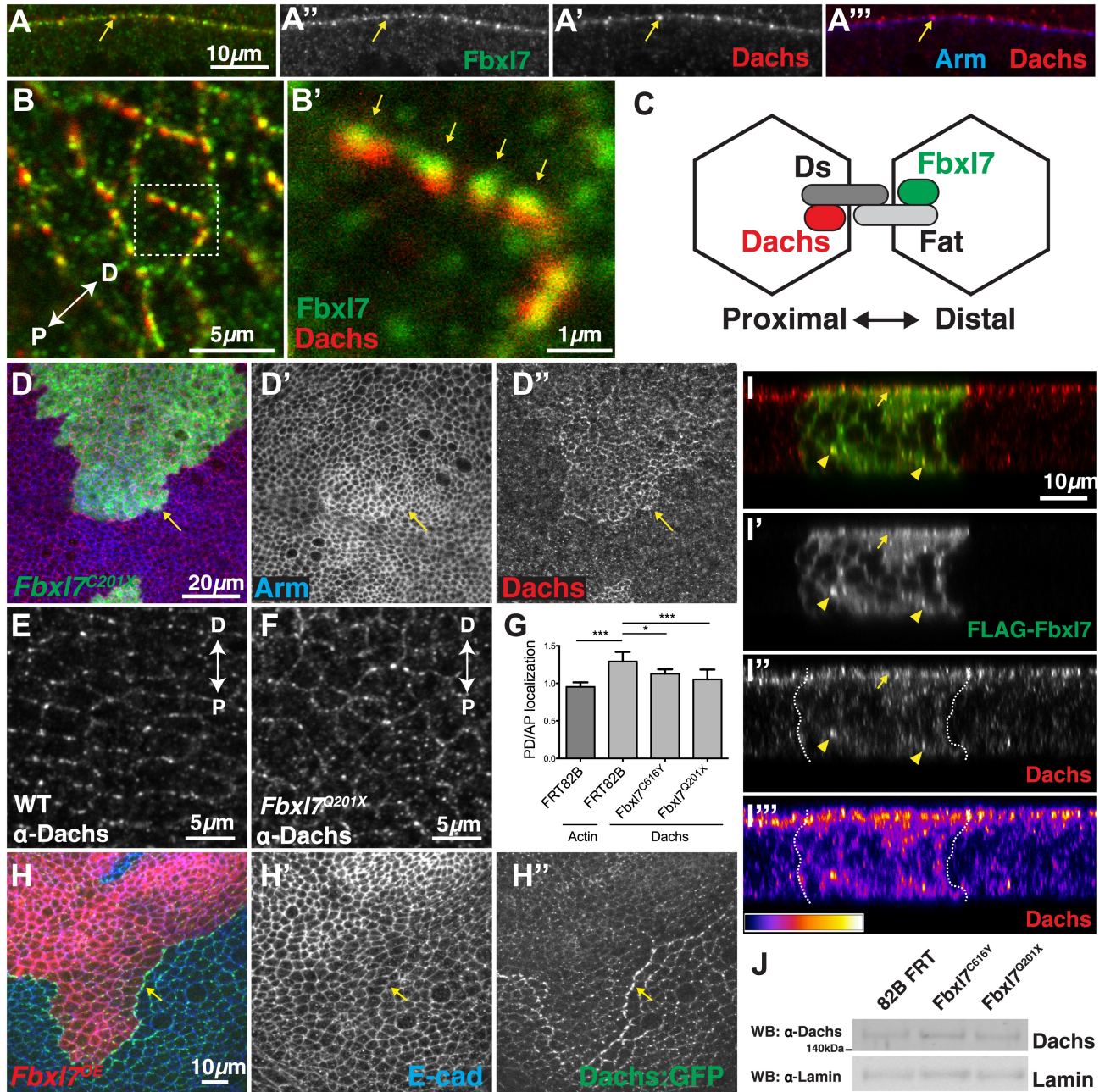


Figure 2.8: Fbx17 regulates the localization of Dachs.

(A-A'') Confocal slice through a bend in the wing disc showing (A') Dachs (red) and (A'') Fbx17 (green) localize at subapical membrane. (A''') Like Fbx17, Dachs is apical to the adherens junction marked by Arm (blue). (B-B') Confocal slice through the apical surface of the wing disc, specifically the dorsal edge of the pouch, showing Dachs (red) and Fbx17 (green) staining. Dachs and Fbx17 puncta abut each other on either side of the cell boundary. Proximodistal axis indicated as P $\leftrightarrow$ D. (C) Diagram of polarized wing disc cells in which Dachs is enriched on the distal side and Fbx17 is on the proximal side, linked by their association to Dachsous and Fat, respectively, which bind across cells. (D-D'') Apical confocal slice of MARCM *Fbx17<sup>Q201X</sup>* clones (green) and staining for Arm (blue) and Dachs (red). Dachs levels are elevated in clones. (E-G) Apical confocal slice with staining for Dachs in (E) wild-type or (F) *Fbx17<sup>Q201X</sup>* discs. Images are from the dorsal edge of the pouch and are aligned so the proximodistal axis is vertical. Dachs enrichment on P/D membrane, seen in (E) wild-type discs, is impaired in (F) *Fbx17<sup>Q201X</sup>* discs. (G) Quantification of Dachs P/D enrichment in wing discs. Dachs is localized in a P/D direction, whereas Actin is not. Dachs P/D asymmetry is impaired in both *Fbx17<sup>C616Y</sup>* and *Fbx17<sup>Q201X</sup>* discs. Significance calculated with one-way ANOVA test. \*\*\*  $p \leq 0.001$ , \*  $p \leq 0.05$ . Error bars indicate SD. (H-H'') Apical confocal slice of FLAG-Fbx17 overexpressing clones (red, cells marked by RFP) and staining for anti-GFP (green, Dachs:GFP) and E-cad (blue). Apical Dachs levels within the clone are reduced, and Dachs is enriched at the edge of the clone. (I-I'') Confocal z-section of a wing disc with a FLAG-Fbx17 expressing clone (green) and stained for Dachs (red). FLAG-Fbx17 and Dachs co-localize to apical membrane (arrow) and intracellular puncta (arrowheads). (I''-I''') Cytoplasmic levels of Dachs are slightly elevated within the clone. (I''') Heat map of I''. (J) Western blots from wing disc lysates. Endogenous Dachs protein levels are not changed in *Fbx17* mutant wing discs compared to control.

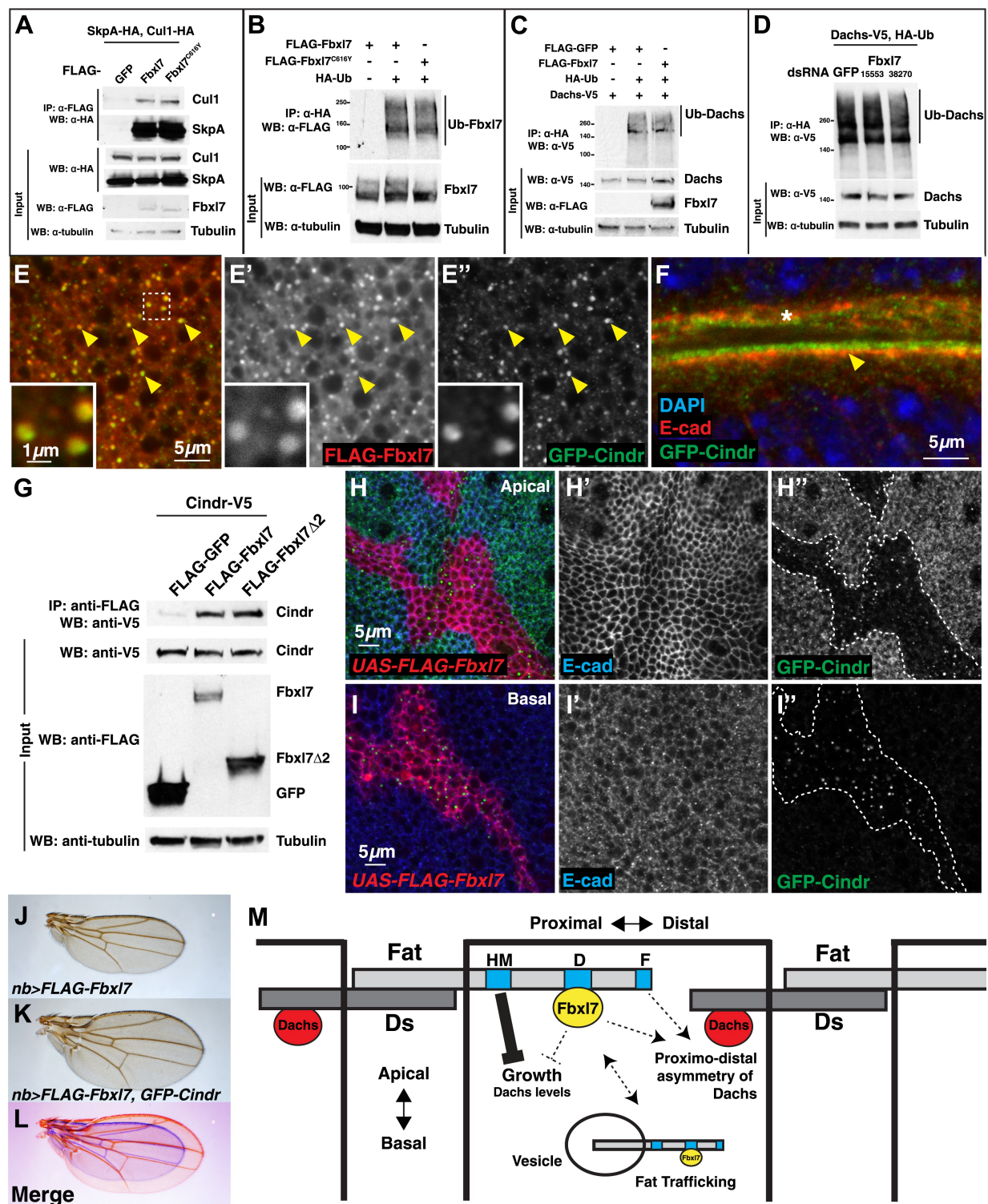


Figure 2.9: Fbx17 does not affect Dachs ubiquitylation, and Fbx17 affects the localization of Cindr.

(A) Co-immunoprecipitation assay from S2 cells. SkpA-HA and Cul1-HA immunoprecipitates with FLAG-Fbx17. (B) In-vivo Fbx17 ubiquitylation assay in S2 cells. FLAG-Fbx17 and FLAG-Fbx17<sup>C616Y</sup> are ubiquitylated in vivo. (C-D) In-vivo Dachs ubiquitylation assay in S2 cells. Dachs-V5 is ubiquitylated under wild-type conditions, and does not change with (C) overexpression of FLAG-Fbx17 or (D) knockdown of Fbx17 with two different dsRNAs. (E-E'') Confocal slice showing localization of FLAG-Fbx17 (red) and GFP-Cindr (green) in puncta (arrowheads). (F) Confocal slice through a bend in the wing disc. GFP-Cindr (green) localizes to subapical membrane, apical to E-cad (red). Asterisk indicates an adjacent bend in the tissue. (G) Co-immunoprecipitation experiment in S2 cells. Cindr-V5 pulls down with full length FLAG-Fbx17, and FLAG-Fbx17 $\Delta$ 2, which contains only the LRR domains. (H-I'') Confocal slice in a disc with clones overexpressing FLAG-Fbx17 (red, cells marked by myr-RFP) in a *GFP-Cindr* background. (H-H'') An apical plane shows loss of apical GFP-Cindr within the clone, and (I-I'') a basal plane shows accumulation of GFP-Cindr in puncta. (J) Compared to (J) *nb>FLAG-Fbx17* alone, (K) overexpressing GFP-Cindr partially rescues the small wing phenotype. (L) Merge shows J blue and K in red. (M) Model of Fbx17 as a component of Fat signaling. Not drawn to scale.

Oligo name	Sequence
Not1-Fbx17-F	CGGCGGCGGCCGCTTCGCACAAGACTAGCAACCG
Xba1-Fbx17-R	GCCGTCTAGATCAACAGAATCCCGGATTTG
C616Y-SDM-F	GTGTGTCCGACTACCTGAACATCAC
C616Y-SDM-R	GTGATGTTTCAGGTAGTCGGACACAC
Not1-Fbx17 $\Delta$ 1-F	CGGCGGCGGCCGCTTGGAACCGCAAAGGTCCC
Not1-Fbx17 $\Delta$ 2-F	CGGCGGCGGCCGCTTCGCTGCGGGGCGAGCACT
Xba1-Fbx17 $\Delta$ 3-R	GCGGTCTAGATTCAGGGCGGCGGTCCAATGGC
Not1-GFP-F	GGCGGAGGTGCGGCCGCTGTGAGCAAGGGCGAGGAG
Xba1-GFP-R	ACAAAGATCCTCTAGATCACTTGTACAGCTCGTCCA
Not1-SkpA-F	CGCGTCGCGGCCGCCACCATGCCCAGCATCAAGTTGC
Xba1-SkpA-R	GCCGTCTAGAGACTTCTCCTCGCACCCTCGT
Kpn1-Cul1-F	CTAGTGGTACCCACCATGAACCGCTCCGGCAAT
Not1-Cul1-R	GACGCGGCGGCCGCTGGCGAGATACTATATGTGTCTTTG
Not1-Cul1DN-R	GACGCGGCGGCCGCTCACGACCATCACCTGGTTAAGA
Not1-Fat1CD-F	CGTCGCGGCCGCAAATGGAGAGGCTACTGCTCC
Xba1-Fat1CD-R	GCGCGTCTAGATTACGTAGAATCGAGACCGAGGA
Fat61SDM-F	GCAGCCGCGCATTCTCATTTTGCACGACATTTCCGG
Fat61SDM-R	CCGAAATGTCGTGCAAATGAGAATGCGCGGCTGC
EcoRI-HA-Ub-F	CGCGTCGAATTCCAAAATGTACCCATACGATGTTCC AGATTACGCTCAAATTTTCGTTAAGACCCTCACTG
Xba1-Ub-R	GCCGTCTAGACTAGCCACCACGCAGACGCAG
Not1-cindr-F	CGCGTCGCGGCCGCCACCATGGAAAACAACATCTGTGCA
Xba1-cindr-R	GCCGTCTAGAGAACTTTCGTCACGCACTG
DRSC15513-F	TAATACGACTCACTATAGGGCGACCTTTGAGTTGAGAGG
DRSC15513-R	TAATACGACTCACTATAGGGGCGAGTCGCTCGTTCCC
DRSC38270-F	TAATACGACTCACTATAGGGATCTGAACGCTCGAGGATGT
DRSC38270-R	TAATACGACTCACTATAGGGCCAAAAGTCCGTGTATGGCT
GFPdsRNA-F	TAATACGACTCACTATAGGGATGGTGAGCAAGGGCGAG
GFPdsRNA-R	TAATACGACTCACTATAGGGCTTGTACAGCTCGTCCATGC

Table 2.1: Oligonucleotide sequences

<b>Protein</b>	<b>Localization</b>	<b>Overlap w/ FLAG-Fbx17?</b>	<b>BL#</b>
Rab1	Endoplasmic reticulum	no	24104
Rab2		no	23246
Rab3		no	9763
Rab4	Early endosomes	no	9767
Rab5	Early endosomes	no	24616
Rab6	Golgi	no	23251
Rab7	Late endosomes	no	23270; 23641
Rab8		no	23272
Rab9		no	9784
Rab9Db		no	50774
Rab9E		no	9833
Rab9Fb		no	23276
Rab10		no	9789
Rab11	Recycling endosomes	no	9790
Rab14		no	9794
Rab18		no	9796
Rab19		no	24150
Rab21		no	23242
Rab23		no	9802
Rab26		no	23244
Rab27		no	24769
Rab30		no	9812
Rab32		no	9815
Rab35		no	9821
Rab39		no	9825
Rab40		no	9830
RabX1		no	23274
RabX2		no	23275
RabX4		no	9851
RabX5		no	9854
RabX6		no	23278
Galt	Golgi	no	30902
KDEL	Endoplasmic reticulum	no	9898
FYVE	PI(3)P-bearing endosomes	no	42712
hLC3	Autophagosomes	no	8730
Atg8a	Autophagosomes	no	52005
Lamp1	Lysosomes	no	

nSyb	Synaptic vesicles	no	6922
Grasp65	Golgi	no	8508
SKL	peroxisomes	no	28882
gammaCOP	Golgi	no	29711
mCD8	membrane and secretory vesicles	no	5130
Chc	Clathrin-coated vesicles	no	
Clc	Clathrin-coated vesicles	no	7101
Sqh	Myosin II	no	42234
Cnn	Centrosomes	no	7255
Snx3	Retromer	rare	
Vps35	Retromer	some	
Vps29	Retromer	rare	
Wls	Membrane/retromer	no	
Ena	Adherens junctions	no	28798
Cindr	Intercellular bridges, apical membrane	yes	50802
Scraps	Anillin	no	51348
Septin2	Septin2	no	26257
Pav	Ring canals	no	
Pod1	Actin/microtubules	no	8800
Klp61F	Mitotic spindles	no	35509

Table 2.2: Co-localization of FLAG-Fbx17 and vesicle markers

## Chapter 3

A JNK-CtBP pathway regulates the growth effector *bantam* in *Drosophila*

### 3.1 Abstract

Multicellular organisms require strict growth control mechanisms to ensure an organ reaches but does not grossly exceed its appropriate size and shape. In an unbiased mosaic screen for genes involved in growth regulation, we identified a loss-of-function allele of the gene *CtBP* that conferred a growth advantage to homozygous mutant tissue. *CtBP* encodes a widely conserved transcriptional co-repressor with a critical function in development, yet its role in regulating tissue growth is unclear. We found that CtBP functions as a negative regulator of growth by restricting the expression of the growth-promoting microRNA *bantam* (*ban*). Though *ban* is a known target of the Hippo pathway effector Yorkie (Yki), reduction of CtBP function in the absence of Yki still leads to the upregulation of a reporter for a 410-basepair minimal enhancer of *ban*. Investigation into how *ban* could be regulated independent of Yki revealed that *ban* enhancer activity is responsive to the Jun N-terminal Kinase (JNK) pathway. JNK signaling has been broadly studied as a stress-response pathway, with both pro-apoptotic and pro-proliferative functions. How such varied cellular responses are balanced by a single pathway remains an unanswered question. Our work suggests that CtBP may interact with specific components of AP-1, the downstream transcriptional effector of the JNK pathway, thereby switching AP-1 from a transcriptional activator to a repressor to mediate distinct signaling outcomes.

### 3.2 Introduction

Tissue growth is a fundamental aspect of animal development. Strict control mechanisms are needed to ensure that an organ does not exceed its correct size, and to allow for growth re-initiation upon tissue damage. How our organs—and the individual cells therein—“know” when to expand, and when to stop growing, are fascinating questions for developmental biologists.

The Hippo pathway is essential for normal development and plays a key role in growth control, through the coordinated regulation of cell proliferation and apoptosis (Huang et al., 2005). Many of the pathway components found in *Drosophila* are shared among diverse metazoans, with great functional conservation in mammals (Sebé-Pedrós, et al., 2012; Zhao et al., 2011). The *Drosophila* Hippo pathway restricts tissue growth by inhibiting the nuclear localization of the transcriptional coactivator Yorkie (Yki) (Huang et al., 2005). Under pro-growth conditions, Yki can accumulate in the nucleus, where it activates numerous target genes, some of which are known to contribute to organ growth—e.g. *cyclin E*, *diap1*, and *bantam*.

While we are far from a complete understanding of the “transcriptional program” of Yki that defines its role in developmental growth, mounting evidence suggests that the components of this program are likely subject to multiple regulatory inputs. Indeed, many studies have demonstrated that Yki-dependent regulatory enhancers often contain consensus binding sites for the transcriptional effectors of other conserved signaling pathways (Pascual

et al., 2017). The regulation of “shared targets” by Yki and other transcriptional effectors could provide a conserved mechanism by which tissue growth is kept in check.

A transcription factor that has been shown to have binding sites in the genetic loci for many Yki targets is AP-1 (Pascual et al., 2017), the downstream transcriptional effector of the c-Jun amino-terminal kinase (JNK) pathway (Eferl and Wagner, 2003). The JNK pathway is a kinase cascade involved in several morphogenetic processes during development and is activated in response to various stress stimuli. JNK signaling has been shown to trigger apoptosis or tumorigenesis, depending on the genetic context, via activation of AP-1. AP-1 are homodimeric and heterodimeric protein complexes consisting of the bZIP-domain containing proteins Fos and Jun. How the same pathway can give rise to such distinct outputs remains a key question.

JNK signaling has been shown to activate Yki activity during tissue regeneration and tumorigenesis (Sun and Irvine, 2011; Sun and Irvine 2013; Enomoto and Igaki, 2013; Enomoto et al., 2015), yet its role in regulating developmental growth is less understood. Recent work has suggested that a low level of JNK activity is normally present in the developing *Drosophila* wing imaginal disc and promotes tissue growth by stimulating Yki activity independent of AP-1 (Willsey et al., 2016).

Here we describe a novel function for the transcriptional co-repressor CtBP in regulating tissue growth by restricting the expression of the growth effector *bantam*. We show that CtBP regulates a minimal *ban* enhancer via both Yki-dependent and Yki-independent mechanisms, and that JNK activity is necessary and sufficient to activate this enhancer. We find that CtBP may regulate this enhancer by antagonizing JNK signaling, and point to a possibility for distinct functions of Fos proteins in mediating this effect. Taken together, our findings support a role for JNK signaling in regulating the transcriptional program underlying developmental growth.

### 3.3 Materials and Methods

#### Cloning and molecular biology

##### *Drosophila* stocks and husbandry

Crosses were maintained on standard fly food at 25°C unless otherwise noted. For experiments sensitive to the effects of developmental staging and vial density, egg deposition was limited to a 4 h window.

The *CtBP*<sup>A147T</sup> allele is an EMS mutation induced on an *FRT82B* chromosome. The *CtBP*<sup>Q229\*</sup> allele (BDSC 1663) has been described as a null allele and was recombined onto the parental *FRT82B* chromosome for use in this study. The *CtBP*<sup>N148fs</sup> mutation was generated on the *FRT82B* chromosome using CRISPR/Cas9 and a guide RNA targeting codon 148.

Transgenic *UAS-CtBP-HA* stocks for overexpression of each unique CtBP protein isoform were generated for this study and integrated at the attP40 landing site.

Additional stocks used were: *FRT82B* (Xu and Rubin, 1993), *GFP-ban* (bantam sensor, Brennecke et al., 2003); *ban3-GFP* (Matakatsu and Blair); *ex<sup>697</sup>* (Boedigheimer and Laughon, 1993); *Diap1 3.5-GFP* (Zhang et al., 2008); *FRT42D yki<sup>B5</sup>* (Huang et al., 2005); *FRT42D MARCM*; *UAS-ban-sponge* (Becam et al., 2011); *UAS-Fos.D* (Ling et al., 2012).

Remaining stocks used in this study were from, or derived from, the Bloomington Stock Center (Bloomington, IN): *FRT82B ubi-RFPnls* (BDSC 30555); *FRT82B MARCM* (BDSC 30036); *UbxFlp*; *FRT42D GFP*; *FRT82B RFP* (BDSC 43340); *FRT82B kay<sup>ED6315</sup>* (BDSC 41772); *brC12-lacZ* (BDSC 44256); *puc<sup>A251.1F3</sup>* (BDSC 11173); *nub-Gal4* (BDSC 25754); *ptc-Gal4* (BDSC 2017); *UAS-GFP* (BDSC 6874); *UAS-yellow-shRNA* (BDSC 64527); *UAS-CtBP-shRNA* (BDSC 32889); *UAS-puc-shRNA* (BDSC 53019); *UAS-Hep-WT* (BDSC 9308); *UAS-Bsk-DN* (BDSC 9311); *UAS-bsk-shRNA* (BDSC 57035); *UAS-Fos* (BDSC 7213); *UAS-fos-shRNA* (BDSC 33379); *UAS-Jun* (BDSC 7216).

## Clonal analysis

For the clone and twin-spot quantification experiments shown in Figure 3.1, clones were induced 48 h after egg deposition with a  $45 \pm 15$  min heat-shock at 37°C and wing imaginal discs were dissected 72 h later. For an individual mosaic disc, the total clone area was determined by tracing all the RFP-negative clones and adding up their areas, and the total twin-spot area was determined by tracing all the 2×RFP-positive clones and adding up their areas.

For the MARCM experiments shown in Figures 3.2 and 3.3, clones were induced 48 h after egg deposition with an hour-long 37°C heat-shock, and wing imaginal discs were dissected 72 h later. Individual clones were traced using the Polygon tool and measured in ImageJ.

## Immunostaining and antibodies

Imaginal discs were dissected from wandering third instar larvae were fixed in PBS + 4% paraformaldehyde for 20 minutes at room temperature, washed and permeabilized in PBS + 0.1% Triton-X, and blocked in PBS + 0.1% Triton-X + 5% goat serum (G9023, Sigma) or donkey serum (D9663, Sigma). Primary antibody stains were performed overnight at 4°C, while secondary antibody stains were performed for 2-4 hours at room temperature.

Primary antibodies were diluted in the same solution used for the blocking step and used at the following concentrations: 1:50 goat anti-dCtBP (dN-20, Santa Cruz Biotechnology); 1:500 rabbit anti-cleaved DCP-1 (9578S, Cell Signaling Technology); 1:500 rabbit anti-β-Galactosidase (559762, MP Biomedicals); 1:500 mouse anti-β-Galactosidase (Sigma); 1:500 mouse anti-GFP; 1:500 rabbit anti-HA (C29F4, Cell Signaling Technology); 1:400 guinea pig anti-Yki; 1:1000 rabbit anti-dFos (a gift from D. Bohmann). Alexa Fluor-conjugated secondary antibodies were from Thermo Fisher Scientific and diluted 1:500 in the appropriate

blocking solution. Nuclei were visualized with DAPI (1:1000). Tissues were mounted in SlowFade Diamond Antifade Mountant (Thermo Fisher Scientific).

Confocal images were obtained on a Zeiss LSM 700 and processed using ImageJ.

## Imaging and processing of adult structures

Adult structures were imaged using a Leica transmitted light microscope (TL RCI, Germany). For adult wing experiments, wings were removed from adult females and mounted onto slides using Gary's Magic Mounting Medium. The outline of each wing was traced using the Polygon tool beginning at the alar-costal break, and the bound area was quantified in ImageJ.

## 3.4 Results

### CtBP is a negative regulator of tissue growth

In an unbiased mosaic screen for genes involved in growth regulation (described in Tapon et al., 2001), we identified an allele of the gene *CtBP* that conferred a growth advantage to homozygous mutant tissue. Mutant clones of this allele, *CtBP<sup>A147T</sup>*, generated by *eyFlp/FRT*-mediated mitotic recombination, were overrepresented in the adult eye when compared to clones of the parental *FRT82B* chromosome (Figure 3.1A-B). *CtBP* encodes a widely conserved transcriptional co-repressor and was originally identified for its ability to bind the C-terminus of the adenovirus E1A oncoprotein in mammalian cells (Boyd et al., 1993). Subsequent work has shown that, in both vertebrates—which have two *CtBP* genes—and invertebrates—which have just one—the CtBP proteins can form interactions with a large number of DNA-binding transcriptional repressors to regulate gene expression (reviewed in Turner and Crossley, 2001; and Chinnadurai, 2007). Many of these repressors possess a PxDSL motif that is important for CtBP-binding. In *Drosophila*, the *CtBP* gene is predicted to produce multiple short (379-386 a.a.) and long (473-481 a.a.) protein isoforms via alternative splicing (Figures 3.1N, 3.2A).

The *CtBP<sup>A147T</sup>* allele failed to complement a previously described null allele of *CtBP* (*CtBP<sup>87De-10</sup>*, which we will refer to henceforth by its nonsense mutation *CtBP<sup>Q229\*</sup>*). This null allele causes embryonic lethality in homozygous animals, while animals homozygous for the *CtBP<sup>A147T</sup>* allele survive to the late pupal stage, suggesting that the *CtBP<sup>A147T</sup>* allele recovered in our screen is likely a hypomorph. It has been reported previously that *CtBP<sup>Q229\*</sup>* clones are larger than wild-type clones in mosaic eye imaginal discs (Hoang et al., 2010). We observe this result as well (Figure 3.1G), with adult eyes consequently exhibiting large mutant clones (Figure 3.1C). In addition to this published null allele, we used CRISPR/Cas9-directed mutagenesis to generate a 13-bp deletion in the first coding exon of *CtBP* on the *FRT82B* chromosome. The deletion causes a frameshift mutation, *CtBP<sup>N148fs</sup>*,

and consequent premature stop codon. Mutant clones of this likely null allele also display a growth advantage in mosaic eyes (Figure 3.1D).

Owing to its pleiotropic effects on gene expression, *Drosophila* CtBP has been implicated in a number of developmental processes, including embryonic segmentation (Poortinga et al., 1998; Nibu et al., 1998) and appendage patterning (Biryukova and Heitzler, 2008; Hoang et al., 2010), yet less is known about its specific function in tissue growth control. Though our results support a previous report’s findings that CtBP regulates cell proliferation within the developing eye (Hoang et al., 2010), whether this growth function extends beyond eye development has not been shown. To address this, we generated *CtBP* mutant clones throughout the imaginal discs using *hsFlp/FRT*-mediated mitotic recombination. Because the *CtBP* mutation is flipped over an FRT chromosome bearing a fluorescent marker, we could directly compare the area of *CtBP* mutant tissue—marked by the absence of the fluorescent marker—to that of the wild-type twin-spot tissue. We found that for all three *CtBP* alleles, homozygous mutant clones comprised nearly twice as much of the whole wing disc as did twin-spot tissue, while in control mosaic discs, the total areas of unmarked and twin-spot tissue are roughly the same (Figure 3.1E-M). We also noticed that, particularly for the two null alleles, *CtBP* mutant clones had smooth edges (Figure 3.1G-H, K-L).

Overexpressing each individual protein isoform of CtBP in the wing pouch consistently led to an overall size reduction of the adult wing, as well as ectopic vein tissue, likely reflecting CtBP’s dual roles in growth and patterning (Figure 3.2B-E). However, the severity of these phenotypes was variable between isoforms and even when assessing the effects of a single isoform, particularly those that fell into the “short” category. In general, overexpression of the “long” isoforms resulted in smaller, rounder wings and mild ectopic vein formation (Figure 3.2C), while overexpression of the “short” isoforms caused a proportionally reduced wing size and excessive ectopic veins (Figure 3.2D). Though the differences observed between the short and long isoform overexpression phenotypes support the idea that distinct CtBP isoforms may have unique biological functions, we chose not to pursue these differences further. In summary, the phenotypes associated with both *CtBP* loss-of-function and overexpression indicate a negative growth-regulatory function for CtBP.

## CtBP limits tissue growth by repressing *bantam* expression

We next sought to understand why *CtBP* mutant clones are overgrown. Given CtBP’s identity as a transcriptional co-repressor, we explored the possibility that CtBP may normally restrict tissue growth by regulating the expression of known growth effectors. We focused on readouts of the Hippo pathway due to its evolutionarily conserved function as a key regulator of organ size. We tested the effects of manipulating CtBP function on *in vivo* transcriptional reporters for the Yki target genes *bantam* (*ban*), *expanded* (*ex*), and *diap1*, as well as the protein expression pattern of Yki. In *CtBP<sup>Q229\*</sup>* clones, expression of a *ban3-GFP* enhancer reporter (Figure 3.3A-A’’; Matakatsu and Blair, 2012) was increased, particularly along clonal boundaries (arrowhead in Figure 3.3A’-A’’). We also observed a slight upregulation of *ex* (Figure 3.3B-B’’), as assessed by a *ex<sup>lacZ</sup>* enhancer trap (*ex<sup>697</sup>* [Boedigheimer and

Laughon, 1993]) though this seemed to occur just along the cells in contact with wild-type tissue (arrowhead in Figure 3.3B'-B''). Expression of a *diap1-GFP* transgenic reporter (Zhang et al., 2008) was unchanged in *CtBP<sup>Q229\*</sup>* clones (Figure 3.3C-C''). An antibody stain for Yki was not appreciably altered by loss of *CtBP*, showing, if anything, a slight decrease in overall levels within a *CtBP<sup>Q229\*</sup>* clone (Figure 3.3D-D'').

The *ban* gene encodes a microRNA (miRNA) that promotes growth by stimulating cell proliferation and inhibiting apoptosis (Brennecke et al., 2003). Consistent with the observed increase in *ban3-GFP* enhancer activity, a *GFP-ban* sensor, which inversely reports *ban* miRNA levels (Brennecke et al., 2003) showed decreased GFP levels in *CtBP<sup>Q229\*</sup>* clones (Figure 3.4A-A''), indicated higher levels of *ban* miRNA activity. Conversely, Flp-out Gal4 clones that overexpress CtBP show higher *GFP-ban* sensor expression, indicating reduced *ban* miRNA levels (Figure 3.4B-B''). We note that this effect is shown via overexpression of the short CtBP.I-HA isoform (Figure 3.4B-B''), but we also tested the short CtBP.A-HA and long CtBP.E-HA isoforms and observed increased *GFP-ban* in clones overexpressing these isoforms as well (not shown).

Our results suggest that increased *ban* expression may be responsible for the overgrowth phenotype of *CtBP* mutant tissue. To confirm this model, we tested whether reducing *ban* levels can suppress the overgrowth of *CtBP* mutant clones using the MARCM technique, which allows for the expression of UAS transgenes within mosaic clones (Lee and Luo, 1999). Expression of a previously described *ban* sponge transgene (*ban-sp.*), which contains repeated *ban*-binding sites to deplete the endogenous pool of available *ban* miRNA (Becam et al., 2011), significantly reduced the growth of *CtBP<sup>Q229\*</sup>* MARCM clones (compare Figure 3.4D to 3.4E; quantified in 3.4G). The average size of *CtBP<sup>Q229\*</sup>* clones expressing *ban-sp.* did not differ significantly from that of control *FRT82B* clones expressing *ban-sp.* (compare Figure 3.4D to 3.4F; quantified in 3.4G). Taken together, these results suggest a role for CtBP in regulating tissue growth via repression of the growth-promoting miRNA *ban*.

## CtBP regulates a minimal *bantam* enhancer, *brC12* via Yorkie-dependent and Yorkie-independent mechanisms

CtBP is thought to be incapable of binding DNA itself and so we next wondered what factors might mechanistically link CtBP to *ban* regulation. Within the *ban3* enhancer sequence used to generate the *ban3-GFP* reporter is a roughly 400-basepair sequence, *brC12* (Figure 3.5A), that has been previously shown to function as a Yki-dependent minimal *ban* enhancer (Oh and Irvine, 2011). When we tested whether this enhancer is sensitive to changes in *CtBP*, we detected upregulation of a *brC12-lacZ* reporter gene in *CtBP<sup>Q229\*</sup>* MARCM clones (Figure 3.5B-B'). Overexpressing CtBP in *CtBP<sup>Q229\*</sup>* MARCM clones could fully suppress this increased enhancer activity (we show use of the long isoform E in Figure 3.5C-C' but also observed a similar effect using the short isoform A). By identifying a minimal sequence by which CtBP is capable of regulating *ban*, we sought to use this readout to further probe the mechanism linking CtBP to growth.

Because the minimal *brC12* enhancer is known to be regulated in a Yki-dependent manner, we next tested whether *yki* is required for the increased reporter activity caused by loss of *CtBP*. This was done by generating *yki*<sup>B5</sup>; *CtBP*<sup>Q229\*</sup> double-mutant clones using UbxFlp and double FRT chromosomes and assaying *brC12-lacZ* reporter activity (Figure 3.5D-F). Because the *yki* and *CtBP* alleles are carried on separate FRT chromosomes, they can be independently flipped over uniquely marked FRT chromosomes (Figure 3.5D-D'). As outlined in Fig. 3.5D'', this will result in four genetically-distinct populations of cells distinguishable by their fluorescent markers: (1) cells that lack *yki* function but have at least one functional copy of *CtBP* are red; (2) cells that lack *CtBP* function but have at least one functional version of *yki* are green; (3) cells that have at least one functional copy of both *yki* and *CtBP* are yellow; and (4) cells that are double-mutant lack all fluorescent markers and hence appear black. Consistent with previous reports and the results shown in Figure 3.5B-B', *brC12-lacZ* reporter activity is completely abolished in *yki* single-mutant tissue (single-asterisk in Figure 3.5F-F') and is elevated in *CtBP* single-mutant tissue (double-asterisk in Figure 3.5F-F') as compared to wild-type tissue (dotted outline in Figure 3.5F-F'). If regulation of *brC12* enhancer activity by CtBP were solely Yki-dependent, then double-mutant tissue would be predicted to have the same level of reporter activity as that found in *yki* single-mutant tissue. In fact, *brC12-lacZ* expression actually appeared slightly higher in the double-mutant tissue (solid outline in Figure 3.5F-F') than in the *yki* single-mutant tissue (single-asterisk in Figure 3.5F-F'), but was still lower than that of the *CtBP* single-mutant tissue. This intermediate phenotype suggests that there is both a Yki-dependent and Yki-independent component by which CtBP regulates *ban* enhancer activity.

### ***brC12* activity depends on a basal level of JNK signaling**

We sought to further explore the Yki-independent component to *ban* regulation. We identified a putative AP-1 binding site, TGAGTCA (Olive et al., 1997), within a highly conserved region of the *brC12* sequence (Figure 3.6A). AP-1 is the downstream transcriptional effector of the JNK pathway (Figure 3.6B), suggesting that *ban* enhancer activity may be regulated by JNK signaling. To test this, we assayed the effects of various JNK pathway manipulations on the *brC12-lacZ* reporter, using a *ptc-Gal4* driver. As shown in Figure 3.6C and C'', this reporter displays a relatively uniform expression pattern throughout the wing imaginal disc. Blocking JNK signaling via expression of a dominant-negative version of the Drosophila JNK protein Basket (Bsk-DN) (Figure 3.6D) completely abolished reporter expression within the *ptc-Gal4* stripe (Figure 3.6D''). This suggests that *ban* enhancer activity is dependent on a basal level of JNK signaling that is normally present throughout undamaged discs.

Because the JNK pathway is known to promote apoptosis (Igaki, 2009), this can complicate interpretation of *brC12-lacZ* expression changes under conditions of JNK pathway over-activation, as growth effectors are often upregulated to compensate for loss of tissue. For instance, elevating pathway activity via knockdown of the JNK phosphatase Puckered (Puc) resulted in an increase in both *brC12-lacZ* expression (Figure 3.6E'') and apoptosis, as detected by DCP-1 staining (Figure 3.6E'''). However, when we mildly activated JNK

signaling by overexpressing the JNK kinase Hemipterous (Hep), we observed elevated levels of *brC12-lacZ* expression (Figure 3.6F'') without an appreciable increase in apoptosis (Figure 3.6F'''). Taken together, our results suggest that activity of the minimal *ban* enhancer is JNK-dependent and may be uncoupled from the role of JNK signaling in apoptosis.

## CtBP regulates *brC12* activity by antagonizing JNK signaling

Previously, our group has reported that loss of *CtBP* function results in the upregulation of several reporters of AP-1 activity (Worley et al., 2018), suggesting that JNK and CtBP may have opposing effects on shared transcriptional targets. Since we have demonstrated the minimal *ban* enhancer is activated by JNK signaling, we hypothesized CtBP may normally antagonize this effect, which could explain why *brC12-lacZ* expression is increased in *CtBP* mutant tissue. To determine if CtBP regulates the *ban* enhancer in a JNK-dependent manner, we co-expressed Bsk-DN with CtBP-targeting shRNA using *ptc-Gal4* and examined reporter expression. Due to persistent knockdown of the CtBP protein, as revealed by CtBP immunostaining, in cells that previously but stopped expressing *Gal4*, we consistently observed increased levels of the *brC12-lacZ* reporter outside of the current *ptc-Gal4* expression domain, indicated by UAS-GFP expression (marked by yellow brackets in Figure 3.7A-B). Taking advantage of the persistent CtBP knockdown caused by *ptc-Gal4*-driven expression of the *CtBP-shRNA* transgene, we co-expressed the shorter-lived Bsk-DN protein, whose function is presumably limited to the current *ptc>GFP* domain, to assess enhancer activity in *CtBP*-knockdown tissue with or without JNK signaling (Figure 3.7B-B'). Whereas *brC12-lacZ* levels were increased in cells lacking CtBP alone (marked by yellow brackets in Figure 3.7B-B'), knocking down CtBP and blocking JNK signaling brought reporter expression down to levels similar to what we observed in the non-*Gal4/UAS*-expressing tissue (Figure 3.7B'). Thus, JNK signaling is required for the full upregulation of *brC12* activity caused by loss of *CtBP*. Notably, co-expression of Bsk-DN and CtBP-shRNA did not appear to reduce reporter levels to the same extent observed when overexpressing Bsk-DN alone (compare Figure 3.6D'' to 3.7B'), suggesting that there are still distinct mechanisms by which CtBP and the JNK pathway regulate the *brC12* enhancer.

## Loss of distinct Fos isoforms leads to increased *brC12* enhancer activity

Given CtBP's identity as a transcriptional co-repressor, one possible mechanism by which CtBP could antagonize JNK activity is through a functional interaction with AP-1. The AP-1 complex is typically thought of as a transcriptional activator and is formed by heterodimeric interactions between the transcription factors Jun (also known as Jra) and Fos (also known as Kayak and Fra). Intriguingly, protein sequence analysis reveals that 2 of the 5 predicted isoforms of Fos, isoform A and isoform G, possess the canonical CtBP binding motif, PxDSL (Figure 3.8A). Thus, we speculated that CtBP could be recruited to the *ban* locus by AP-1 complexes containing these Fos proteins to mediate transcriptional repression. We therefore

reasoned that eliminating these isoforms might phenocopy the effect of inactivating *CtBP*. To test this, we took advantage of a  $\sim 17$ kb chromosomal deletion, *Df(3R)ED6315*, removes 3 of the 4 alternatively spliced 5' exons of the *fos* gene and spans the transcriptional start sites for 3 of the 5 isoforms, including A and G (Figure 3.8A). When we made mitotic clones that are homozygous for this deletion (Figure 3.8B-B''), we observed elevated *brC12-lacZ* reporter levels within these clones (Figure 3.8B''). The chromosomal region that is removed by the *Df(3R)ED6315* deficiency also contains two additional genes, *fos intronic gene (fig)* (Figure 3.8A) and the lncRNA *CR46110* (not shown), neither of which have well-characterized functions. While we cannot exclude the possibility that elimination of one or more of these factors may be causing the observed increase in enhancer activity, given the analysis presented thus far, we take this result to suggest that some Fos isoforms may have a repressive function.

To determine if all Fos isoforms restrict *brC12* enhancer activity, we knocked down *fos* using an shRNA that targets all isoforms (Figure 3.8C). Expressing this shRNA using *ptc-Gal4* had no appreciable effect on *brC12-lacZ* expression (Figure 3.8C-C'). Immunostaining with an anti-Fos antibody confirmed Fos knockdown in the *ptc-Gal4* expression domain and also revealed that Fos is present at very low levels throughout the disc proper (Figure 3.8C'''), where most of our analyses of the *brC12-lacZ* reporter have so far been performed. Greater Fos protein expression was instead observed in the peripodial epithelium (Figure 3.8D-D'), wherein *ptc-Gal4* expression is limited to only a thin strip of cells (Figure 3.8D).

The results presented in this section are so far consistent with three possible models. In one, Fos is not required for regulation of *brC12* enhancer activity, which is why *fos* knockdown had no effect on *brC12-lacZ* expression, and, despite the apparent AP-1 binding site identified in the minimal *ban* enhancer, JNK signaling activates the enhancer via a Fos/AP-1 independent mechanism. In this scenario, *brC12* reporter activity is sensitive to loss of some other factor removed by the *Df(3R)ED6315* deficiency. A second model predicts that while Fos/AP-1 is normally involved in transcriptional activation, certain Fos isoforms may function, either primarily or in certain contexts, as transcriptional repressors. The result of knocking down all Fos isoforms could simply represent an "averaging" of these opposing effects. A third model could involve a hybrid of the first two models, in which JNK signaling activates the *ban* minimal enhancer via both AP-1-independent and AP-1-dependent mechanisms.

## **The *brC12* enhancer is activated by Fos in an isoform-specific manner**

If distinct Fos isoforms do have specific effects on the *brC12* enhancer, then overexpressing each isoform individually could offer insights into their specific functions. Due to limitations in available transgenic fly lines, we were able to assess the overexpression effects of only two isoforms, D and A, both of which are predicted to be affected by the *Df(3R)ED6315* deficiency. Overexpression of isoform D (also known as the  $\alpha$  isoform but which we will

henceforth refer to as Fos.D; Figure 3.8E) resulted in an upregulation of *brC12-lacZ* expression (Figure 3.8E''), indicating that Fos.D is capable of activating the minimal enhancer. Overexpression of one of the PxDLS-containing Fos isoforms, isoform A (also known as the  $\beta$  isoform but which we will henceforth refer to as Fos.A; Figure 3.8F), had no effect on *brC12* enhancer activity (Figure 3.8F''). Staining with an antibody that recognizes all Fos isoforms revealed that ectopic Fos.A was stably expressed (Figure 3.8F''), to a greater degree, in fact, than ectopic Fos.D (Figure 3.8E''). Because Fos and Jun together have been shown to form more stable protein-DNA complexes and thereby activate transcription to a greater extent than either of the proteins alone (Perkins et al., 1990), we also co-expressed Fos.A with Jun (Figure 3.8G). This did not result in any appreciable change in *brC12* enhancer activity (Figure 3.8G'') but was sufficient to upregulate a known target, *mmp1* (as assessed by MMP1 antibody staining; Figure 3.8G''). Thus, Fos.A does not appear to regulate the minimal *ban* enhancer. While this study did not directly test the effects of overexpressing the Fos isoform G (Fos.G), since it is the other isoform affected by the *Df(3R)ED6315* deficiency and is predicted to bind CtBP (Figure 3.8A), it is possible that the upregulation in *brC12* activity observed in *Df(3R)ED6315* clones (Figure 3.8B'') is caused by loss of *fos.G*. Furthermore, Fos.A may still be capable of repressing *brC12* activity, but this may require a greater abundance of CtBP. Finally, since Fos.D was capable of activating the minimal enhancer (Figure 3.8'') yet was predicted to be compromised by the *Df(3R)ED6315* deficiency (Figure 3.8A), then one might expect—as we have suggested was the case when all *fos* isoforms were knocked down—that *Df(3R)ED6315* clones should have exhibited a similar averaging of *brC12* activation and repression effects. One possibility is that the levels of each isoform may differ within a tissue, and so the effects of losing some of all Fos isoforms will most closely match the functional loss of those isoforms that are most abundant.

## CtBP may regulate a subset of AP-1 target genes

Since our group has previously shown that transcriptional reporters of AP-1—namely *AP-1-GFP*, *dilp8-GFP*, and *mmp1-lacZ*—are autonomously upregulated in *CtBP* mutant clones (Worley et al., 2018), we wondered if CtBP is a general negative regulator of AP-1 targets. *puc* is a transcriptional target of JNK signaling. Because it encodes a phosphatase for JNK, its expression forms a negative feedback loop on JNK activity (Figure 3.6B). We examined the expression of a *puc-lacZ* enhancer trap (*puc<sup>A251.1F3</sup>*) when *CtBP* is knocked down. As this *lacZ* enhancer trap is also an allele of *puc*, heterozygosity for *puc-lacZ* should provide a sensitized background with a modest elevation in overall JNK activity throughout the animal. Normally, *puc-lacZ* expression in the wing imaginal disc is uniformly low throughout the disc proper (Figure 3.9A'-C') but is strongly detected in the stalk and peripodial epithelium. Knocking down *CtBP* using *ptc-Gal4* did not affect *puc-lacZ* expression within the area of knockdown in the pouch (Figure 3.9D', F-F') but did result in its upregulation within a region of the dorsal hinge (Figure 3.9 E-E'). While *ptc-Gal4* expression is restricted to the stripe of anterior cells along the compartment boundary, we observed *puc-lacZ* induction in both compartments. This ectopic *puc-lacZ* expression is accompanied by a disruption in

tissue morphology, reminiscent of the ectopic fold phenotypes associated with altered Dpp signaling (Liu et al., 2016). CtBP is known to antagonize Dpp signaling (Hasson et al., 2001), and so this phenotype likely reflects an interaction between elevated levels of Dpp and JNK activation (resulting from the *puc-lacZ* allele). As a test of this, we co-expressed *CtBP-shRNA* with Bsk-DN (3.9G-I'). Indeed, this abolished the upregulation of *puc-lacZ* within the dorsal hinge, though it did not prevent formation of an ectopic fold in this region (Figure 3.9H-H'). Strikingly, this also resulted in activation of the *puc* reporter within a group of cells in the pouch (Figure 3.9I-I') that was not observed under conditions of *CtBP* alone (Figure 3.9F-F'). These cells did not appear to have the morphology characteristic of cells undergoing apoptosis. Because *puc-lacZ* expression was not uniformly increased within the area of *CtBP* knockdown, this suggests that CtBP is not a general regulator of AP-1 target genes.

### 3.5 Discussion

In this study, we demonstrate a role for the transcriptional corepressor CtBP in restricting tissue growth during *Drosophila* development, in part by regulating the expression of the growth-promoting microRNA *ban*. Our work extends a previously reported role for CtBP in regulating cell proliferation in the developing eye (Hoang et al., 2010). Our finding that *CtBP* mutant clones are overgrown in other tissues, namely the wing imaginal disc, suggests that CtBP has important functions in ensuring proper organ size throughout the animal. While CtBP is widely conserved among eukaryotes, *ban* is specific to invertebrates (Brennecke et al., 2003), making it difficult to extend the implications of our findings to other systems. Indeed, the functions of the two *CtBP* genes in mammals in the context of growth is already quite complicated, and includes both tumor-suppressive and oncogenic capabilities (reviewed in Chinnadurai, 2007).

Our investigation into the mechanism by which CtBP represses *ban* led us to uncover a role for the JNK pathway in regulating the activity of a minimal *ban* enhancer, *brC12*. The widely conserved JNK kinase cascade is known to be activated in response to a variety of stress stimuli and has key roles in regeneration and tumorigenesis. However, its function in developmental growth is less understood. It has been reported that a localized stripe of phosphorylated ('active') JNK (pJNK) along the anterior-posterior (A/P) compartment boundary in the wing imaginal disc is critical for proper disc growth and that inhibiting this JNK activity results in a reduction in overall wing size (Willsey et al., 2016). In our study, we did not specifically quantify the effects of similarly performed JNK pathway manipulations on tissue size, and could not observe any consequence of the reported pJNK stripe. However, our finding that the *brC12-lacZ* reporter can detect a seemingly uniform basal level of JNK signaling throughout the wing imaginal disc (Figure 3.6D) is consistent with the idea that low levels of JNK activity are important for normal growth. We note that we were unsuccessful at correlating the observed changes in *brC12* enhancer activity caused by JNK pathway manipulations with an appropriate modulation of the *GFP-ban* sensor. Further investigation

into whether *ban* expression is truly increased—and is necessary—for JNK-dependent tissue growth would aid our understanding of how JNK signaling regulates developmental growth.

While we have shown that the *brC12* enhancer is activated by both Yki-dependent and Yki-independent mechanisms, this study has not clarified which of these branches involves JNK signaling. In fact, JNK pathway regulation of the *brC12* enhancer may even involve Yki-dependent and Yki-independent components. Clearly the mechanism by which JNK signaling regulates *brC12* enhancer activity remains an open question. We have identified a consensus AP-1 binding site within a conserved region of this enhancer sequence, but have not yet determined whether this site is functional. In the report by Willsey et al. (2016), it was determined that JNK signaling regulates wing size independent of AP-1 because knocking down *fos* and *jun*, both individually and together, did not affect overall wing size. Taking into account only the results of our experiments knocking down *fos* (Figure 3.8C) or overexpressing Fos.A either alone (Figure 3.8F) or with Jun (Figure 3.8G)—each of which caused no obvious change in *brC12-lacZ* expression—it would be reasonable to conclude that JNK signaling similarly regulates *brC12* enhancer activity independent of AP-1. However, our observations that ectopic expression of the Fos.D isoform (Figure 3.8E) and that mitotic clones that are homozygous for a deficiency predicted to cause functional loss of the D, A, and G *fos* isoforms (Figure 3.8B) activate the *brC12* enhancer suggest that, while its role may be complex, Fos/AP-1 still regulates the minimal enhancer. Based on our prediction that the A and G isoforms can bind CtBP, we propose that these Fos isoforms may restrict target gene transcription by recruitment of CtBP to genetic loci defined by their AP-1 binding sites. Future studies will determine whether CtBP does indeed form a physical interaction with these Fos isoforms and, if so, whether these interactions mediate a repressive function for Fos. Additional analysis of the growth functions of the untested Fos isoforms would also provide a better understanding of the functional requirement for Fos in regulating *brC12* enhancer activity.

The idea that CtBP, through its interactions with distinct Fos isoforms, may switch AP-1 from a transcriptional activator to a repressor is an exciting one, and could be generalized to other examples of AP-1-dependent transcriptional regulation. In fact, a study of circadian rhythm behavior has previously demonstrated a unique requirement for Fos.D in regulating *Clock* (*Clk*) expression via its isoform-specific interaction with the *Clk* repressor VRI (Ling et al., 2012). Thus, the distinct N-terminal regions of the Fos isoforms may form interactions with unique binding partners, which may in turn confer distinct functions in a variety biological processes. Because the JNK pathway is activated by multiple and diverse stimuli to mediate varied—and, at times, seemingly contradictory—cellular outcomes, an important question has been how activation of a single pathway can elicit distinct responses. Our work suggests that the functions of distinct Fos isoforms could provide insight into this question.

### 3.6 Figures

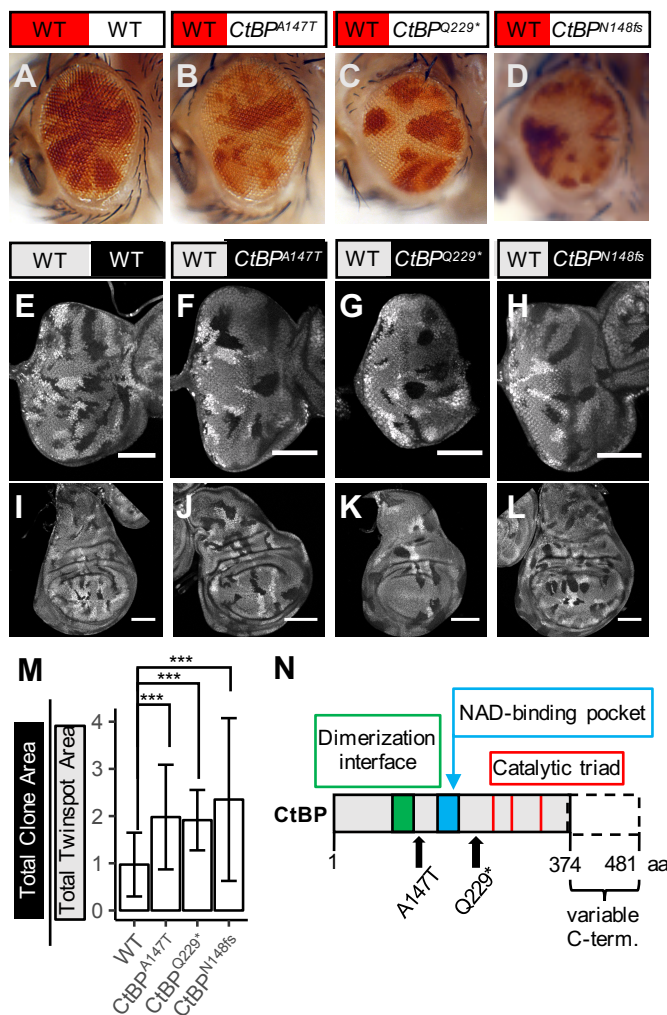


**Figure 3.1: Mutations in *CtBP* result in increased tissue growth.** (A-D) Mosaic adult eye assay. Mutant tissue is marked by the absence of red pigment. (A) Control mosaic eyes. (B) *CtBP*<sup>A147T</sup>, (C) *CtBP*<sup>Q229\*</sup>, and (D) *CtBP*<sup>N148fs</sup> mosaic eyes have more mutant tissue. (E-L) *hsFlp*-induced mosaic eye (E-H) and wing (I-L) imaginal discs. Mutant tissue is marked by the absence of a fluorescent marker. Scale bars, 100  $\mu$ m. (M) Graph showing the ratio of total mutant tissue to total wild-type twin-spot tissue measured from mosaic wing discs of the genotypes shown in I-L.  $n=12, 9, 9,$  and  $5$  discs per genotype, respectively. Data are presented as mean  $\pm$  SD. Statistical significance was determined using one-way ANOVA with Tukey's post-hoc test.  $***p \leq 0.001$ . (N) Protein model of *Drosophila CtBP* showing general domain structures and the three coding mutations used in this study. The gray region is shared by all predicted isoforms.



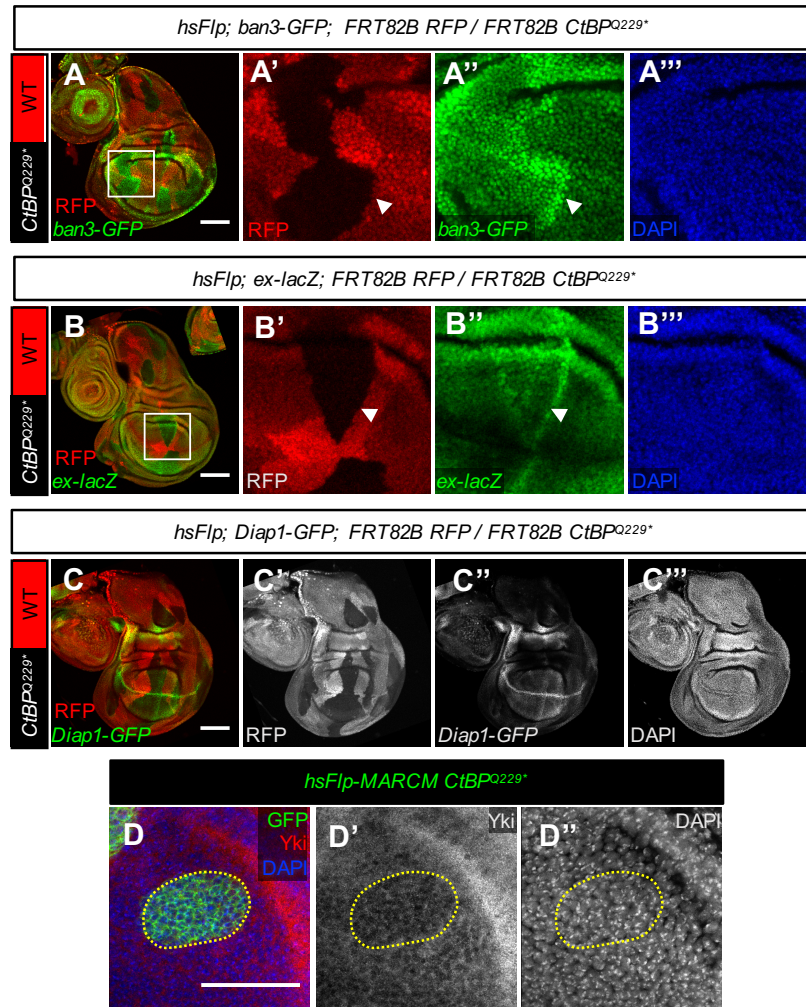


Figure 3.3: **Analysis of Yki activity in *CtBP* mutant clones.** (A-C) Analysis of *in vivo* transcriptional reporters for Yorkie targets in mosaic wing imaginal discs. Wild-type cells are marked with RFP and *CtBP<sup>Q229\*</sup>* clones are unmarked. (A-B) Mutant clones show increased levels of *ban3-GFP* (A'', green) and *ex-lacZ* (B'', green), particularly along clonal boundaries (arrowheads). Boxes indicate areas enlarged in A'-A''' and B'-B'''. Scale bars, 100  $\mu\text{m}$ . (C-C'') *Diap1-GFP* expression is only not appreciably altered in *CtBP<sup>Q229\*</sup>* clones. Scale bar, 100  $\mu\text{m}$ . (D-D'') An antibody stain for endogenous Yki shows that it is weakly decreased in a MARCM *CtBP<sup>Q229\*</sup>* clone (outlined). Scale bar, 50  $\mu\text{m}$ . DAPI shows nuclei.

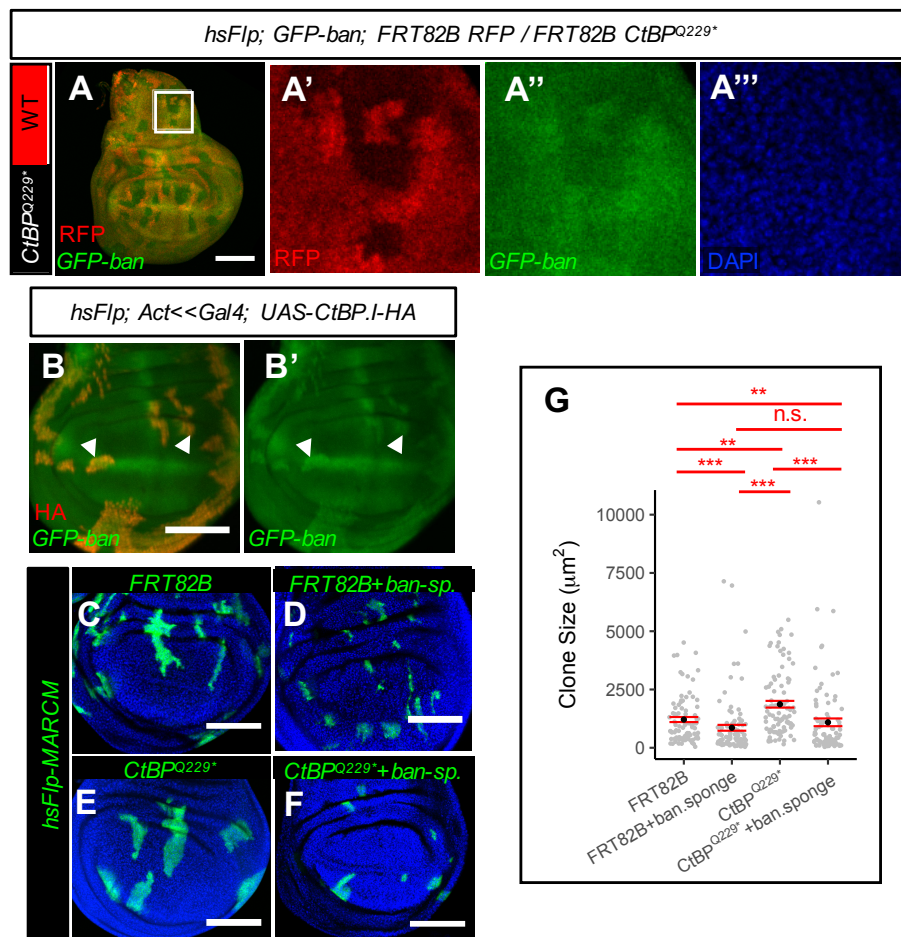


Figure 3.4: **Increased *ban* activity is required for overgrowth of *CtBP* clones.** (A-B) Analysis of the *GFP-ban* sensor, which inversely reports *ban* microRNA activity, in clones mutant for or overexpressing *CtBP*. (A-A''') *CtBP<sup>Q229\*</sup>* clones (unmarked) have lower levels of the *GFP-ban* sensor (green). Box indicates areas enlarged in subsequent panels. (B-B') Flp-out Gal4 clones overexpressing *CtBP* show higher levels of the *GFP-ban* sensor (green). Use of the short isoform *CtBP.I-HA* is shown and the clones were detected by HA staining (red). Arrowheads show examples of increased *GFP-ban* sensor. (C-G) MARCM clone size assay. MARCM Gal4 clones (green) were induced by expression of *hsFlp* following a 1-hour heat-shock at  $\sim 48$  hours after egg-lay. Discs were dissected  $\sim 72$  hours ACI. Shown are representative wing pouches with (A) *FRT82B* control clones, (B) *FRT82B* control clones overexpressing a *ban* sponge (*ban-sp.*), (C) *CtBP<sup>Q229\*</sup>* mutant clones, and (D) *CtBP<sup>Q229\*</sup>* mutant clones overexpressing *ban-sp.* (E) Quantification of individual clone sizes (in pixels) from the genotypes shown in C (n=87), D (n=97), E (n=92), and F (n=90), respectively. All data points (gray dots) are shown along with mean (black dots) and SEM (red error bars). Statistical significance was taken as  $p \leq 0.05$  and assessed by performing pairwise comparisons of each MARCM condition using a Wilcoxon rank sum test. \*\*\*  $p \leq 0.001$ . \*\*  $p \leq 0.01$ . All scale bars in figure,  $100 \mu\text{m}$ . DAPI shows nuclei (blue).

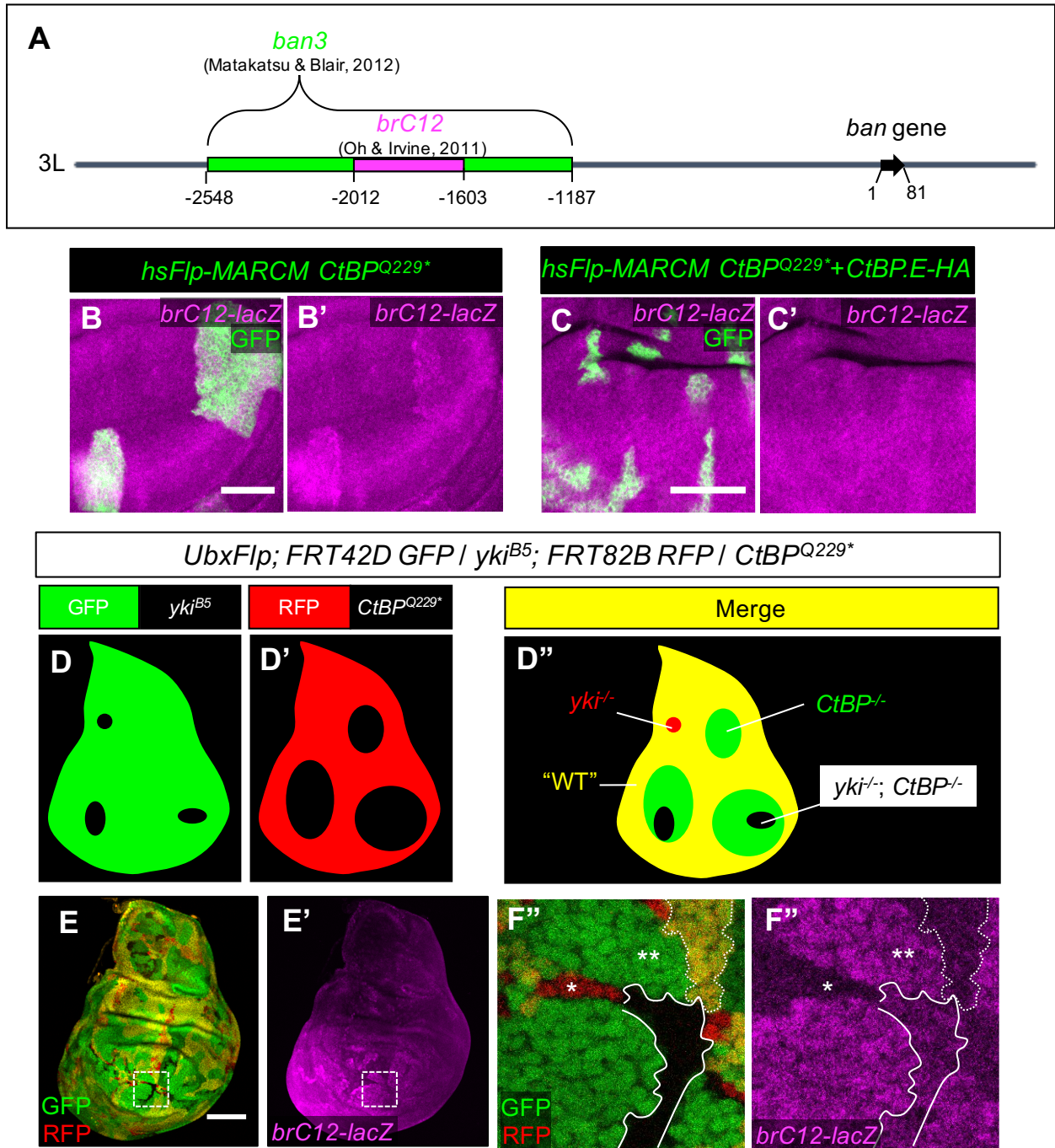


Figure 3.5: CtBP regulates a minimal *ban* enhancer, *brC12* via Yki-dependent and Yki-independent mechanisms.

(A) A schematic of the *ban* locus showing the enhancer regions that were cloned into the *ban3-GFP* (green) and *brC12-lacZ* (magenta) reporter transgenes. (B-B') *CtBP<sup>Q229\*</sup>* MARCM clones (green) show increased expression of a minimal bantam enhancer reporter, *brC12-lacZ*. Scale bar, 50  $\mu\text{m}$ . (C-C') CtBP overexpression in *CtBP<sup>Q229\*</sup>* clones via the MARCM technique could fully suppress the upregulation of *brC12-lacZ* (use of the long isoform E is shown). Scale bar, 50  $\mu\text{m}$ . (D-F) Expression levels of the *brC12-lacZ* were assessed in *yki<sup>B5</sup>;CtBP<sup>Q229\*</sup>* double-mutant clones. (D-D'') A schematic showing the technique used to generate the double-mutant clones shown in (E-F). *UbxFlp*-induced mitotic recombination independently generates (D) GFP-negative *yki<sup>B5</sup>* clones and (D') RFP-negative *CtBP<sup>Q229\*</sup>* clones, resulting in (D'') four genetically-distinct cell populations: clones mutant for *yki* but wild-type for *CtBP* are red, clones mutant for *CtBP* but wild-type for *yki* are green, clones that have at least one functional copy of both *CtBP* and *yki* are yellow, and double-mutant clones lack all fluorescent markers and hence appear black. (E-F) Clones of all four genotypes could be recovered in a single disc, allowing for assessment of the *brC12-lacZ* reporter in each. Scale bar, 100  $\mu\text{m}$ . (F-F'') A magnification of the dashed boxes in E-E'. Compared to wild-type tissue (dotted outline), the *brC12-lacZ* reporter is increased in *CtBP* mutant tissue (double-asterisk) and decreased in *yki* mutant tissue (single-asterisk). Double-mutant tissue (solid outline) shows intermediate levels of the *brC12-lacZ* reporter.



(A) Sequence alignment of a region of the *brC12* enhancer with putative AP-1 consensus site (magenta). The DNA sequences of the *ban* locus from seven fly species were obtained from Oh and Irvine (2011). Asterisks mark nucleotides identical in all seven species. The region shown is spanned by nucleotides 67-128 of the enhancer, using the *D. melanogaster* sequence as a reference. (B) A schematic of the JNK pathway. (C-F) Manipulations of different JNK pathway components were performed by expressing various UAS-transgenes in the *ptc*-domain (green) and the effects on the *brC12-lacZ* reporter (magenta) were assessed in wing imaginal discs. Boxes indicate the areas of the wing pouch that are enlarged in subsequent panels. DAPI shows nuclei (blue). (C-C'') A control disc showing *brC12-lacZ* reporter expression when a neutral transgene, yellow-shRNA, is expressed. (D-D'') Blocking JNK signaling using a dominant-negative form of Bsk/JNK reduces *brC12-lacZ* expression levels. (E-E'') Strong pathway activation via knockdown of *puc* (E'') upregulates *brC12-lacZ* expression but also leads to (E''') apoptosis. (F-F'') Elevating JNK pathway activity via expression of a wild-type form of Hep/JNKK causes (F'') upregulation of *brC12-lacZ* without increasing (F''') apoptosis. Scale bars, 100  $\mu\text{m}$ .

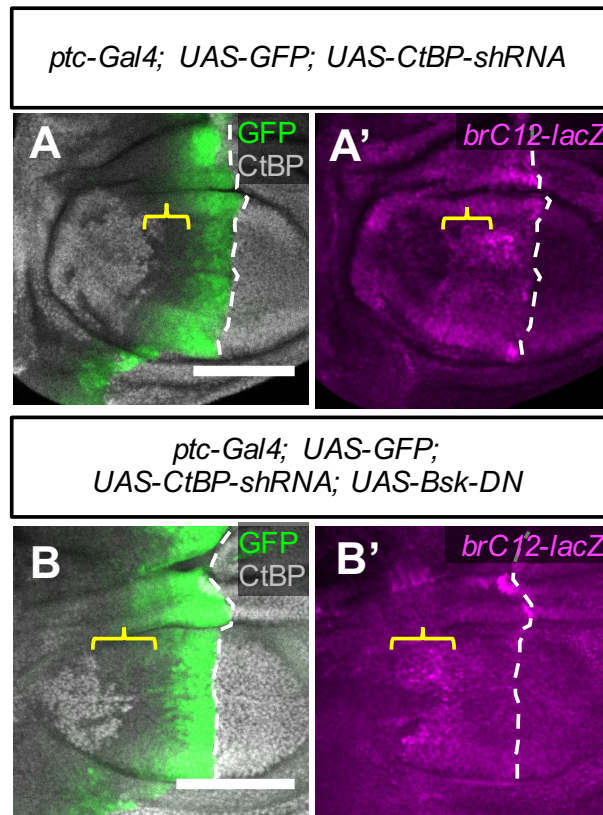


Figure 3.7: **Blocking JNK signaling abrogates the increased *brC12* activity caused by loss of *CtBP*** (A) *CtBP*-shRNA expression using *ptc-Gal4* effectively knocks down *CtBP* in the *ptc*-domain (GFP) and results in prolonged *CtBP* knockdown in cells that expressed *ptc* earlier in development (yellow bracket). (A') Upregulation of *brC12-lacZ* is observed in *CtBP*-knockdown tissue, including in tissue no longer expressing *ptc-Gal4* (yellow bracket). (B) Co-expression of a dominant-negative form of Bsk/JNK (B') suppresses the *brC12-lacZ* upregulation caused by *CtBP* knockdown. Yellow bracket shows that in a region of the disc in which *CtBP* knockdown persists but JNK signaling is not blocked, the *brC12-lacZ* reporter remains elevated. Scale bars, 100  $\mu\text{m}$ .

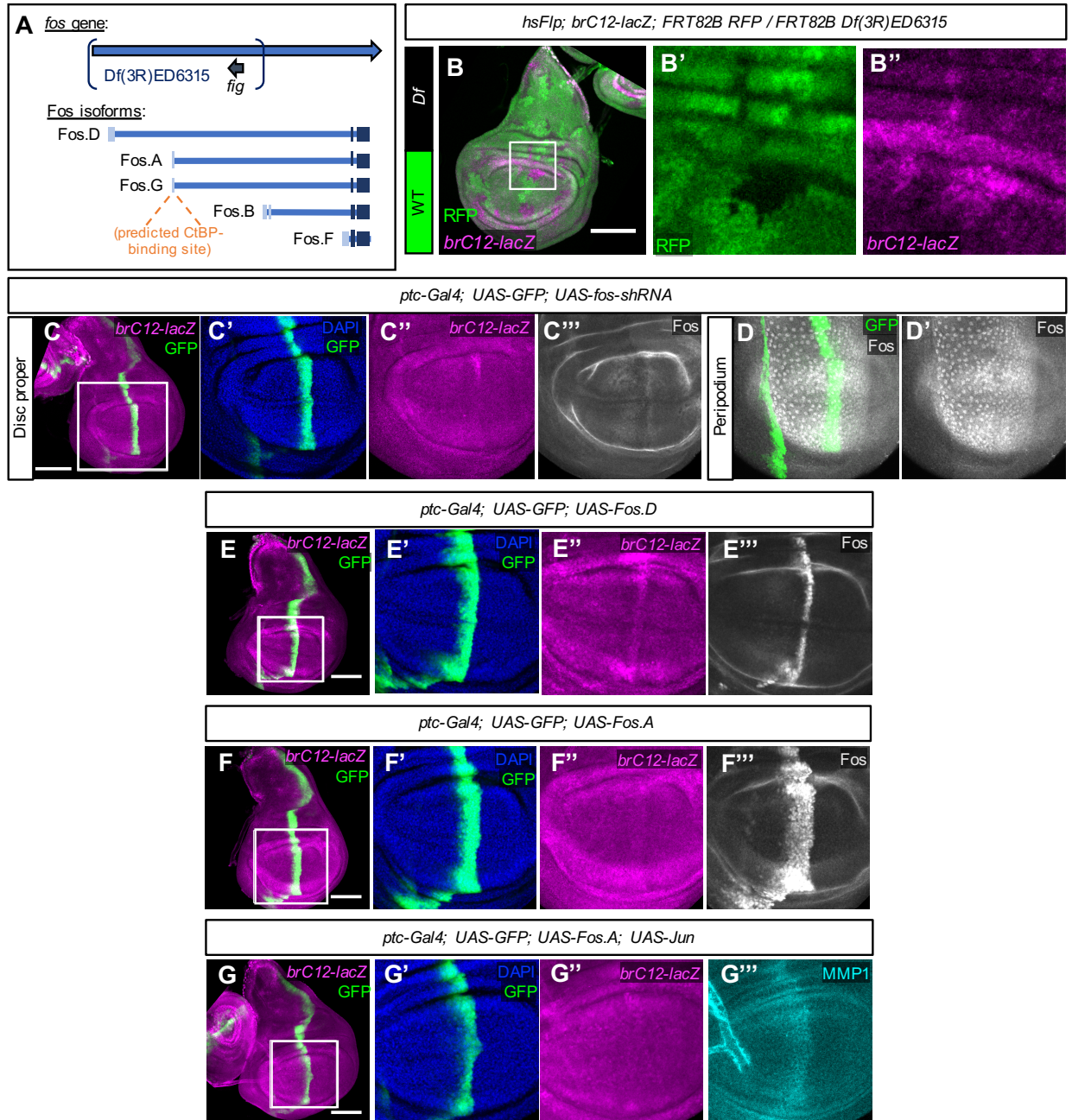


Figure 3.8: Loss of distinct Fos isoforms leads to *brC12-lacZ* upregulation

(A) A model of the *fos* genetic locus showing the 17-kb region removed by the *ED6315* deficiency (brackets) and five predicted protein isoforms. The dark blue boxes represent coding exons shared by all isoforms while the light blue boxes represent coding exons present in only some isoforms. Intronic regions are represented by the horizontal lines; non-coding exons are not displayed. Isoforms A and G share identical first exons, containing a predicted CtBP-binding motif, PADLS. (B-B'') RFP-negative clones that are homozygous for the *ED6315* deletion show increased levels of (B'') *brC12-lacZ*. (C-G) Different *fos* manipulations were performed by expressing various UAS-transgenes in the *ptc*-domain (green) and the effects on the *brC12-lacZ* reporter (magenta) were assessed in wing imaginal discs. Boxes indicate the areas of the wing pouch that are enlarged in subsequent panels. DAPI shows nuclei (blue).

(C) Knockdown of *fos* via expression of an shRNA predicted to target all isoforms does not show changes in (C'') *brC12-lacZ* reporter expression. (C''') Fos protein levels (as detected by the Fos antibody) are low throughout the disc proper. (D-D') The region of the same disc in C'-C''' showing high Fos protein detection in the peripodium. (E-E''') Overexpression of Fos.D, validated by (E''') Fos antibody staining, results in increased (E'') *brC12-lacZ* expression. (F-F''') Overexpression of Fos.A, validated by (F''') Fos antibody staining, does not affect (F'') *brC12-lacZ* expression. (G-G''') Co-expression of Fos.A and Jun does not affect (G'') *brC12-lacZ* expression but does show increased levels of (G''') MMP1 protein. All scale bars in figure, 100  $\mu\text{m}$ .

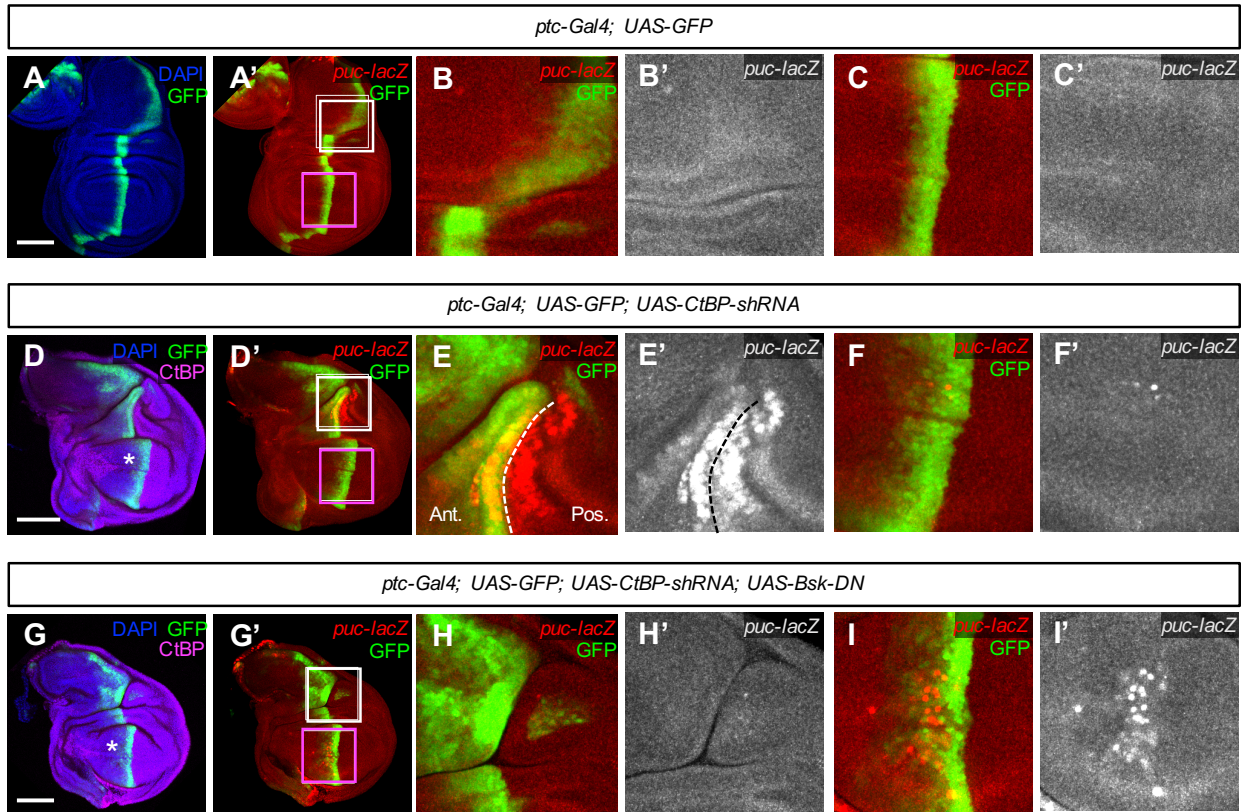


Figure 3.9: **CtBP inactivation does not autonomously upregulate *puc-lacZ* expression.** *puc* activity was monitored using the *puc<sup>A251.1F3</sup>-lacZ* enhancer trap. The white boxes in (A'), (D'), and (G') show the areas enlarged in (B-B'), (E-E'), and (H-H'), respectively, while the magenta boxes show the areas enlarged in (C-C'), (F-F'), and (I-I'). (A-C) A control disc showing low background levels of *puc-lacZ* expression. (D-F) Knocking down *CtBP* using *ptc-Gal4* (green) upregulates (E-E') *puc-lacZ* expression only in a group of cells within the dorsal hinge and not (F-F') in the pouch. (E-E') *puc-lacZ* is activated in cells on both sides of the compartment boundary (dashed line) and is accompanied by ectopic folds in the tissue. "Ant."=Anterior. "Pos."=Posterior. (G-I) Co-expression of a dominant-negative form of Bsk/JNK (H-H') suppresses induction of *puc-lacZ* in the dorsal hinge but does not eliminate all ectopic folds, and (I-I') results in autonomous *puc-lacZ* upregulation in the pouch. Asterisks in D and G show persistent *CtBP* knockdown as assessed by CtBP antibody stain (magenta). All scale bars, 100  $\mu\text{m}$ .

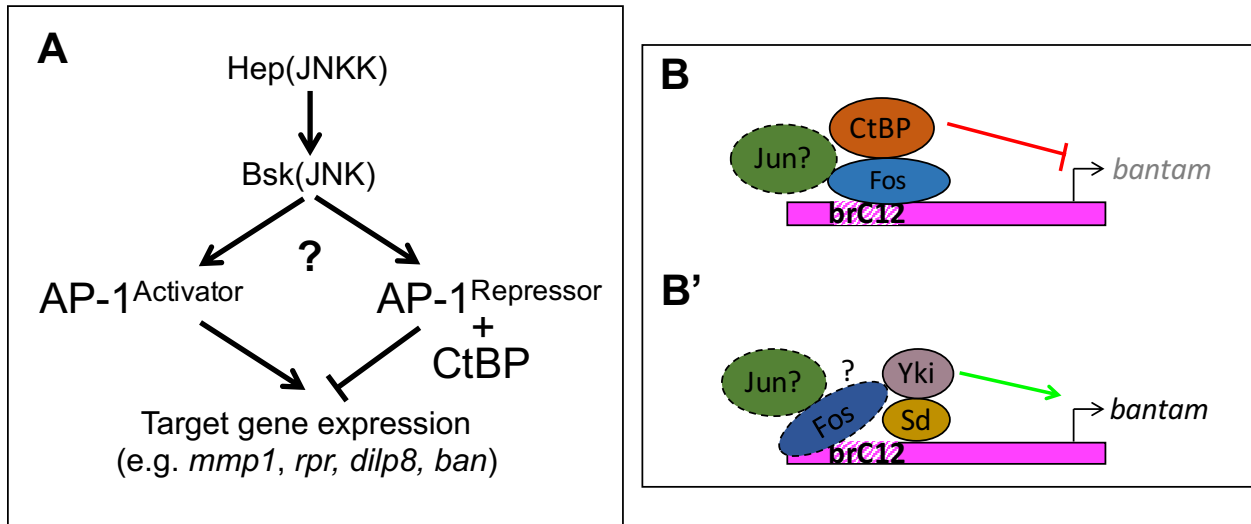


Figure 3.10: **A model for how CtBP could switch AP-1 from a transcriptional activator to repressor.** (A) A pathway showing how JNK activity could result in divergent transcriptional outputs. (B-B') A model of the *ban* locus showing how distinct transcriptional regulators downstream of JNK activity could lead to (B) transcriptional repression and (B') transcriptional activation.

## Chapter 4

# Discovery and applications of persistent RNAi-mediated knockdown in *Drosophila*

This chapter is a partial reproduction of the following paper:

Bosch, J. A., Sumabat, T. M., and Hariharan, I. K. (2016). Persistence of RNAi-Mediated Knockdown in *Drosophila* Complicates Mosaic Analysis Yet Enables Highly Sensitive Lineage Tracing. *Genetics*, 203(1), 109-118.

For the cited work, my contributions were to Figures 4.1C-D,F and 4.2A-B and to Table 4.1. I helped conceive the project with JAB, performed immunohistochemistry and imaging with JAB, and edited the manuscript with JAB and IKH. The results shown in Figure 4.1G are unpublished.

## 4.1 Abstract

RNA interference (RNAi) has emerged as a powerful way of reducing gene function in *Drosophila melanogaster* tissues. By expressing synthetic short hairpin RNAs (shRNAs) using the Gal4/UAS system, knockdown is efficiently achieved in specific tissues or in clones of marked cells. Here we show that knockdown by shRNAs is so potent and persistent that even transient exposure of cells to shRNAs can reduce gene function in their descendants. When using the FLP-out Gal4 method, in some instances we observed unmarked “shadow RNAi” clones adjacent to Gal4-expressing clones, which may have resulted from brief Gal4 expression following recombination but prior to cell division. Similarly, Gal4 driver lines with dynamic expression patterns can generate shadow RNAi cells after their activity has ceased in those cells. Importantly, these effects can lead to erroneous conclusions regarding the cell autonomy of knockdown phenotypes. We have investigated the basis of this phenomenon and suggested experimental designs for eliminating ambiguities in interpretation. We have also exploited the persistence of shRNA-mediated knockdown to design a sensitive lineage-tracing method, i-TRACE, which is capable of detecting even low levels of past reporter expression. Using i-TRACE, we demonstrate transient infidelities in the expression of some cell-identity markers near compartment boundaries in the wing imaginal disc.

## 4.2 Introduction

RNA interference (RNAi) is an endogenous gene-silencing mechanism in eukaryotic cells that has been harnessed as a powerful reverse genetics tool (Hannon, 2002). RNAi is initiated by short interfering RNAs (siRNAs) or microRNAs (miRNAs) that target messenger RNAs for degradation or translational inhibition in a sequence-specific manner (Wilson and Doudna, 2013). Importantly, RNAi can be artificially induced by gene-specific hairpin RNAs that are processed into siRNAs (Fire et al., 1998; Paddison et al., 2002). These RNAi reagents, along with completely sequenced genomes, have enabled experimenters to perform loss-of-function studies in diverse organisms (Mohr et al., 2014).

An important consideration for knockdown experiments is whether RNAi-mediated knockdown is sustained or transient. In *Caenorhabditis elegans* (Sijen et al., 2001) and plants (Vaistij et al., 2002), siRNAs undergo amplification by RNA-dependent RNA polymerases (RdRPs), leading to a long-lasting RNAi response. In contrast, *Drosophila* and vertebrates do not have RdRP homologs (Zong et al., 2009) and RNAi is normally transient (Chi et al., 2003; Roignant et al., 2003). The development of transgenic strategies to express RNA hairpins has overcome this problem, and RNAi can be induced, sustained, and/or repressed using different promoter sequences (Perrimon et al., 2010; Livshits and Lowe, 2013). This ability to control RNAi in a temporal manner in vivo has proven essential for generating reversible phenotypes (Livshits and Lowe, 2013) and for dissecting the biological functions of pleiotropic genes (Perrimon et al., 2010).

In *Drosophila*, accurate control of where and when RNAi occurs is critical for evaluat-

ing the effects of knockdown in specific cell populations *in vivo* (Perrimon et al., 2010). Spatiotemporal control of RNAi-mediated knockdown is most often accomplished using the Gal4/*UAS* system (Fischer et al., 1988; Brand and Perrimon, 1993), where cell/tissue-specific Gal4 transgenes drive co-expression of hairpin RNAs and cellular markers (e.g., *UAS-GFP*) under *UAS* control. These hairpin transgenes are available either as long double-stranded RNAs (dsRNAs) or as short hairpin RNAs (shRNAs) embedded within a *miR-1* microRNA backbone (Perrimon et al., 2010), with the latter thought to be more effective at gene silencing (Ni et al., 2011). Gal4 transgenes, are also used as reporters of endogenous gene expression (Fischer et al., 1988; Brand and Perrimon, 1993), and, for many Gal4 lines, expression may dynamically change on a timescale of hours or days during development (Yeh et al., 1995; Evans et al., 2009), homeostasis (Micchelli and Perrimon, 2006; Buchon et al., 2009), or environmental changes (Halfon et al., 1997; Agaisse et al., 2003). Several studies in mammalian cell culture and *in vivo* models have shown that protein levels do not recover immediately after turning off RNAi, usually requiring >2 days (Gupta et al., 2004; Dickins et al., 2005; Bartlett and Davis, 2006; Zhang et al., 2007; Baccarini et al., 2011). Despite the known potential for RNAi persistence to occur, no studies to date have documented or addressed how this can affect Gal4-regulated knockdown experiments that require precise temporal and spatial resolution *in vivo*.

Here, we demonstrate in *Drosophila* tissues that even transient production of shRNAs leads to persistent gene knockdown after Gal4 expression has ceased. We show that this phenomenon can, in the context of common experimental designs, lead to false interpretations about the identity of cells undergoing knockdown, and we provide experimental workarounds to address this issue. Furthermore, we exploit RNAi persistence to develop a novel lineage-tracing tool called i-TRACE that we demonstrate can be used to identify instances where even brief changes in gene expression have occurred during the generation of specific cell lineages.

## 4.3 Materials and Methods

### *Drosophila* stocks and husbandry

Crosses were maintained on standard fly food at 25°C unless otherwise noted.

Most transgenic stocks were obtained or derived from the Bloomington Stock Center and are listed here with corresponding stock numbers (BL#): *ptc-Gal4* (BL2017), *en-Gal4* (BL30564), *dpp-Gal4* (BL1553), *nb-Gal4* (BL25754), *ap-Gal4* (BL3041), *UAS-GFP* (BL6874), *UAS-RFPnls* (BL30556), *UAS-mCD8.ChRFP* (BL27391), *UAS-GFP-shRNA#1* Chr. II (BL41557), *UAS-GFP-shRNA#1* Chr. III (BL41556), *UAS-GFP-dsRNA* (BL9330), *UAS-RFP-shRNA* (BL35785), *UAS-crb-shRNA* (BL40869), *UAS-crb-dsRNA* (BL27697), *hsp70-GFP* (BL51354), *ubi-GFPnls* (BL5189), *ubi-RFPnls* (BL34500), *UAS-Nslmb-vhhGFP4* (BL38421), *tub-Gal80ts* (BL7108), *G-TRACE* (BL28281), *hsFLP* (BL8862), *Act5c-FRT-CD2-FRT-Gal4* (BL4780), and *Act5c-FRT-y<sup>+</sup>-FRT-Gal4* (BL3953). Additional stocks with BL#s are listed

in Table 4.1.

The remaining stocks used originated from the publications noted: *ci-Gal4* (Crocker et al., 2006), *hh-Gal4* (Tanimoto et al., 2000), *esg-Gal4* (Micchelli and Perrimon, 2006), *FRT40A MARCM* (Lee and Luo, 1999), *FRT40A* (Xu and Rubin, 1993), *FRT42D yki<sup>B5</sup>* (Huang et al., 2005), and *FRT42D MARCM* (Lee and Luo, 1999).

## Dissections, antibody staining, and microscopy

Unless otherwise noted, all tissues were dissected with forceps in glass well dishes with 1 PBS. Tissues were fixed in 4% paraformaldehyde in 1 PBS for 20 min. After washing in 1 PBS, tissues were stained with DAPI (1 ng/ $\mu$ l) in 1 PBS for 1 hr, washed with 1 PBS, and mounted onto slides with Vectashield mounting media (Vector Labs) or SlowFade Gold mounting medium (Life Technologies). Mounted samples were imaged on a Zeiss 700 or 780 confocal microscope. Confocal slices were processed with ImageJ software (NIH).

For wing imaginal discs, wandering third instar larvae were bisected and inverted to expose the imaginal discs to fixative. For immunostaining of wing discs, fixed carcasses with attached wing discs were permeabilized with PBS+0.1% Triton-X100 for 20 min, blocked with PBS+0.1% Triton-X100+5% normal goat serum for 1 hr, and incubated with primary antibodies diluted in blocking solution overnight at 4°C. Samples were washed three times in PBS+0.1% Triton-X100 for 15 min each. Subsequent steps involving staining using secondary antibodies were the same as primary antibodies. Antibodies used were the following: mouse anti-Arm (1:100, N2 7A1; Developmental Studies Hybridoma Bank) and rat anti-Crb (1:500) (Richard et al., 2006).

For adult midguts, females 1 week post eclosion were starved for 4 hr to purge any gut contents that are autofluorescent. This was performed by placing adults into empty vials containing filter paper soaked with 4% sucrose. Adult midguts were dissected from decapitated animals by gently pulling out the gut and placing it into fixative.

For experiments requiring heat-shock induction of the *hs-FLP* transgene in wing imaginal discs, ~72 hr after egg deposition larvae were placed in a 37°C water bath for 15–30 min (for FLP-out Gal4 experiments) or 1–2 hr (for MARCM experiments) and returned to 25°C. Larvae were dissected as wandering third instar larvae.

For experiments requiring heat-shock induction of the *hsp70-GFP* transgene, crosses were incubated at 37°C for 30 min, returned to 25°C, and dissected 2 hr later. Non-heat-shocked controls were kept at 25°C until dissection.

For heat-shift experiments involving *tub-Gal80ts*, eggs from crosses were initially incubated at 18°C (permissive temperature, Gal4 off). Vials were incubated at 29°C (nonpermissive temperature, Gal4 on) for 16 hr until dissected as wandering third instar larvae. Controls were kept at the same temperature throughout development (18°C or 29°C).

## 4.4 Results

### Transient expression of shRNAs causes persistent knockdown in unmarked “shadow RNAi” cells

The FLP-out Gal4 system (Pignoni and Zipursky 1997) can be used to induce RNAi in a clonal lineage of cells that stably express Gal4. Clones are generated using a heat-shock-inducible *FLP* transgene, which catalyzes the removal of a transcriptional stop upstream of the Gal4-coding sequence (Figure 4.1A). While using this system, we unexpectedly found that clonal expression of shRNAs causes knockdown in cells that do not express Gal4. For example, in larvae that ubiquitously express GFP (*ubi-GFP*), we generated Gal4 clones that express red fluorescent protein (*UAS-RFP*) and shRNA targeting *GFP* (*UAS-GFP-shRNA*) and dissected wing discs 48 hr after clone induction (ACI). As expected, RFP-expressing clones knock down GFP (Figure 4.1B). However, we also observed patches of cells that knock down GFP but do not express RFP. We refer to this unexpected cell type as “shadow RNAi” cells since these cells exhibit knockdown of their target gene but do not express Gal4 as assessed by the absence of RFP expression.

Importantly, we find that shadow RNAi cells are produced when shRNAs target the endogenous genes, *crumbs* (*crb*) and *CtBP* (Figure 4.1C–D and Table 4.1). Furthermore, *crb* shadow RNAi cells exhibited a known *crb* mutant phenotype characterized by altered localization of Crb where they contact wild-type cells (Figure 4.1D) (Pellicka et al., 2002; Chen et al., 2010; Hafezi et al., 2012). These results suggest that production of shadow RNAi cells may be an inherent phenomenon when using the FLP-out Gal4 system, as opposed to sporadic effects such as chromosomal instability or epigenetic silencing of transgenes.

We note that tests of three other endogenous genes (*fat*, *gigas*, and *dachshund*) did not obviously generate shadow RNAi cells. In addition, when we repeated FLP-out Gal4 experiments using dsRNAs targeting GFP (*UAS-GFP-dsRNA*), we found that shadow RNAi cells were not clearly visible and may have exhibited only weak knockdown. These results are summarized in Table 4.1. Therefore, shadow RNAi cells may manifest only when targeting particular genes or when using certain RNAi reagents.

Several observations of shadow RNAi cells hint at a mechanism by which they are generated. Shadow RNAi cells nearly always appear as cohesive groups in contact with Gal4 clones (Figure 4.1B–C), which is a well-documented behavior of sister clones in the imaginal disc (Xu and Rubin 1993). Furthermore, in cases where shadow RNAi cells exhibit partial knockdown of the target gene (Figure 4.1B), each cell within a cohesive group shows the same level of knockdown, suggesting a synchronized reversal of RNAi over time. Indeed, we find that knockdown in shadow RNAi cells is barely visible at 72 hr ACI (not shown), suggesting that knockdown is not sustained as in Gal4-expressing clones. These observations suggest that shadow RNAi cells produced using the FLP-out Gal4 system are a sister lineage to Gal4 clones and that knockdown persists for up to 3 days after being transiently induced.

To explain our observations with the FLP-out Gal4 system, we propose that shRNAs are transiently expressed in an ancestral mother cell that gave rise to Gal4-expressing clones and

sister shadow RNAi clones. This event could occur during G2 when cells have duplicated their genome if one of two *Act-FRT-stop-FRT-Gal4* transgenes undergoes recombination and briefly expresses Gal4 before cell division (Figure 4.1E). In contrast, recombination during G1, or recombination of both *Act-FRT-stop-FRT-Gal4* transgenes, would not be expected to generate shadow RNAi clones. To test this model, we performed clonal RNAi experiments using the MARCM (Mosaic Analysis with a Repressible Cell Marker) system, which restricts Gal4 activity until after two daughter cells are produced and the levels of the Gal80 repressor in the cytoplasm decay (Lee and Luo 1999). Consistent with this hypothesis, when using MARCM to express shRNAs that target *crb*, we find that Crb protein is knocked down only in the Gal4 clone (Figure 4.1F). This result rules against the possibility that shRNA or Gal4 molecules are transferred from the Gal4 clone into shadow RNAi clones.

One finding that seemed inconsistent with our model was that when we generated MARCM clones that are homozygous null for the pro-growth gene *yorkie* (*yki*) and express shRNAs targeting *RFP* in a *ubi-RFP* genetic background, we observed RFP knockdown in unmarked clones (Figure 4.1G). Similar shadow RNAi clones were observed when we generated *yki* MARCM clones expressing *CtBP*-targeting shRNAs and performed antibody staining for CtBP (results not shown). If, as our model predicts, shadow RNAi is the result of transient shRNA production, then these observations are unexpected because all cells, prior to clone induction, should have been continuously expressing *Gal80*, thereby preventing any production (transient or otherwise) of the shRNA. In cultured mammalian cells, functional loss of YAP, the mammalian ortholog of Yki, has been shown to delay the abscission of dividing cells (Bui et al., 2016). If such a role in cytokinesis is conserved between YAP and Yki, then this could account for the shadow RNAi observed with *yki* MARCM clones (See Discussion).

Our results suggest that persistent RNAi-mediated knockdown occur primarily due to the transient expression of shRNAs. To verify this using an independent method, we used the *patched-Gal4* (*ptc-Gal4*) enhancer trap line that expresses Gal4 in the *ptc* expression pattern (Hinz et al., 1994). In early wing disc development, *ptc-Gal4* is expressed in all cells of the anterior compartment and later becomes restricted to a thin stripe of anterior cells that border the posterior compartment (Phillips et al., 1990; Evans et al., 2009). When we used *ptc-Gal4* to express shRNAs targeting *GFP* (Figure 4.2A) or *crb* (Figure 4.2B), we observed knockdown of the target gene within cells of the stripe currently expressing Gal4, as well as cells far anterior to the stripe that no longer express Gal4 (assessed by a fluorescent protein expressed under UAS control). In contrast, dsRNAs targeting *GFP* transcript or a nanobody fusion that degrades GFP protein (Caussinus et al., 2012) cause knockdown of GFP fluorescence mainly within the *ptc*-expressing stripe, although some cells immediately anterior to the stripe have reduced GFP levels (Table 4.1). Similarly, dsRNAs that target *crb* cause knockdown only within the *ptc*-expressing stripe (Table 4.1). To directly test if past expression of *ptc-Gal4* in more anterior regions of the wing disc is required to generate shadow RNAi cells, we used a temperature-sensitive Gal80 transgene (McGuire et al., 2003) to restrict expression of Gal4 to a 16-hr window immediately preceding dissection (Figure 4.2D). Under these conditions, shadow RNAi cells are not observed, suggesting that the

shadow RNAi cells were generated by prior expression of the shRNA in those cells.

## Investigation of mechanisms contributing to the persistence of RNAi-mediated knockdown

Our observation that it takes  $\sim 3$  days to reverse the effects of GFP knockdown is consistent with reports in mammalian cell culture and *in vivo* mouse models (Gupta et al., 2004; Dickins et al., 2005; Bartlett and Davis 2006; Zhang et al., 2007; Baccarini et al., 2011), although our experiments were performed at a comparably lower temperature (25°C). In these mammalian systems, it is generally thought that reversal from RNAi occurs by siRNA degradation and/or dilution with cell divisions (Dickins et al., 2005; Baccarini et al., 2011). Yet, considering this explanation, we were surprised by the high degree of persistent GFP knockdown following a short pulse of shRNA expression (Figure 4.1, B–D). Therefore, we considered the possibility that RNAi was being actively maintained in some manner.

Active maintenance of RNAi has been demonstrated in different species, such as RNAi amplification in *C. elegans* (Sijen et al., 2001; Alder et al., 2003) or RNAi-induced transcriptional silencing (RITS) (Verdel et al., 2004) in *S. pombe*. In addition, Piwi-interacting RNAs (piRNAs) target transcripts via an amplifying "ping-pong" cycle (Brennecke et al., 2007). Initiation of each of these mechanisms requires the presence of target transcripts. Therefore, we tested whether RNAi persistence in *Drosophila* tissues occurs when the target gene is not expressed until immediately before dissection. This was accomplished using a heat-shock-inducible GFP transgene (*hs-GFP*) that is highly expressed when animals are incubated at 37°C (Figure 4.3). Using *ptc-Gal4* to express *GFP-shRNA* in a *hs-GFP* background, and inducing GFP expression 2 hr before dissection, we find that GFP knockdown occurs in the *ptc* stripe (RFP+) as well as in cells far anterior (RFP-) (Figure 4.3C). We do not detect GFP fluorescence without heat shock and observe tissue autofluorescence only at higher exposure settings (Figure 4.3B'). These results suggest that previous expression of transcripts is not required for RNAi persistence in shadow RNAi cells.

We also systematically tested the requirement of genes that might promote RNAi persistence based on mechanisms that operate in other systems. This was accomplished by knocking down each gene while monitoring transient knockdown of a ubiquitously expressed RFP (*ubi-RFP*) using the *ptc-Gal4* expression system. Our goal was to identify genes that are selectively required for RNAi persistence in cells anterior to the *ptc* stripe. We tested *Drosophila* orthologs of genes involved in RITS, chromatin-remodeling genes, and machinery involved in miRNA, siRNA, and piRNA processing. With one exception, none of the genes when knocked down abolished persistent RNAi of the *ubi-RFP* reporter gene (Figure 4.4). The exception was *Ago2* RNAi, which nearly abolishes RFP knockdown in all cells expressing *ptc-Gal4* (Figure 4.4C). This result is consistent with the known role of Ago2 to bind siRNAs and coordinate RNAi-induced silencing complex (RISC) degradation of target transcripts (Ni et al., 2011). In summary, our results favor a model where the persistence of RNAi is simply the result of a slow rate of degradation of shRNAs and/or their siRNA

derivatives.

## **i-TRACE: a novel lineage analysis tool based on RNAi**

Since even transient expression of an shRNA could generate persistent knockdown (Figure 4.1B–C), we explored its use as a lineage-tracing tool. To facilitate RNAi-based lineage tracing with Gal4 lines, we constructed a fly strain containing three transgenes: (1) a reporter of Gal4 activity (e.g., *UAS-RFP*), (2) a ubiquitously expressed target gene (e.g., *ubi-GFP*), and (3) a Gal4-controlled shRNA (e.g., *UAS-GFP-shRNA*) (Figure 4.5A). Therefore, when this triple-transgenic line is crossed with a Gal4 line, F1 progeny will contain cells and tissues that report real-time Gal4 expression (RFP+, GFP–) and recent Gal4 expression (RFP–, GFP–) (Figure 4.5B). Since exogenous fluorescent transgenes are used, the tissues being analyzed are wild type and antibody staining is not necessary. We refer to this system as “i-TRACE” (RNAi-Technique for Real-time And Clonal Expression), which shares a similar naming convention with G-TRACE, a recombination-based lineage-tracing technique (Evans et al., 2009). We compared i-TRACE with G-TRACE using several well-characterized Gal4 lines.

*dpp-Gal4* expresses in the anterior wing disc at early developmental stages and becomes restricted to a thin stripe of cells at the border between anterior and posterior compartments (Masucci et al., 1990; Evans et al., 2009). Using i-TRACE, we observed large regions of the anterior wing disc that previously expressed *dpp-Gal4* (Figure 4.5C). Using G-TRACE (Figure 4.5D), we find that the region of lineage-traced cells is patchier and restricted to a smaller domain. *nubbin-Gal4* (*nb-Gal4*) expresses in the wing disc pouch, and the outer edge of this domain is thought to shift throughout larval development (Zirin and Mann 2007). Using i-TRACE, we confirmed this phenomenon by finding a thin ring of cells outside of the *nb-Gal4* domain that previously expressed Gal4 (Figure 4.5E). In contrast, when using G-TRACE, this ring of past expression is not visible (Figure 4.5F). Thus, in at least these two cases, i-TRACE appears more sensitive than G-TRACE.

*escargot-Gal4* (*esg-Gal4*) expresses in two cell types of the adult midgut: intestinal stem cells and their immediate descendants called enteroblasts (EBs) (Micchelli and Perrimon 2006). EBs give rise to two differentiated cell types that no longer express *esg-Gal4*: enterocytes and enteroendocrine cells. Together, these four cell types compose the entire midgut epithelium. Using i-TRACE with *esg-Gal4*, we observed that all cells of the midgut are GFP– (Figure 4.5G). These cells include enterocytes, which are discernible by their large nuclear size (Micchelli and Perrimon 2006). In contrast, muscle cells that surround the midgut epithelium express GFP, confirming that animals contain the *ubi-GFP* transgene. This result supports the model that differentiated cell types in the midgut epithelium are descendants of a lineage that expressed *esg-Gal4*. Using G-TRACE with *esg-Gal4* demonstrates similar results to i-TRACE (Figure 4.5H).

In summary, our analysis of several Gal4 lines using the i-TRACE system suggests that it is a useful tool for simultaneously visualizing past and present gene expression.

## Reversible changes in compartment identity markers are revealed using i-TRACE

During animal development, boundaries between gene expression domains are important to physically separate cells of different function (Dahmann et al., 2011). In the *Drosophila* wing disc, four compartments are separated by two boundaries, the anterior/posterior (A/P) boundary, and the dorsal/ventral (D/V) boundary (Figure 4.6A). The A/P boundary is specified during embryogenesis and the D/V boundary at the end of the first larval instar. Lineage-tracing techniques have demonstrated that cells initially specified in one compartment do not normally switch identities (Garcia-Bellido et al., 1973). We set out to test this model by analyzing the expression patterns of several compartment-specific Gal4 lines with i-TRACE.

The A/P boundary is specified by the selector gene *engrailed* (*en*) (Kornberg et al., 1985), which expresses in all cells of the posterior compartment and activates transcription of *hedgehog* (*hh*) (Tabata et al., 1992). Using i-TRACE to analyze *hh-Gal4*, we observed present expression in the posterior compartment of the third instar wing disc (Figure 4.6B), consistent with previous studies (Tanimoto et al., 2000). Surprisingly, in all discs imaged (>20), we also observed patches of shadow RNAi cells in the anterior compartment (Figure 5B), indicating that *hh-Gal4* was previously expressed in these cells.

To determine if other markers of compartment identity transiently express outside of their canonical compartment, we analyzed the expression patterns of additional Gal4 lines with i-TRACE in the third instar wing disc. *cubitus interruptus* (*ci*), an essential component of the *hh* pathway, is repressed in the posterior compartment by *en* and thus is expressed only in the anterior compartment (Eaton and Kornberg 1990). Using i-TRACE to analyze *ci-Gal4*, we find the expected current expression in the anterior compartment, but also evidence of past expression in cells of the posterior compartment (Figure 4.6C). In addition, a subset of posterior shadow RNAi cells actively express *ci-Gal4* (Figure 4.6C'). *apterous* (*ap*) is a selector gene expressed in the dorsal compartment of the wing disc (Blair et al., 1994). Using i-TRACE to analyze *ap-Gal4*, we observe cells in the ventral compartment that previously expressed Gal4 (Figure 4.6D). In summary, our results with i-TRACE suggest that the expression of each of four different compartment-specific Gal4 lines (*hh-Gal4*, *en-Gal4*, *ci-Gal4*, and *ap-Gal4*) is not completely restricted to its specific compartment.

Several similarities in the characteristics of shadow RNAi patches produced from different compartment Gal4 lines suggest that they are clones that originate close to the compartment boundary. First, these cells appear as cohesive groups with similar levels of knockdown, suggesting that they belong to a shared clonal lineage that underwent several cell divisions after expression of Gal4 (Xu and Rubin 1993). Second, these patches are frequently elongated in the proximo/distal direction, an indicator that there is significant proliferation after the labeling event (Baena-Lopez et al., 2005). Third, these patches lie in proximity to the compartment boundary defined by the particular Gal4 line. These results suggest that cells located at wing-disc compartment boundaries can transiently express at least some markers of the opposite compartment (Figure 4.6E).

## 4.5 Discussion

In this study, we show that transient expression of shRNAs in *Drosophila* tissues can cause persistent knockdown in cells that outlasts co-expressed marker transgenes. We term this effect “shadow RNAi,” since cells with persistent knockdown are not discernible without visualizing target gene expression. Although this effect was obvious when targeting three different genes, *GFP*, *RFP*, *crb*, and *CtBP*, it is possible that other genes may behave differently. Indeed, we were unsuccessful in observing shadow RNAi cells for three other genes (*fat*, *gigas*, and *dachshund*) in the wing disc using FLP-out Gal4 (Table 4.1). While these could represent technical failures, it is also possible that gene-specific factors influence the susceptibility to shadow RNAi, such as transcript/protein expression levels or stability. Similarly, different RNAi reagents may or may not cause shadow RNAi. For both *GFP* and *crb*, we found that an shRNA transgene was much more effective than a long dsRNA transgene in generating shadow RNAi (Table 4.1). This difference may simply be explained by better knockdown efficiency using shRNAs compared to dsRNAs, as has been observed previously (Ni et al., 2011). Alternatively, shRNAs, which are embedded in a *miR-1* microRNA backbone (Ni et al., 2011), might be more stable in cells than long dsRNAs or produce greater numbers of siRNAs. Importantly, it is possible that other hairpin transgenes, derived from different sources or that target different regions of a transcript, may behave differently.

Since shadow RNAi cells can have mutant phenotypes, as shown in this chapter with *crb* (Figure 4.1D) and previously with *CtBP* (Figure 3.7), it is important that researchers take this phenomenon into consideration, especially when drawing conclusions about the cell autonomy of mutant phenotypes caused by RNAi-induced knockdown. For some experiments, simply identifying where shadow RNAi cells are located may allow a proper interpretation of results. To test if an shRNA generates shadow RNAi cells *in vivo*, it is critical to visualize target gene expression while conducting knockdown. Although we used antibodies to detect protein levels, *in situ* hybridization to detect transcript levels may also be effective. Complementary to testing an shRNA, a Gal4 line can be assayed with i-TRACE to determine if it causes persistent RNAi of a fluorescent reporter transgene.

We also suggest methods to limit the generation of shadow RNAi cells. For example, including a temperature-sensitive Gal80 transgene can allow more refined temporal control over when Gal4 is turned on (e.g., Figure 4.2, C–E), thus giving shadow RNAi cells less time to form. Alternatively, based on our experiments with *GFP* and *crb* knockdown, using long dsRNAs instead of shRNAs seems to prevent formation of shadow RNAi cells. If performing clonal experiments using shRNAs, our work suggests that the MARCM system may be beneficial in minimizing the phenomenon of shadow RNAi clones, provided that these clones are not otherwise genetically predisposed to cellular abnormalities that may promote shadow RNAi. For instance, we still observed shadow RNAi for multiple target genes outside of *yki*<sup>-/-</sup> clones generated by the MARCM technique (Figure 4.1G). If Yki shares a function with its mammalian ortholog YAP in promoting proper cytokinesis (Bui et al., 2016), then a possible explanation for this result is that a delay in abscission between the *yki*<sup>-/-</sup> cell and its *Gal80*<sup>+/+</sup> sister cell generated by the recombination event could allow for the exchange of Gal4 and/or

shRNA molecules. It has been suggested that YAP's function in regulating cytokinesis is distinct from its function as a transcriptional coactivator, instead involving a role in coordinating proper localization of protein complexes critical for executing cytokinesis (Bui et al., 2016). Though preliminary, our results suggest that Yki could possess a similar non-transcriptional function in regulating cell division and merit further investigation. Moreover, our use of the MARCM technique coupled with detection of shadow RNAi in uncovering this potential function for Yki reveals that such a system could enable future studies of cellular abscission.

As an outcome of our work describing RNAi persistence *in vivo*, we developed the i-TRACE system as a novel method to monitor dynamic gene expression from Gal4 reporter lines. The i-TRACE system fills an important gap in existing genetic methods. For example, real-time detection of Gal4 expression is accomplished with a reporter under UAS control (Fischer et al., 1988; Brand and Perrimon 1993) but cannot be used to report past expression of Gal4. Conversely, recombination-based methods are used to stably mark cell lineages that previously expressed Gal4 (Evans et al., 2009), but can overlook short-term changes in gene expression that occur after stable recombination. The i-TRACE system can be used as a lineage-tracing tool for visualizing recent gene expression, since reporter knockdown in marked cells reverses after  $\sim 72$  hr. In addition, in at least some situations, the i-TRACE system appears to be a more sensitive reporter of past Gal4 expression than G-TRACE.

Only rarely has a switch in compartment identity been observed near lineage-restricted boundaries, such as in the *Drosophila* embryo (Gettings et al., 2010) and in the wing discs during regeneration (Herrera and Morata 2014). Our data demonstrate that cells located at lineage-restricted boundaries of the wing disc can transiently express Gal4 reporters of the opposite compartment identity (Figure 4.6E), raising the possibility that boundary cells may be less committed to their respective compartmental identities than previously thought, although they ultimately seem to maintain their originally fated compartmental identities. An important caveat is that Gal4 reporter transgenes might not accurately reflect transcription of the endogenous gene. Therefore, it remains unknown whether boundary cells express endogenous identity genes of the opposite compartment and whether this results in transient cell-fate changes. Careful imaging of endogenous compartment identity gene expression in developing wing discs may help resolve this issue. Furthermore, other possibilities such as direct transfer of Gal4 or shRNAs between cells at the boundary also merit consideration.

## 4.6 Figures

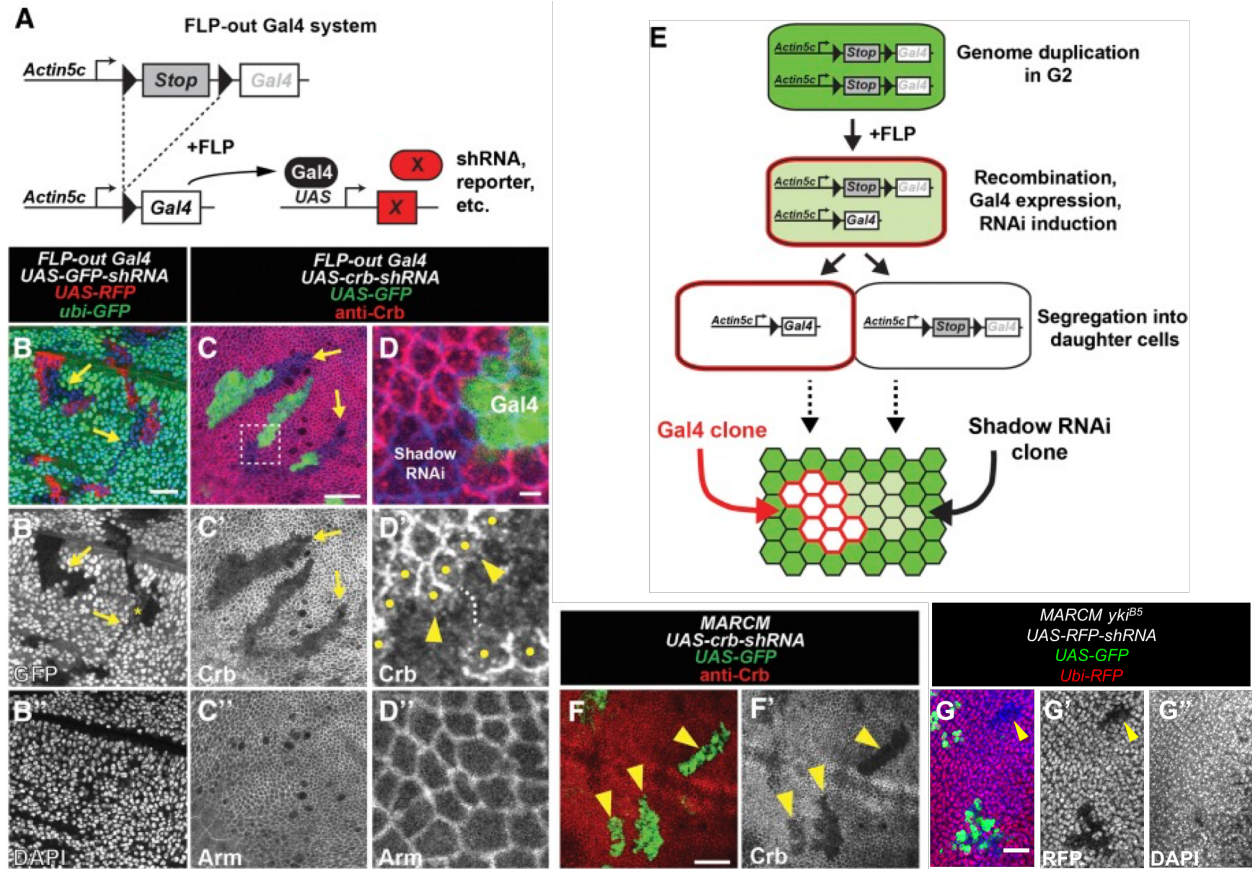


Figure 4.1: Gene knockdown in shadow RNAi clones when using the FLP-out Gal4 system.

(A) Genetic diagram of the FLP-out Gal4 system. The *Actin5c* promoter drives constitutive expression of Gal4 after FLP/FRT recombination. (B–D) FLP-out Gal4 clones in the wing imaginal disc. (B) Gal4 clones express RFP (red) and *GFP-shRNA*, causing knockdown of GFP (green). Shadow RNAi clones knock down GFP but do not express RFP (arrows). Asterisk in B' indicates shadow RNAi clone with intermediate levels of knockdown. Cell nuclei labeled with DAPI (blue). Bar, 20  $\mu\text{m}$ . (C) Gal4 clones express GFP (green) and *crb-shRNA* and knock down Crb protein (red). Shadow RNAi clones knock down Crb protein (arrows). Arm staining (blue) shows cell membrane. Bar, 20  $\mu\text{m}$ . (D) Magnification of region in C. Arrowheads indicate that Crb protein is missing on the membrane of wild-type cells (dots) that contact Gal4 and shadow RNAi cells. Bar, 2  $\mu\text{m}$ . (E) Model for generation of shadow RNAi clones. Prior to cell division, recombination during G2 causes expression of Gal4 (red) and knockdown of target gene expression (green). Following cell division, target gene knockdown persists in non-Gal4-expressing cells (shadow RNAi clone). (F) MARCM Gal4 clones in the wing disc (arrowheads). Gal4 clones express GFP (green) and *crb-shRNA* and knock down Crb protein (red). Bar, 20  $\mu\text{m}$ . (G) *yki<sup>B5</sup>* MARCM Gal4 clones in the eye disc express GFP (green) and *RFP-shRNA* and knock down ubiquitously expressed RFP protein (red). Shadow RNAi clone shows knockdown of RFP but does not express GFP (arrowhead). Cell nuclei labeled with DAPI (blue). Bar, 20  $\mu\text{m}$ . All panels with (') or (") designation show isolated greyscale channels of the merged image in their respective parental panel.

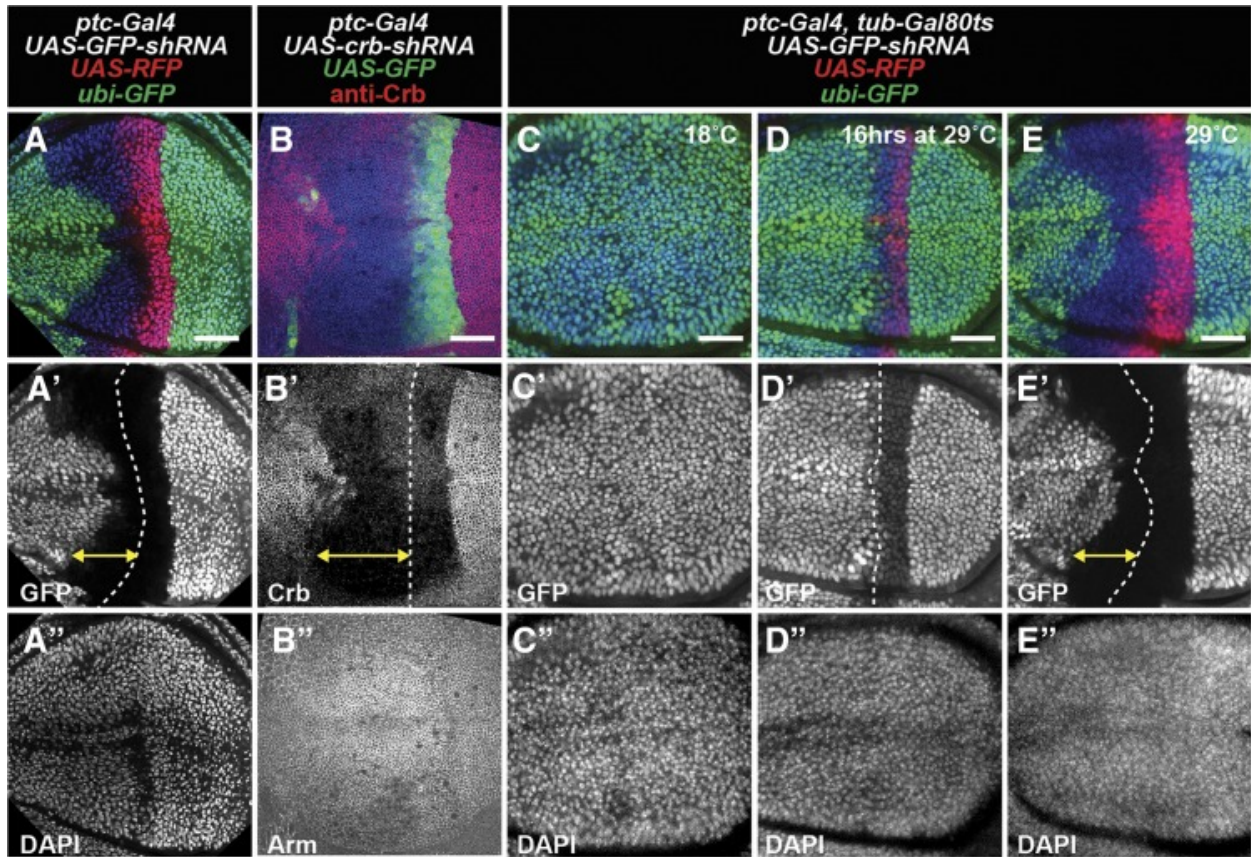


Figure 4.2: **Gene knockdown in shadow RNAi cells caused by dynamic expression of *ptc-Gal4*.** (A–E) Wing imaginal discs with RNAi under control of *ptc-Gal4*. (A) *ptc-Gal4* expression of RFP (red) and *GFP-shRNA* cause knockdown of GFP (green). Cell nuclei labeled with DAPI (blue). (B) *ptc-Gal4* expression of GFP (green) and *crb-shRNA* cause knockdown of Crb protein (red). Arm staining (blue) shows cell membrane. (C–E) Temperature control of *ptc-Gal4* expression with *tub-Gal80ts*. *ptc-Gal4* expression of RFP (red) and *GFP-shRNA* cause knockdown of GFP (green). Cell nuclei labeled with DAPI (blue). (C) Larvae always kept at 18°C. (D) Larvae shifted from 18°C to 29°C 16 hr before dissection. (E) Larvae always kept at 29°C. Double arrow in A', B', and E' indicates RNAi persistence in cells anterior to the *ptc* stripe. Bars, 50  $\mu\text{m}$ . All panels with (') or (") designation show isolated greyscale channels of the merged image in their respective parental panel.

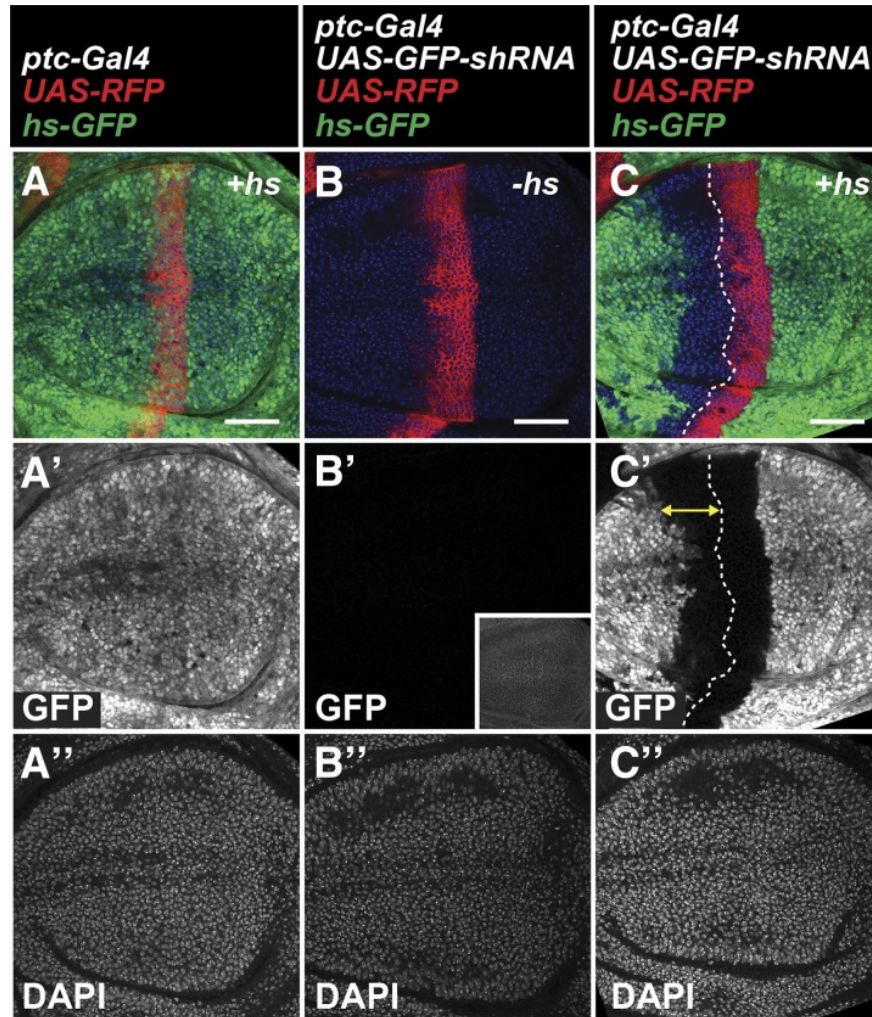


Figure 4.3: **RNAi persistence does not require past expression of target transcripts.** (A–C) Wing imaginal discs with *ptc-Gal4* expression of RFP (red). All discs contain the *hs-GFP* transgene. GFP (green) expression is induced with a heat shock (hs) 2 hr before dissection. Cell nuclei labeled with DAPI (blue). (A) Heat-shock induction of GFP (green) with no *GFP-shRNA*. (B) Expression of *GFP-shRNA* with no heat shock. (B') Inset shows maximum exposure. (C) Expression of *GFP-shRNA* with heat shock. Double arrow in C' indicates RNAi persistence in cells anterior to the *ptc* stripe. Bars, 50  $\mu\text{m}$ . All panels with (') or (") designation show isolated greyscale channels of the merged image in their respective parental panel.

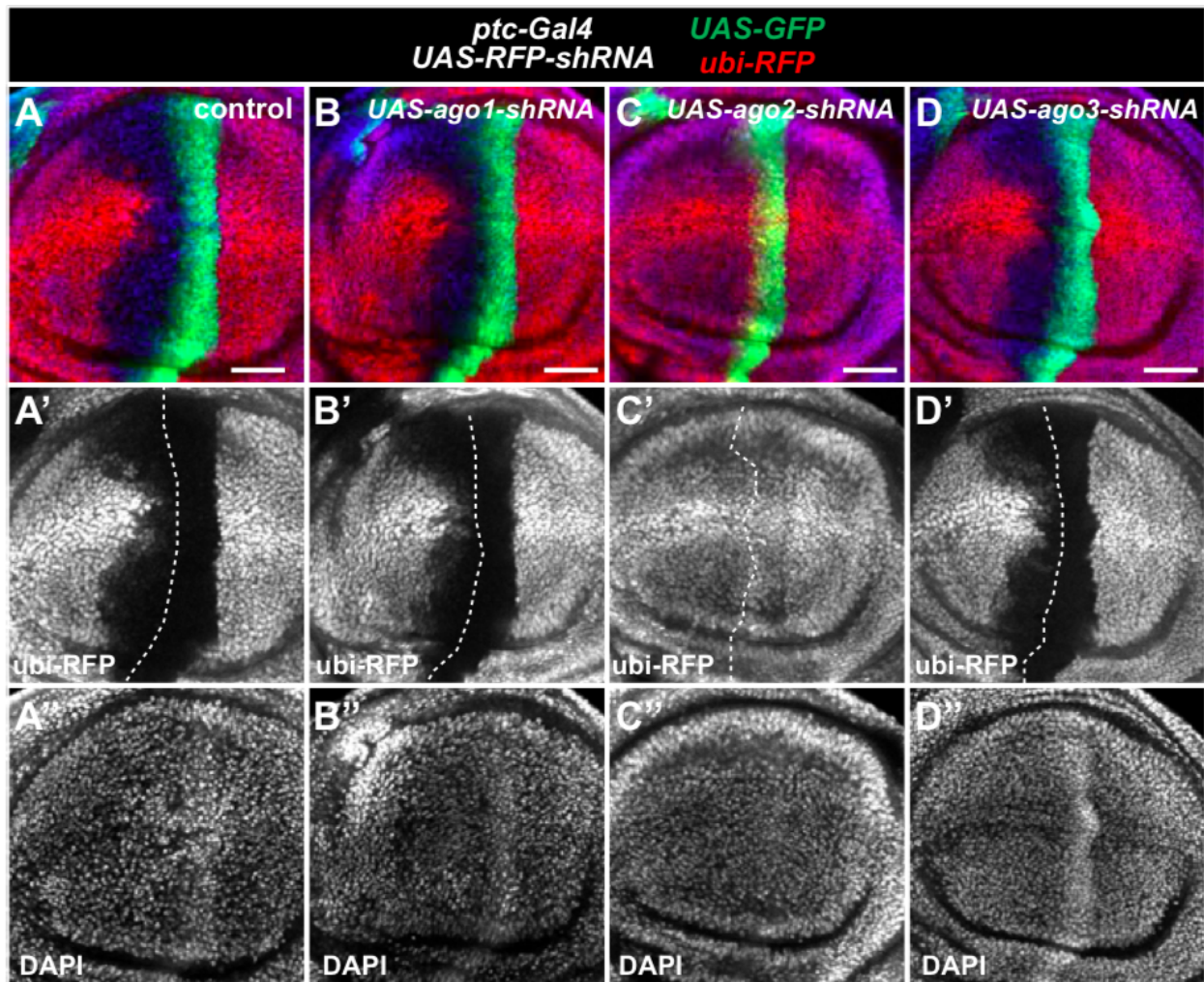


Figure 4.4: RNAi persistence requires Ago2 but not other RISC components. (A–D) Wing imaginal disc with *ptc-Gal4* expression of GFP (green) and *RFP-shRNA*, in an *ubi-RFP* background. Cell nuclei labeled with DAPI (blue). (A) Control disc. Expression of (B) *ago1-shRNA*, (C) *ago2-shRNA*, or (D) *ago3-shRNA*. Scale bars are 50 $\mu$ m.

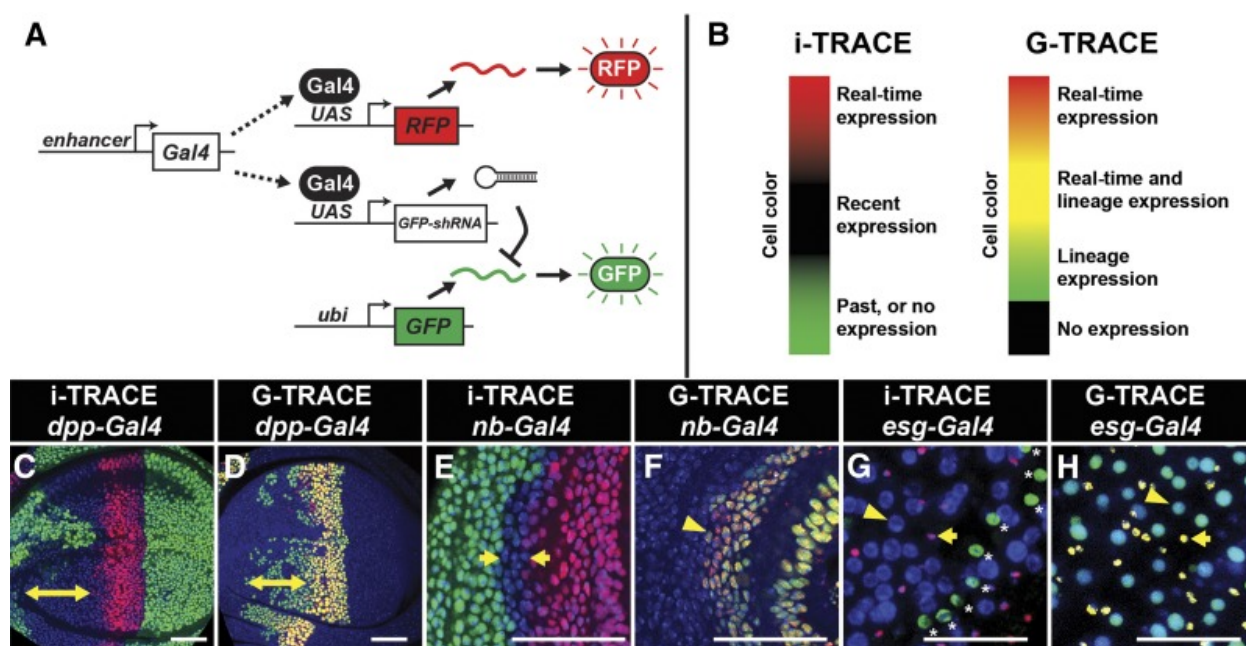


Figure 4.5: **The i-TRACE system.** (A) Diagram of the genetic components that form the i-TRACE system. Enhancer-driven expression of Gal4 induces RFP and *GFP-shRNA* in cells. *GFP-shRNA* targets ubiquitously expressed GFP transcripts from *ubi-GFP*. (B) A comparison of cell color representations between the i-TRACE and G-TRACE systems. (C–H) Analysis of enhancer-Gal4 expression with i-TRACE and G-TRACE. Cell nuclei labeled with DAPI (blue). Bars, 50  $\mu\text{m}$ . (C and D) *dpp-Gal4* expression in the wing imaginal disc. Double arrows indicate RNAi persistence in C, or recombined lineage in D, in cells anterior to the *ptc* stripe. (E and F) *nb-Gal4* expression in the wing imaginal disc. (E) Arrows indicate region of past expression at outer edge of pouch. (F) Arrowhead indicates outer boundary of *nb-Gal4* expression. (G and H) *esg-Gal4* expression in the adult midgut. Arrows indicate RFP+ nuclei; arrowheads indicate enterocyte nuclei. Asterisks in G indicate overlying muscle nuclei with GFP expression.

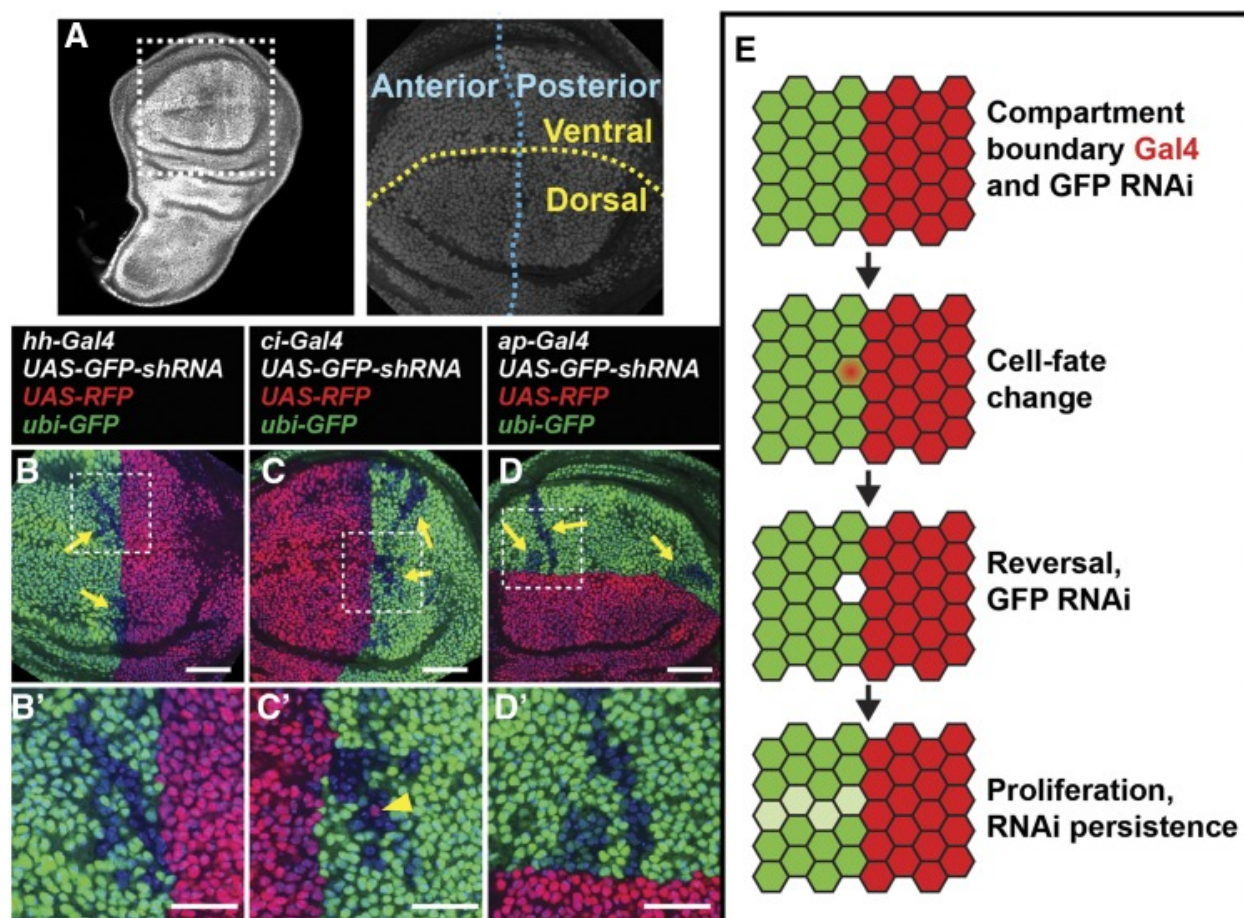


Figure 4.6: **Reversible cell-fate switching at compartment boundaries in the wing disc.** (A) Wandering third instar wing disc expressing *ubi-GFP*. Boxed area indicates magnified pouch region with overlay of compartment boundaries, ventral-dorsal (horizontal yellow line) and anterior-posterior (vertical blue line). (B–D) i-TRACE analysis of compartment-specific Gal4 lines in the wing disc. (B) *hh-Gal4* (posterior expression). (C) *ci-Gal4* (anterior expression). (D) *ap-Gal4* (dorsal expression). Cell nuclei labeled with DAPI (blue). Arrows indicate shadow RNAi cells in the opposite compartment to enhancer-Gal4 expression. Boxes indicate magnifications in B', C', and D'. Arrowhead in C' indicates a posterior RFP+ cell. Bars, 50  $\mu\text{m}$  in B, C, D; 25  $\mu\text{m}$  in B', C', and D'.

<b>Target</b>	<b>Knockdown type</b>	<b>BL#</b>	<b>FLPout-Gal4 phenotype</b>	<b>ptc-Gal4 phenotype</b>
<i>ubi-GFP</i>	dsRNA	9330	rare and faint shadow RNAi	faint shadow RNAi anterior to ptc stripe
<i>ubi-GFP</i>	shRNA	41556	obvious shadow RNAi	obvious shadow RNAi anterior to ptc stripe
<i>hs-GFP</i>	shRNA	41555	-	obvious shadow RNAi anterior to ptc stripe
<i>ubi-GFP</i>	deGradFP	38421	-	faint shadow RNAi anterior to ptc stripe
<i>ubi-RFP</i>	shRNA	35785	obvious shadow RNAi	obvious shadow RNAi anterior to ptc stripe
<i>crb</i>	dsRNA	27697	-	no shadow RNAi anterior to ptc stripe
<i>crb</i>	shRNA	40869	obvious shadow RNAi	obvious shadow RNAi anterior to ptc stripe
<i>CtBP</i>	shRNA	32889	obvious shadow RNAi	obvious shadow RNAi anterior to ptc stripe
<i>gigas</i>	shRNA	34737	no shadow RNAi	-
<i>ft</i>	shRNA	34970	no shadow RNAi	-
<i>dac</i>	shRNA	35022	no shadow RNAi	-

Table 4.1: Summary of genes targeted by RNAi and knockdown transgenes tested

# References

- Adams, M. D. and J. J. Sekelsky (2002). From sequence to phenotype: reverse genetics in *Drosophila melanogaster*. *Nature Reviews Genetics* 3:189 EP –.
- Aegerter-Wilmsen, T., C. M. Aegerter, E. Hafen, and K. Basler (2007). Model for the regulation of size in the wing imaginal disc of *Drosophila*. *Mechanisms of development* 124 (4):318–326.
- Agaisse, H., U.-M. Petersen, M. Boutros, B. Mathey-Prevot, and N. Perrimon (2003). Signaling role of hemocytes in *Drosophila* JAK/STAT-dependent response to septic injury. *Developmental cell* 5 (3):441–450.
- Alder, M. N., S. Dames, J. Gaudet, and S. E. Mango (2003). Gene silencing in *Caenorhabditis elegans* by transitive RNA interference. *Rna* 9 (1):25–32.
- Alexandre, C., A. Baena-Lopez, and J.-P. Vincent (2013). Patterning and growth control by membrane-tethered Wingless. *Nature* 505:180 EP –.
- Ambegaonkar, A. A., G. Pan, M. Mani, Y. Feng, and K. D. Irvine (2012). Propagation of Dachsous-Fat planar cell polarity. *Current Biology* 22 (14):1302–1308.
- Baccarini, A., H. Chauhan, T. J. Gardner, A. D. Jayaprakash, R. Sachidanandam, and B. D. Brown (2011). Kinetic analysis reveals the fate of a microRNA following target regulation in mammalian cells. *Current biology* 21 (5):369–376.
- Baena-López, L. A., A. Baonza, and A. García-Bellido (2005). The orientation of cell divisions determines the shape of *Drosophila* organs. *Current Biology* 15 (18):1640–1644.
- Bartlett, D. W. and M. E. Davis (2006). Insights into the kinetics of siRNA-mediated gene silencing from live-cell and live-animal bioluminescent imaging. *Nucleic acids research* 34 (1):322–333.
- Baumgartner, R., I. Poernbacher, N. Buser, E. Hafen, and H. Stocker (2010). The WW Domain Protein Kibra Acts Upstream of Hippo in *Drosophila*. *Developmental Cell* 18 (2):309–316.
- Becam, I., N. Rafel, X. Hong, S. M. Cohen, and M. Milán (2011). Notch-mediated repression of bantam miRNA contributes to boundary formation in the *Drosophila* wing. *Development* 138 (17):3781–3789.
- Bennett, F. C. and K. F. Harvey (2006). Fat cadherin modulates organ size in *Drosophila* via the Salvador/Warts/Hippo signaling pathway. *Current Biology* 16 (21):2101–2110.

- Biryukova, I. and P. Heitzler (2008). Drosophila C-terminal binding protein, dCtBP is required for sensory organ prepatterning and sharpens proneural transcriptional activity of the GATA factor Pnr. *Developmental biology* 323 (1):64–75.
- Biteau, B., J. Karpac, D. Hwangbo, and H. Jasper (2011). Regulation of Drosophila lifespan by JNK signaling. *Experimental gerontology* 46 (5):349–354.
- Blair, S. S., D. L. Brower, J. B. Thomas, and M. Zavortink (1994). The role of apterous in the control of dorsoventral compartmentalization and PS integrin gene expression in the developing wing of Drosophila. *Development* 120 (7):1805–1815.
- Boedigheimer, M. and A. Laughon (1993). Expanded: a gene involved in the control of cell proliferation in imaginal discs. *Development* 118 (4):1291–1301.
- Boone, E., J. Colombani, D. S. Andersen, and P. Léopold (2016). The Hippo signalling pathway coordinates organ growth and limits developmental variability by controlling dilp8 expression. *Nature Communications* 7:13505 EP –.
- Bosch, M., F. Serras, E. Martín-Blanco, and J. Bagaña (2005). JNK signaling pathway required for wound healing in regenerating Drosophila wing imaginal discs. *Developmental biology* 280 (1):73–86.
- Bossuyt, W., C. Chen, Q. Chen, M. Sudol, H. McNeill, D. Pan, A. Kopp, and G. Halder (2014). An evolutionary shift in the regulation of the Hippo pathway between mice and flies. *Oncogene* 33 (10):1218.
- Bosveld, F., I. Bonnet, B. Guirao, S. Tlili, Z. Wang, A. Petitalot, R. Marchand, P.-L. Bardet, P. Marcq, F. Graner, et al. (2012). Mechanical control of morphogenesis by Fat/Dachsous/Four-jointed planar cell polarity pathway. *Science* 336 (6082):724–727.
- Boyd, J. M., T. Subramanian, U. Schaeper, M. La Regina, S. Bayley, and G. Chinnadurai (1993). A region in the C-terminus of adenovirus 2/5 E1a protein is required for association with a cellular phosphoprotein and important for the negative modulation of T24-ras mediated transformation, tumorigenesis and metastasis. *The EMBO journal* 12 (2):469–478.
- Brand, A. H. and N. Perrimon (1993). Targeted gene expression as a means of altering cell fates and generating dominant phenotypes. *development* 118 (2):401–415.
- Brennecke, J., A. A. Aravin, A. Stark, M. Dus, M. Kellis, R. Sachidanandam, and G. J. Hannon (2007). Discrete small RNA-generating loci as master regulators of transposon activity in Drosophila. *Cell* 128 (6):1089–1103.
- Brennecke, J., D. R. Hipfner, A. Stark, R. B. Russell, and S. M. Cohen (2003). bantam encodes a developmentally regulated microRNA that controls cell proliferation and regulates the proapoptotic gene hid in Drosophila. *Cell* 113 (1):25–36.
- Brittle, A., C. Thomas, and D. Strutt (2012). Planar polarity specification through asymmetric subcellular localization of Fat and Dachsous. *Current biology* 22 (10):907–914.
- Brittle, A. L., A. Repiso, J. Casal, P. A. Lawrence, and D. Strutt (2010). Four-jointed modulates growth and planar polarity by reducing the affinity of dachsous for fat. *Current Biology* 20 (9):803–810.
- Bryant, P. J. (1971). Regeneration and duplication following operations in situ on the imaginal discs of Drosophila melanogaster. *Developmental biology* 26 (4):637–651.

- Bryant, P. J., B. Huettner, L. I. Held Jr, J. Ryerse, and J. Szidonya (1988). Mutations at the fat locus interfere with cell proliferation control and epithelial morphogenesis in *Drosophila*. *Developmental biology* 129 (2):541–554.
- Bryant, P. J. and P. Levinson (1985). Intrinsic growth control in the imaginal primordia of *Drosophila*, and the autonomous action of a lethal mutation causing overgrowth. *Developmental biology* 107 (2):355–363.
- Buchon, N., N. A. Broderick, S. Chakrabarti, and B. Lemaitre (2009). Invasive and indigenous microbiota impact intestinal stem cell activity through multiple pathways in *Drosophila*. *Genes & development* 23 (19):2333–2344.
- Bui, D. A., W. Lee, A. E. White, J. W. Harper, R. C. Schackmann, M. Overholtzer, L. M. Selfors, and J. S. Brugge (2016). Cytokinesis involves a nontranscriptional function of the Hippo pathway effector YAP. *Sci. Signal.* 9 (417):ra23–ra23.
- Carrano, A. C., E. Eytan, A. Hershko, and M. Pagano (1999). SKP2 is required for ubiquitin-mediated degradation of the CDK inhibitor p27. *Nature cell biology* 1 (4):193.
- Caussinus, E., O. Kanca, and M. Affolter (2012). Fluorescent fusion protein knockout mediated by anti-GFP nanobody. *Nature Structural and Molecular Biology* 19 (1):117.
- Chen, C.-L., K. M. Gajewski, F. Hamaratoglu, W. Bossuyt, L. Sansores-Garcia, C. Tao, and G. Halder (2010a). The apical-basal cell polarity determinant Crumbs regulates Hippo signaling in *Drosophila*. *Proceedings of the National Academy of Sciences* 107 (36):15810–15815.
- (2010b). The apical-basal cell polarity determinant Crumbs regulates Hippo signaling in *Drosophila*. *Proceedings of the National Academy of Sciences of the United States of America* 107 (36):15810–15815.
- Chi, J.-T., H. Y. Chang, N. N. Wang, D. S. Chang, N. Dunphy, and P. O. Brown (2003). Genomewide view of gene silencing by small interfering RNAs. *Proceedings of the National Academy of Sciences* 100 (11):6343–6346.
- Chinnadurai, G. (2007). CtBP family proteins. *GtBP Family Proteins*. Springer, 1–17.
- Cho, E., Y. Feng, C. Rauskolb, S. Maitra, R. Fehon, and K. D. Irvine (2006). Delineation of a Fat tumor suppressor pathway. *Nature genetics* 38 (10):1142.
- Clark, H. F., D. Brentrup, K. Schneitz, A. Bieber, C. Goodman, and M. Noll (1995). Dachsous encodes a member of the cadherin superfamily that controls imaginal disc morphogenesis in *Drosophila*. *Genes & Development* 9 (12):1530–1542.
- Colombani, J., D. S. Andersen, and P. Léopold (2012). Secreted peptide Dilp8 coordinates *Drosophila* tissue growth with developmental timing. *Science* 336 (6081):582–585.
- Coon, T. A., J. R. Glasser, R. K. Mallampalli, and B. B. Chen (2012). Novel E3 ligase component FBXL7 ubiquitinates and degrades Aurora A, causing mitotic arrest. *Cell cycle* 11 (4):721–729.
- Cooper, G. M. (2000). “The Molecular Composition of Cells”. *The Cell: A Molecular Approach*. 2nd ed.
- Crocker, J. A., S. L. Ziegenhorn, and R. A. Holmgren (2006). Regulation of the *Drosophila* transcription factor, Cubitus interruptus, by two conserved domains. *Developmental biology* 291 (2):368–381.

- Dahmann, C., A. C. Oates, and M. Brand (2011). Boundary formation and maintenance in tissue development. *Nature Reviews Genetics* 12 (1):43.
- Deng, H., W. Wang, J. Yu, Y. Zheng, Y. Qing, and D. Pan (2015). Spectrin regulates Hippo signaling by modulating cortical actomyosin activity. *eLife* 4:ed. by J. Rossant, e06567.
- Desai, R., R. Sarpal, N. Ishiyama, M. Pellikka, M. Ikura, and U. Tepass (2013). Monomeric  $\alpha$ -catenin links cadherin to the actin cytoskeleton. *Nature cell biology* 15 (3):261.
- Dickins, R. A., M. T. Hemann, J. T. Zilfou, D. R. Simpson, I. Ibarra, G. J. Hannon, and S. W. Lowe (2005). Probing tumor phenotypes using stable and regulated synthetic microRNA precursors. *Nature genetics* 37 (11):1289.
- Dubatolova, T and L Omelyanchuk (2004). Analysis of cell proliferation in Drosophila wing imaginal discs using mosaic clones. *Heredity* 92 (4):299.
- Dui, W., W. Lu, J. Ma, and R. Jiao (2012). A systematic phenotypic screen of F-box genes through a tissue-specific RNAi-based approach in Drosophila. *Journal of Genetics and Genomics* 39 (8):397–413.
- Dupont, S., L. Morsut, M. Aragona, E. Enzo, S. Giulitti, M. Cordenonsi, F. Zanconato, J. Le Digabel, M. Forcato, S. Bicciato, N. Elvassore, and S. Piccolo (2011). Role of YAP/TAZ in mechanotransduction. *Nature* 474:179 EP –.
- Eaton, S. and T. B. Kornberg (1990). Repression of ci-D in posterior compartments of Drosophila by engrailed. *Genes & Development* 4 (6):1068–1077.
- Eferl, R. and E. F. Wagner (2003). AP-1: a double-edged sword in tumorigenesis. *Nature Reviews Cancer* 3 (11):859.
- Enomoto, M. and T. Igaki (2013). Src controls tumorigenesis via JNK-dependent regulation of the Hippo pathway in Drosophila. *EMBO reports* 14 (1):65–72.
- Enomoto, M., D. Kizawa, S. Ohsawa, and T. Igaki (2015). JNK signaling is converted from anti-to pro-tumor pathway by Ras-mediated switch of Warts activity. *Developmental biology* 403 (2):162–171.
- Evans, C. J., J. M. Olson, K. T. Ngo, E. Kim, N. E. Lee, E. Kuoy, A. N. Patananan, D. Sitz, P. Tran, M.-T. Do, et al. (2009). G-TRACE: rapid Gal4-based cell lineage analysis in Drosophila. *Nature methods* 6 (8):603.
- Fabricius, J. C. (1778). *Philosophia entomologica*. Impensis Carol. Ernest. Bohnii.
- Fanto, M., L. Clayton, J. Meredith, K. Hardiman, B. Charroux, S. Kerridge, and H. McNeill (2003). The tumor-suppressor and cell adhesion molecule Fat controls planar polarity via physical interactions with Atrophin, a transcriptional co-repressor. *Development* 130 (4):763–774.
- Feng, Y. and K. D. Irvine (2007). Fat and expanded act in parallel to regulate growth through warts. *Proceedings of the National Academy of Sciences* 104 (51):20362–20367.
- (2009). Processing and phosphorylation of the Fat receptor. *Proceedings of the National Academy of Sciences* 106 (29):11989–11994.
- Fernández, B. G., P. Gaspar, C. Brás-Pereira, B. Jezowska, S. R. Rebelo, and F. Janody (2011). Actin-Capping Protein and the Hippo pathway regulate F-actin and tissue growth in Drosophila. *Development* 138 (11):2337–2346.

- Ferreira, A. and M. Milán (2015). Dally Proteoglycan Mediates the Autonomous and Nonautonomous Effects on Tissue Growth Caused by Activation of the PI3K and TOR Pathways. *PLoS Biology* 13 (8):1–28.
- Fire, A., S. Xu, M. K. Montgomery, S. A. Kostas, S. E. Driver, and C. C. Mello (1998). Potent and specific genetic interference by double-stranded RNA in *Caenorhabditis elegans*. *nature* 391 (6669):806.
- Fischer, J. A., E. Giniger, T. Maniatis, and M. Ptashne (1988). GAL4 activates transcription in *Drosophila*. *Nature* 332 (6167):853.
- Fletcher, G. C., A. Elbediwy, I. Khanal, P. S. Ribeiro, N. Tapon, and B. J. Thompson (2015). The Spectrin cytoskeleton regulates the Hippo signalling pathway. *The EMBO Journal* 34 (7):940–954.
- Froldi, F., M. Ziosi, F. Garoia, A. Pession, N. A. Grzeschik, P. Bellosta, D. Strand, H. E. Richardson, A. Pession, and D. Grifoni (2010). The lethal giant larvae tumour suppressor mutation requires dMyc oncoprotein to promote clonal malignancy. *BMC biology* 8 (1):33.
- Galan, J.-M. and M. Peter (1999). Ubiquitin-dependent degradation of multiple F-box proteins by an autocatalytic mechanism. *Proceedings of the National Academy of Sciences* 96 (16):9124–9129.
- García-Bellido, A. and J. R. Merriam (1971). Parameters of the wing imaginal disc development of *Drosophila melanogaster*. *Developmental biology* 24 (1):61–87.
- García-Martínez, V., D. Macías, Y. Ganan, J. García-Lobo, M. Francia, M. Fernández-Teran, and J. Hurlé (1993). Internucleosomal DNA fragmentation and programmed cell death (apoptosis) in the interdigital tissue of the embryonic chick leg bud. *Journal of Cell Science* 106 (1):201–208.
- Garelli, A., A. M. Gontijo, V. Miguela, E. Caparros, and M. Dominguez (2012). Imaginal discs secrete insulin-like peptide 8 to mediate plasticity of growth and maturation. *Science* 336 (6081):579–582.
- Genevet, A., M. C. Wehr, R. Brain, B. J. Thompson, and N. Tapon (2010). Kibra Is a Regulator of the Salvador/Warts/Hippo Signaling Network. *Developmental Cell* 18 (2-3):300–308.
- Gettings, M., F. Serman, R. Rousset, P. Bagnolini, L. Almeida, and S. Noselli (2010). JNK signalling controls remodelling of the segment boundary through cell reprogramming during *Drosophila* morphogenesis. *PLoS biology* 8 (6):e1000390.
- González-Gaitán, M., M. P. Capdevila, and A. García-Bellido (1994). Cell proliferation patterns in the wing imaginal disc of *Drosophila*. *Mechanisms of development* 46 (3):183–200.
- Gunage, R. D., H. Reichert, and K. VijayRaghavan (2014). Identification of a new stem cell population that generates *Drosophila* flight muscles. *Elife* 3.
- Guo, T., Y. Lu, P. Li, M.-X. Yin, D. Lv, W. Zhang, H. Wang, Z. Zhou, H. Ji, Y. Zhao, et al. (2013). A novel partner of Scalloped regulates Hippo signaling via antagonizing Scalloped-Yorkie activity. *Cell research* 23 (10):1201.

- Gupta, S., R. A. Schoer, J. E. Egan, G. J. Hannon, and V. Mittal (2004). Inducible, reversible, and stable RNA interference in mammalian cells. *Proceedings of the National Academy of Sciences* 101 (7):1927–1932.
- Hadorn, E. (1963). Differenzierungsleistungen wiederholt fragmentierter Teilstücke männlicher Genitalscheiben von *Drosophila melanogaster* nach Kultur in vivo. *Developmental Biology* 7:617–629.
- Hafezi, Y., J. A. Bosch, and I. K. Hariharan (2012). Differences in levels of the transmembrane protein Crumbs can influence cell survival at clonal boundaries. *Developmental biology* 368 (2):358–369.
- Haglund, K., N. Shimokawa, I. Szymkiewicz, and I. Dikic (2002). Cbl-directed monoubiquitination of CIN85 is involved in regulation of ligand-induced degradation of EGF receptors. *Proceedings of the National Academy of Sciences* 99 (19):12191–12196.
- Halder, G. and R. L. Johnson (2011). Hippo signaling: growth control and beyond. *Development* 138 (1):9–22.
- Halfon, M. S., H. Kose, A. Chiba, and H. Keshishian (1997). Targeted gene expression without a tissue-specific promoter: creating mosaic embryos using laser-induced single-cell heat shock. *Proceedings of the National Academy of Sciences* 94 (12):6255–6260.
- Halme, A., M. Cheng, and I. K. Hariharan (2010). Retinoids regulate a developmental checkpoint for tissue regeneration in *Drosophila*. *Current Biology* 20 (5):458–463.
- Hamaratoglu, F., M. Willecke, M. Kango-Singh, R. Nolo, E. Hyun, C. Tao, H. Jafar-Nejad, and G. Halder (2006). The tumour-suppressor genes NF2/Merlin and Expanded act through Hippo signalling to regulate cell proliferation and apoptosis. *Nature cell biology* 8 (1):27.
- Hannon, G. J. (2002). RNA interference. *Nature* 418 (6894):244.
- Hariharan, I. K. (2015). Organ size control: lessons from *Drosophila*. *Developmental cell* 34 (3):255–265.
- Harrison, R. G. (1924). Some unexpected results of the heteroplasic transplantation of limbs. *Proceedings of the National Academy of Sciences* 10 (2):69–74.
- Hasson, P., B. Müller, K. Basler, and Z. Paroush (2001). Brinker requires two corepressors for maximal and versatile repression in Dpp signalling. *The EMBO journal* 20 (20):5725–5736.
- Herrera, S. C. and G. Morata (2014). Transgressions of compartment boundaries and cell reprogramming during regeneration in *Drosophila*. *Elife* 3.
- Hinz, U., B. Giebel, and J. Campos-Ortega (1994). The basic-helix-loop-helix domain of *Drosophila* lethal of scute protein is sufficient for proneural function and activates neurogenic genes. *Cell* 76 (1):77–87.
- Hoang, C. Q., M. E. Burnett, and J. Curtiss (2010). *Drosophila* CtBP regulates proliferation and differentiation of eye precursors and complexes with Eyeless, Dachshund, Dan, and Danr during eye and antennal development. *Developmental Dynamics* 239 (9):2367–2385.
- Huang, J., S. Wu, J. Barrera, K. Matthews, and D. Pan (2005). The Hippo signaling pathway coordinately regulates cell proliferation and apoptosis by inactivating Yorkie, the *Drosophila* Homolog of YAP. *Cell* 122 (3):421–434.

- Hufnagel, L., A. A. Teleman, H. Rouault, S. M. Cohen, and B. I. Shraiman (2007). On the mechanism of wing size determination in fly development. *Proceedings of the National Academy of Sciences* 104 (10):3835–3840.
- Igaki, T. (2009). Correcting developmental errors by apoptosis: lessons from *Drosophila* JNK signaling. *Apoptosis* 14 (8):1021–1028.
- Igaki, T., R. A. Pagliarini, and T. Xu (2006). Loss of cell polarity drives tumor growth and invasion through JNK activation in *Drosophila*. *Current Biology* 16 (11):1139–1146.
- Irvine, K. D. and K. F. Harvey (2015). Control of organ growth by patterning and hippo signaling in *Drosophila*. *Cold Spring Harbor perspectives in biology* 7 (6):a019224.
- Ishikawa, H. O., H. Takeuchi, R. S. Haltiwanger, and K. D. Irvine (2008). Four-jointed is a Golgi kinase that phosphorylates a subset of cadherin domains. *Science* 321 (5887):401–404.
- Jaszczak, J. S., J. B. Wolpe, A. Q. Dao, and A. Halme (2015). Nitric oxide synthase regulates growth coordination during *Drosophila melanogaster* imaginal disc regeneration. *Genetics* 200 (4):1219–1228.
- Johnson, R. I., S. Bao, and R. L. Cagan (2012). Interactions between *Drosophila* IgCAM adhesion receptors and cindr, the Cd2ap/Cin85 ortholog. *Developmental Dynamics* 241 (12):1933–1943.
- Johnson, R. I., A. Sedgwick, C. D’Souza-Schorey, and R. L. Cagan (2011). Role for a Cindr–Arf6 axis in patterning emerging epithelia. *Molecular biology of the cell* 22 (23):4513–4526.
- Johnson, R. I., M. J. Seppa, and R. L. Cagan (2008). The *Drosophila* CD2AP/CIN85 orthologue Cindr regulates junctions and cytoskeleton dynamics during tissue patterning. *The Journal of cell biology* 180 (6):1191–1204.
- Jursnich, V. A., S. E. Fraser, L. I. Held Jr, J. Ryerse, and P. J. Bryant (1990). Defective gap-junctional communication associated with imaginal disc overgrowth and degeneration caused by mutations of the dco gene in *Drosophila*. *Developmental biology* 140 (2):413–429.
- Khan, S. J., A. Bajpai, M. A. Alam, R. P. Gupta, S. Harsh, R. K. Pandey, S. Goel-Bhattacharya, A. Nigam, A. Mishra, and P. Sinha (2013). Epithelial neoplasia in *Drosophila* entails switch to primitive cell states. *Proceedings of the National Academy of Sciences* 110 (24):E2163–E2172.
- Ko, H. W., J. Jiang, and I. Ederly (2002). Role for Slimb in the degradation of *Drosophila* Period protein phosphorylated by Doubletime. *Nature* 420 (6916):673.
- Koontz, L. M., Y. Liu-Chittenden, F. Yin, Y. Zheng, J. Yu, B. Huang, Q. Chen, S. Wu, and D. Pan (2013). The Hippo effector Yorkie controls normal tissue growth by antagonizing Scalloped-mediated default repression. *Developmental cell* 25 (4):388–401.
- Kornberg, T., I. Sidén, P. O’Farrell, and M. Simon (1985). The engrailed locus of *Drosophila*: in situ localization of transcripts reveals compartment-specific expression. *Cell* 40 (1):45–53.
- Kwon, Y., A. Vinayagam, X. Sun, N. Dephoure, S. P. Gygi, P. Hong, and N. Perrimon (2013). The Hippo signaling pathway interactome. *Science*:1243971.

- Lee, T. and L. Luo (1999). Mosaic analysis with a repressible cell marker for studies of gene function in neuronal morphogenesis. *Neuron* 22 (3):451–461.
- LeGoff, L., H. Rouault, and T. Lecuit (2013). A global pattern of mechanical stress polarizes cell divisions and cell shape in the growing *Drosophila* wing disc. *Development* 140 (19):4051–4059.
- Ling, C., Y. Zheng, F. Yin, J. Yu, J. Huang, Y. Hong, S. Wu, and D. Pan (2010). The apical transmembrane protein Crumbs functions as a tumor suppressor that regulates Hippo signaling by binding to Expanded. *Proceedings of the National Academy of Sciences of the United States of America* 107 (23):10532–10537.
- Ling, J., R. Dubruille, and P. Emery (2012). KAYAK- $\alpha$  modulates circadian transcriptional feedback loops in *Drosophila* pacemaker neurons. *Journal of Neuroscience* 32 (47):16959–16970.
- Liu, S., J. Sun, D. Wang, G. O. Pflugfelder, and J. Shen (2016). Fold formation at the compartment boundary of *Drosophila* wing requires Yki signaling to suppress JNK dependent apoptosis. *Scientific Reports* 6 (38003).
- Livshits, G. and S. W. Lowe (2013). Accelerating cancer modeling with RNAi and nongerm-line genetically engineered mouse models. *Cold Spring Harbor protocols* 2013 (11):pdb-top069856.
- Ma, D., C.-h. Yang, H. McNeill, M. A. Simon, and J. D. Axelrod (2003). Fidelity in planar cell polarity signalling. *Nature* 421 (6922):543.
- Ma, M., X. Cao, J. Dai, and J. C. Pastor-Pareja (2017). Basement Membrane Manipulation in *Drosophila* Wing Discs Affects Dpp Retention but Not Growth Mechanoregulation. *Developmental Cell* 42 (1):97–106.e4.
- Madhavan, M. M. and H. A. Schneiderman (1977). Histological analysis of the dynamics of growth of imaginal discs and histoblast nests during the larval development of *Drosophila melanogaster*. *Wilhelm Roux's archives of developmental biology* 183 (4):269–305.
- Mahoney, P. A., U. Weber, P. Onofrechuk, H. Biessmann, P. J. Bryant, and C. S. Goodman (1991). The fat tumor suppressor gene in *Drosophila* encodes a novel member of the cadherin gene superfamily. *Cell* 67 (5):853–868.
- Mao, Y., A. L. Tournier, P. A. Bates, J. E. Gale, N. Tapon, and B. J. Thompson (2011). Planar polarization of the atypical myosin Dachs orients cell divisions in *Drosophila*. *Genes & development* 25 (2):131–136.
- Mao, Y., B. Kucuk, and K. D. Irvine (2009). *Drosophila* lowfat, a novel modulator of Fat signaling. *Development* 136 (19):3223–3233.
- Mao, Y., C. Rauskolb, E. Cho, W.-L. Hu, H. Hayter, G. Minihan, F. N. Katz, and K. D. Irvine (2006). Dachs: an unconventional myosin that functions downstream of Fat to regulate growth, affinity and gene expression in *Drosophila*. *Development* 133 (13):2539–2551.
- Marie, H., S. J. Pratt, M. Betson, H. Epple, J. T. Kittler, L. Meek, S. J. Moss, S. Troyanovsky, D. Attwell, G. D. Longmore, et al. (2003). The LIM protein Ajuba is recruited to cadherin-dependent cell junctions through an association with  $\alpha$ -catenin. *Journal of Biological Chemistry* 278 (2):1220–1228.

- Martín, F. A., S. C. Herrera, and G. Morata (2009). Cell competition, growth and size control in the *Drosophila* wing imaginal disc. *Development* 136 (22):3747–3756.
- Martín, F. A. and G. Morata (2006). Compartments and the control of growth in the *Drosophila* wing imaginal disc. *Development* 133 (22):4421–4426.
- Masucci, J., R. J. Miltenberger, and F. Hoffmann (1990). Pattern-specific expression of the *Drosophila* decapentaplegic gene in imaginal disks is regulated by 3'cis-regulatory elements. *Genes & development* 4 (11):2011–2023.
- Matakatsu, H. and S. S. Blair (2004). Interactions between Fat and Dachsoos and the regulation of planar cell polarity in the *Drosophila* wing. *Development* 131 (15):3785–3794.
- (2006). Separating the adhesive and signaling functions of the Fat and Dachsoos protocadherins. *Development* 133 (12):2315–2324.
- (2008). The DHHC palmitoyltransferase approximated regulates Fat signaling and Dachsoos localization and activity. *Current Biology* 18 (18):1390–1395.
- (2012). Separating planar cell polarity and Hippo pathway activities of the protocadherins Fat and Dachsoos. *Development* 139 (8):1498–1508.
- McCartney, B., R. Kulikauskas, D. LaJeunesse, and R. Fehon (2000). The neurofibromatosis-2 homologue, Merlin, and the tumor suppressor expanded function together in *Drosophila* to regulate cell proliferation and differentiation. *Development* 127 (6):1315–1324.
- McGuire, S. E., P. T. Le, A. J. Osborn, K. Matsumoto, and R. L. Davis (2003). Spatiotemporal rescue of memory dysfunction in *Drosophila*. *Science* 302 (5651):1765–1768.
- Mesquita, D., A. Dekanty, and M. Milán (2010). A dp53-dependent mechanism involved in coordinating tissue growth in *Drosophila*. *PLoS biology* 8 (12):e1000566.
- Micchelli, C. A. and N. Perrimon (2006). Evidence that stem cells reside in the adult *Drosophila* midgut epithelium. *Nature* 439 (7075):475.
- Milán, M., S. Campuzano, and A. García-Bellido (1996a). Cell cycling and patterned cell proliferation in the *Drosophila* wing during metamorphosis. *Proceedings of the National Academy of Sciences* 93 (21):11687–11692.
- (1996b). Cell cycling and patterned cell proliferation in the wing primordium of *Drosophila*. *Proceedings of the National Academy of Sciences* 93 (2):640–645.
- Mohr, S. E., J. A. Smith, C. E. Shamu, R. A. Neumüller, and N. Perrimon (2014). RNAi screening comes of age: improved techniques and complementary approaches. *Nature reviews Molecular cell biology* 15 (9):591.
- Mori, C., N. Nakamura, S. Kimura, H. Irie, T. Takigawa, and K. Shiota (1995). Programmed cell death in the interdigital tissue of the fetal mouse limb is apoptosis with DNA fragmentation. *The Anatomical Record* 242 (1):103–110.
- Nelson, D. E., S. J. Randle, and H. Laman (2013). Beyond ubiquitination: the atypical functions of Fbxo7 and other F-box proteins. *Open biology* 3 (10):130131.
- Ni, J.-Q., R. Zhou, B. Czech, L.-P. Liu, L. Holderbaum, D. Yang-Zhou, H.-S. Shim, R. Tao, D. Handler, P. Karpowicz, et al. (2011). A genome-scale shRNA resource for transgenic RNAi in *Drosophila*. *Nature methods* 8 (5):405.
- Nibu, Y., H. Zhang, and M. Levine (1998). Interaction of short-range repressors with *Drosophila* CtBP in the embryo. *Science* 280 (5360):101–104.

- Nienhaus, U., T. Aegerter-Wilmsen, and C. M. Aegerter (2009). Determination of mechanical stress distribution in *Drosophila* wing discs using photoelasticity. *Mechanisms of Development* 126 (11):942–949.
- Nolo, R., C. M. Morrison, C. Tao, X. Zhang, and G. Halder (2006). The bantam microRNA is a target of the hippo tumor-suppressor pathway. *Current Biology* 16 (19):1895–1904.
- O’Brochta, D. A. and P. J. Bryant (1985). A zone of non-proliferating cells at a lineage restriction boundary in *Drosophila*. *Nature* 313 (5998):138.
- Oh, H. and K. D. Irvine (2008). In vivo regulation of Yorkie phosphorylation and localization. *Development* 135 (6):1081–1088.
- (2011). Cooperative regulation of growth by Yorkie and Mad through bantam. *Developmental cell* 20 (1):109–122.
- Oh, H., M. Slattery, L. Ma, A. Crofts, K. P. White, R. Mann, and K. D. Irvine (2013). Genome-wide association of Yorkie with chromatin and chromatin remodeling complexes. *Cell reports* 3 (2):309–318.
- Olive, M., D. Krylov, D. R. Echlin, K. Gardner, E. Taparowsky, and C. Vinson (1997). A dominant negative to activation protein-1 (AP1) that abolishes DNA binding and inhibits oncogenesis. *Journal of Biological Chemistry* 272 (30):18586–18594.
- Paddison, P. J., A. A. Caudy, E. Bernstein, G. J. Hannon, and D. S. Conklin (2002). Short hairpin RNAs (shRNAs) induce sequence-specific silencing in mammalian cells. *Genes & development* 16 (8):948–958.
- Pan, D. (2010). The hippo signaling pathway in development and cancer. *Developmental cell* 19 (4):491–505.
- Pan, G., Y. Feng, A. A. Ambegaonkar, G. Sun, M. Huff, C. Rauskolb, and K. D. Irvine (2013). Signal transduction by the Fat cytoplasmic domain. *Development* 140 (4):831–842.
- Park, H.-O., J. Chant, and I. Herskowitz (1993). BUD2 encodes a GTPase-activating protein for Bud1/Rsr1 necessary for proper bud-site selection in yeast. *Nature* 365 (6443):269.
- Parker, N. F. and A. W. Shingleton (2011). The coordination of growth among *Drosophila* organs in response to localized growth-perturbation. *Developmental Biology* 357 (2):318–325.
- Pascual, J., J. Jacobs, L. Sansores-Garcia, M. Natarajan, J. Zeitlinger, S. Aerts, G. Halder, and F. Hamaratoglu (2017). Hippo Reprograms the Transcriptional Response to Ras Signaling. *Developmental cell* 42 (6):667–680.
- Pellikka, M., G. Tanentzapf, M. Pinto, C. Smith, C. J. McGlade, D. F. Ready, and U. Tepass (2002). Crumbs, the *Drosophila* homologue of human CRB1/RP12, is essential for photoreceptor morphogenesis. *Nature* 416 (6877):143.
- Pérez-Garijo, A., E. Shlevkov, and G. Morata (2009). The role of Dpp and Wg in compensatory proliferation and in the formation of hyperplastic overgrowths caused by apoptotic cells in the *Drosophila* wing disc. *Development* 136 (7):1169–1177.
- Perrimon, N., J.-Q. Ni, and L. Perkins (2010). In vivo RNAi: today and tomorrow. *Cold Spring Harbor perspectives in biology* 2 (8):a003640.

- Petrelli, A., G. F. Gilestro, S. Lanzardo, P. M. Comoglio, N. Migone, and S. Giordano (2002). The endophilin–CIN85–Cbl complex mediates ligand-dependent downregulation of c-Met. *Nature* 416 (6877):187.
- Phillips, R. G., I. Roberts, P. W. Ingham, and J. Whittle (1990). The *Drosophila* segment polarity gene *patched* is involved in a position-signalling mechanism in imaginal discs. *Development* 110 (1):105–114.
- Pignoni, F. and S. L. Zipursky (1997). Induction of *Drosophila* eye development by decapentaplegic. *Development* 124 (2):271–278.
- Poortinga, G., M. Watanabe, and S. M. Parkhurst (1998). *Drosophila* CtBP: a Hairy-interacting protein required for embryonic segmentation and Hairy-mediated transcriptional repression. *The EMBO Journal* 17 (7):2067–2078.
- Qing, Y., F. Yin, W. Wang, Y. Zheng, P. Guo, F. Schozer, H. Deng, and D. Pan (2014). The Hippo effector Yorkie activates transcription by interacting with a histone methyltransferase complex through NcoA6. *eLife* 3:ed. by J. Rossant, e02564.
- Rauskolb, C., G. Pan, B. Reddy, H. Oh, and K. D. Irvine (2011). Zyxin links fat signaling to the hippo pathway. *PLoS biology* 9 (6):e1000624.
- Rauskolb, C., S. Sun, G. Sun, Y. Pan, and K. D. Irvine (2014). Cytoskeletal tension inhibits Hippo signaling through an Ajuba-Warts complex. *Cell* 158 (1):143–156.
- Restrepo, S., J. J. Zartman, and K. Basler (2014). Coordination of patterning and growth by the morphogen DPP. *Current Biology* 24 (6):R245–R255.
- Richard, M., F. Grawe, and E. Knust (2006). DPATJ plays a role in retinal morphogenesis and protects against light-dependent degeneration of photoreceptor cells in the *Drosophila* eye. *Developmental dynamics* 235 (4):895–907.
- Rogulja, D., C. Rauskolb, and K. D. Irvine (2008). Morphogen control of wing growth through the Fat signaling pathway. *Developmental cell* 15 (2):309–321.
- Roignant, J.-Y., C. Carré, B. Mugat, D. Szymczak, J.-A. Lepesant, and C. Antoniewski (2003). Absence of transitive and systemic pathways allows cell-specific and isoform-specific RNAi in *Drosophila*. *Rna* 9 (3):299–308.
- Ryoo, H. D., T. Gorenc, and H. Steller (2004). Apoptotic cells can induce compensatory cell proliferation through the JNK and the Wingless signaling pathways. *Developmental cell* 7 (4):491–501.
- Sansores-Garcia, L., W. Bossuyt, K.-I. Wada, S. Yonemura, C. Tao, H. Sasaki, and G. Halder (2011). Modulating F-actin organization induces organ growth by affecting the Hippo pathway. *The EMBO Journal* 30 (12):2325–2335.
- Schmick, M., N. Vartak, B. Papke, M. Kovacevic, D. C. Truxius, L. Rossmannek, and P. I. Bastiaens (2014). KRas localizes to the plasma membrane by spatial cycles of solubilization, trapping and vesicular transport. *Cell* 157 (2):459–471.
- Schubiger, G. (1971). Regeneration, duplication and transdetermination in fragments of the leg disc of *Drosophila melanogaster*. *Developmental biology* 26 (2):277–295.
- Schwank, G. and K. Basler (2010). Regulation of organ growth by morphogen gradients. *Cold Spring Harbor perspectives in biology* 2 (1):a001669.

- Sebé-Pedrós, A., Y. Zheng, I. Ruiz-Trillo, and D. Pan (2012). Premetazoan origin of the Hippo signaling pathway. *Cell reports* 1 (1):13–20.
- Setiawan, L., A. L. Woods, and I. K. Hariharan (2017). The BMP2/4 ortholog Dpp functions as an inter-organ signal that regulates developmental timing in *Drosophila*. *bioRxiv*.
- Sharma, P. and H. McNeill (2013). Chapter Ten - Fat and Dachshous Cadherins. *The Molecular Biology of Cadherins*. Ed. by F. van Roy. Vol. 116. Progress in Molecular Biology and Translational Science. Academic Press, 215–235.
- Shingleton, A. W. (2010). The regulation of organ size in *Drosophila*: physiology, plasticity, patterning and physical force. *Organogenesis* 6 (2):76–87.
- Shingleton, A. W., C. M. Estep, M. V. Driscoll, and I. Dworkin (2009). Many ways to be small: different environmental regulators of size generate distinct scaling relationships in *Drosophila melanogaster*. *Proceedings of the Royal Society B: Biological Sciences* 276 (1667):2625–2633.
- Shraiman, B. I. (2005). Mechanical feedback as a possible regulator of tissue growth. *Proceedings of the National Academy of Sciences of the United States of America* 102 (9):3318–3323.
- Sijen, T., J. Fleenor, F. Simmer, K. L. Thijssen, S. Parrish, L. Timmons, R. H. Plasterk, and A. Fire (2001). On the role of RNA amplification in dsRNA-triggered gene silencing. *Cell* 107 (4):465–476.
- Silva, E., Y. Tsatskis, L. Gardano, N. Tapon, and H. McNeill (2006). The tumor-suppressor gene fat controls tissue growth upstream of expanded in the hippo signaling pathway. *Current Biology* 16 (21):2081–2089.
- Simon, M. A. (2004). Planar cell polarity in the *Drosophila* eye is directed by graded Four-jointed and Dachshous expression. *Development* 131 (24):6175–6184.
- Simon, M. A., A. Xu, H. O. Ishikawa, and K. D. Irvine (2010). Modulation of fat: dachshous binding by the cadherin domain kinase four-jointed. *Current Biology* 20 (9):811–817.
- Skaar, J. R., J. K. Pagan, and M. Pagano (2013). Mechanisms and function of substrate recruitment by F-box proteins. *Nature reviews Molecular cell biology* 14 (6):369.
- Sopko, R., E. Silva, L. Clayton, L. Gardano, M. Barrios-Rodiles, J. Wrana, X. Varelas, N. I. Arbouzova, S. Shaw, S. Saburi, et al. (2009). Phosphorylation of the tumor suppressor fat is regulated by its ligand Dachshous and the kinase discs overgrown. *Current Biology* 19 (13):1112–1117.
- Soubeyran, P., K. Kowanetz, I. Szymkiewicz, W. Y. Langdon, and I. Dikic (2002). Cbl–CIN85–endophilin complex mediates ligand-induced downregulation of EGF receptors. *Nature* 416 (6877):183.
- Strutt, H. and D. Strutt (2002). Nonautonomous planar polarity patterning in *Drosophila*: dishevelled-independent functions of frizzled. *Developmental cell* 3 (6):851–863.
- Su, T., M. Z. Ludwig, J. Xu, and R. G. Fehon (2017). Kibra and Merlin activate the Hippo pathway spatially distinct from and independent of Expanded. *Developmental cell* 40 (5):478–490.e3.

- Sun, G. and K. D. Irvine (2011). Regulation of Hippo signaling by Jun kinase signaling during compensatory cell proliferation and regeneration, and in neoplastic tumors. *Developmental biology* 350 (1):139–151.
- (2013). Ajuba Family Proteins Link JNK to Hippo Signaling. *Science signaling* 6 (292).
- Sutterluty, H, E Chatelain, A Marti, C Wirbelauer, M Senften, and U Muller (15). and W. Krek. 1999. p45SKP2 promotes p27Kip1 degradation and induces S 22 phase in quiescent cells. *Nature Cell Biol* 1:207–14.
- Swarup, S. and E. M. Verheyen (2012). Wnt/wingless signaling in Drosophila. *Cold Spring Harbor perspectives in biology* 4 (6):a007930.
- Tabata, T., S. Eaton, and T. B. Kornberg (1992). The Drosophila hedgehog gene is expressed specifically in posterior compartment cells and is a target of engrailed regulation. *Genes & development* 6 (12b):2635–2645.
- Tamori, Y., E. Suzuki, and W.-M. Deng (2016). Epithelial tumors originate in tumor hotspots, a tissue-intrinsic microenvironment. *PLoS biology* 14 (9):e1002537.
- Tanimoto, H., S. Itoh, P. ten Dijke, and T. Tabata (2000). Hedgehog creates a gradient of DPP activity in Drosophila wing imaginal discs. *Molecular cell* 5 (1):59–71.
- Tapon, N. and K. F. Harvey (2012). The Hippo pathway—from top to bottom and everything in between. *Seminars in cell & developmental biology*. Vol. 23. (7). Academic Press, 768–769.
- Tapon, N., N. Ito, B. J. Dickson, J. E. Treisman, and I. K. Hariharan (2001). The Drosophila tuberous sclerosis complex gene homologs restrict cell growth and cell proliferation. *Cell* 105 (3):345–355.
- Thomas, C. and D. Strutt (2012). The roles of the cadherins Fat and Dachshous in planar polarity specification in Drosophila. *Developmental dynamics* 241 (1):27–39.
- Thompson, B. J. and S. M. Cohen (2006). The Hippo pathway regulates the bantam microRNA to control cell proliferation and apoptosis in Drosophila. *Cell* 126 (4):767–774.
- Thompson, D. W. (1942). *On Growth and Form*. 2nd ed. Cambridge Univ. Press.
- Turner, J. and M. Crossley (2001). The CtBP family: enigmatic and enzymatic transcriptional co-repressors. *Bioessays* 23 (8):683–690.
- Tyler, D. M., W. Li, N. Zhuo, B. Pellock, and N. E. Baker (2007). Genes affecting cell competition in Drosophila. *Genetics* 175 (2):643–657.
- Tyler, S. (2003). Epithelium—the primary building block for metazoan complexity. *Integrative and comparative biology* 43 (1):55–63.
- Uhlirva, M., H. Jasper, and D. Bohmann (2005). Non-cell-autonomous induction of tissue overgrowth by JNK/Ras cooperation in a Drosophila tumor model. *Proceedings of the National Academy of Sciences of the United States of America* 102 (37):13123–13128.
- Vaistij, F. E., L. Jones, and D. C. Baulcombe (2002). Spreading of RNA targeting and DNA methylation in RNA silencing requires transcription of the target gene and a putative RNA-dependent RNA polymerase. *The Plant Cell* 14 (4):857–867.
- Verdel, A., S. Jia, S. Gerber, T. Sugiyama, S. Gygi, S. I. Grewal, and D. Moazed (2004). RNAi-mediated targeting of heterochromatin by the RITS complex. *Science* 303 (5658):672–676.

- Villano, J. L. and F. N. Katz (1995). four-jointed is required for intermediate growth in the proximal-distal axis in *Drosophila*. *Development* 121 (9):2767–2777.
- Vissers, J. H. A., S. A. Manning, A. Kulkarni, and K. F. Harvey (2016). A *Drosophila* RNAi library modulates Hippo pathway-dependent tissue growth. *Nature Communications* 7:10368 EP –.
- Wada, K.-I., K. Itoga, T. Okano, S. Yonemura, and H. Sasaki (2011). Hippo pathway regulation by cell morphology and stress fibers. *Development* 138 (18):3907–3914.
- Wartlick, O., P. Mumcu, F. Jülicher, and M. Gonzalez-Gaitan (2011). Understanding morphogenetic growth control? lessons from flies. *Nature Reviews Molecular Cell Biology* 12 (9):594.
- Watt, K. I., K. F. Harvey, and P. Gregorevic (2017). Regulation of Tissue Growth by the Mammalian Hippo Signaling Pathway. *Frontiers in Physiology* 8:942.
- Weng, R. and S. M. Cohen (2015). Control of *Drosophila* Type I and Type II central brain neuroblast proliferation by bantam microRNA. *Development* 142 (21):3713–3720.
- Wilk, R., J. Hu, D. Blotsky, and H. M. Krause (2016). Diverse and pervasive subcellular distributions for both coding and long noncoding RNAs. *Genes & development* 30 (5):594–609.
- Willecke, M., F. Hamaratoglu, M. Kango-Singh, R. Udan, C.-l. Chen, C. Tao, X. Zhang, and G. Halder (2006). The fat cadherin acts through the hippo tumor-suppressor pathway to regulate tissue size. *Current Biology* 16 (21):2090–2100.
- Williams, R. W. (2000). “Mapping Genes that Modulate Mouse Brain Development: A Quantitative Genetic Approach”. *Mouse Brain Development*. Ed. by A. M. Goffinet and P. Rakic. Berlin, Heidelberg: Springer Berlin Heidelberg, pp. 21–49. ISBN: 978-3-540-48002-0.
- Willsey, H. R., X. Zheng, J. C. Pastor-Pareja, A. J. Willsey, P. A. Beachy, and T. Xu (2016). Localized JNK signaling regulates organ size during development. *Elife* 5.
- Wilson, R. C. and J. A. Doudna (2013). Molecular mechanisms of RNA interference. *Annual review of biophysics* 42:217–239.
- Wolpert, L. (2010). Arms and the Man: The Problem of Symmetric Growth. *PLOS Biology* 8 (9):1–3.
- Worley, M. I., L. A. Alexander, and I. K. Hariharan (2018). CtBP impedes JNK- and Upd/STAT-driven cell fate misspecifications in regenerating *Drosophila* imaginal discs. *eLife* 7:e30391.
- Worley, M. I., L. Setiawan, and I. K. Hariharan (2013). TIE-DYE: a combinatorial marking system to visualize and genetically manipulate clones during development in *Drosophila melanogaster*. *Development* 140 (15):3275–3284.
- Wu, K., S. Y. Fuchs, A. Chen, P. Tan, C. Gomez, Z. Ronai, and Z.-Q. Pan (2000). The SCFHOS/ $\beta$ -TRCP-ROC1 E3 ubiquitin ligase utilizes two distinct domains within CUL1 for substrate targeting and ubiquitin ligation. *Molecular and cellular biology* 20 (4):1382–1393.
- Wu, Y.-C., K.-S. Lee, Y. Song, S. Gehrke, and B. Lu (2017). The bantam microRNA acts through Numb to exert cell growth control and feedback regulation of Notch in tumor-forming stem cells in the *Drosophila* brain. *PLoS genetics* 13 (5):e1006785.

- Xu, T. and G. M. Rubin (1993). Analysis of genetic mosaics in developing and adult *Drosophila* tissues. *Development* 117 (4):1223–1237.
- Xue, Z., M. Wu, K. Wen, M. Ren, L. Long, X. Zhang, and G. Gao (2014). CRISPR/Cas9 Mediates Efficient Conditional Mutagenesis in *Drosophila*. *G3: Genes|Genomes|Genetics* 4 (11):2167–2173.
- Yang, C.-h., J. D. Axelrod, and M. A. Simon (2002). Regulation of Frizzled by fat-like cadherins during planar polarity signaling in the *Drosophila* compound eye. *Cell* 108 (5):675–688.
- Yang, X. and T. Xu (2011). Molecular mechanism of size control in development and human diseases. *Cell research* 21 (5):715.
- Yeh, E., K. Gustafson, and G. L. Boulianne (1995). Green fluorescent protein as a vital marker and reporter of gene expression in *Drosophila*. *Proceedings of the National Academy of Sciences* 92 (15):7036–7040.
- Yen, H.-C. S. and S. J. Elledge (2008). Identification of SCF ubiquitin ligase substrates by global protein stability profiling. *Science* 322 (5903):923–929.
- Yu, J., Y. Zheng, J. Dong, S. Klusza, W.-M. Deng, and D. Pan (2010). Kibra functions as a tumor suppressor protein that regulates Hippo signaling in conjunction with Merlin and Expanded. *Developmental cell* 18 (2):288–299.
- Zhang, J., C. Wang, N. Ke, J. Bliesath, J. Chionis, Q. S. He, Q.-x. Li, J. E. Chatterton, F. Wong-Staal, and D. Zhou (2007). A more efficient RNAi inducible system for tight regulation of gene expression in mammalian cells and xenograft animals. *Rna* 13 (8):1375–1383.
- Zhang, L., F. Ren, Q. Zhang, Y. Chen, B. Wang, and J. Jiang (2008). The TEAD/TEF family of transcription factor Scalloped mediates Hippo signaling in organ size control. *Developmental cell* 14 (3):377–387.
- Zhang, P., C. Pei, X. Wang, J. Xiang, B.-F. Sun, Y. Cheng, X. Qi, M. Marchetti, J.-W. Xu, Y.-P. Sun, B. A. Edgar, and Z. Yuan (2017). A Balance of Yki/Sd Activator and E2F1/Sd Repressor Complexes Controls Cell Survival and Affects Organ Size. *Developmental Cell* 43 (5):603–617.e5.
- Zhao, B., K. Tumaneng, and K.-L. Guan (2011). The Hippo pathway in organ size control, tissue regeneration and stem cell self-renewal. *Nature cell biology* 13 (8):877.
- Zhao, X., C.-h. Yang, and M. A. Simon (2013). The *Drosophila* Cadherin Fat regulates tissue size and planar cell polarity through different domains. *PloS one* 8 (5):e62998.
- Zirin, J. D. and R. S. Mann (2007). Nubbin and Teashirt mark barriers to clonal growth along the proximal–distal axis of the *Drosophila* wing. *Developmental biology* 304 (2):745–758.
- Zong, J., X. Yao, J. Yin, D. Zhang, and H. Ma (2009). Evolution of the RNA-dependent RNA polymerase (RdRP) genes: duplications and possible losses before and after the divergence of major eukaryotic groups. *Gene* 447 (1):29–39.